UNIVERSITA' DEGLI STUDI DI PADOVA

Dipartimento di Tecnica e Gestione dei Sistemi Industriali

Corso di Laurea Magistrale in Ingegneria

dell'Innovazione del Prodotto

Titolo:

''EXPERIMENTAL STUDY ABOUT THERMAL FATIGUE AND EROSION FAILURES ON HPDC DIES.''

Relatore: **Ch. mo Prof Franco Bonollo**

Correlatore: **Ing. Amaya Igartua**, **Ing. Borja Zabala (IK4-TEKNIKER Tribology Unit)**

Laureando: ***Tonino Cundari***

Matricola: ***1062428***

ANNO ACCADEMICO 2015/2016

.

Sommario

ABSTRACT

The objective of this work was to study the phenomena of Thermal fatigue and Erosion that occur in the die during a HPDC process.
It has been demonstrated that there are different wear mechanisms that contribute to damage the High Pressure Die Casting dies, and erosion and thermal fatigue are both the topic of this thesis. Erosion and thermal fatigue are both long term failures, that are very difficult to predict and expensive to repair. Erosion is a mechanical action of the flux against the mould surface, and thermal fatigue is the cracking that results from the repeated compression and tension due to the rapid heating and cooling of the mould surface.

The aim was achieved by the study of the literature of previous tests and by performing some laboratory tests, that have been used to simulate both phenomena and understand them better, in order to predict their appearance in the HPDC moulds. The tests were carried out on AISI H11 and H13 steels, which are the most commonly used die materials hot work tool steels, thanks to their resistance properties.

The results of the experimental study of thermal fatigue confirmed that to a greater amplitude, and at a constant temperature, correspond a less number of residues cycles. From the results of these tests we have managed to identified an equation that can be considered a good starting point to describe the behavior between applied stress and number of residues cycles to rupture. It is however necessary to clarify that is still a work in progress.

The results of the experimental study of the erosion demonstrated that the most affecting parameters are the impact angle and the velocity of the erodent flow. In particular the mass lost values are inversely proportional to the increasing angle, that is larger values of impact angle corresponds to a less mass lost, while the wear depth has a maximum on 45°, a minimum at 15° and an intermediate value at 90°.

SYMBOL INDEX

HPDC = High pressure die-casting;

PID = Proportional-Integral-Derivative;

CL = Constant Load;

CF = Cycle Fatigue;

SSR = Slow Strain Rate;

HTMF = High Temperature Mechanical Fatigue

LCF = Low Cycle Fatigue;

FE = Finite Element;

Chapter 1:

INTRODUCTION

The present work is a little part of an European project that is called ‘’MUSIC’’. Below there is an explanation about the principal points and purposes that this project wants to reach.

‘’High Pressure Die Casting (HPDC) is one of the most representative large-scale production-line in manufacturing field. Due to the high number of process variables involved and to the non-synchronisation of the process control units, HPDC is most “**defect-generating” and “energy-consumption”** processes in EU industry showing less flexibility to any changes in products and in process evolution. The sustainability issue imposes that machines/systems are able to efficiently and ecologically support the

production with higher quality, faster delivery times, and shorter times between successive generations of products.

Therefore, the MUSIC is strongly aimed at leading EU-HPDC factories to cost-based competitive advanced through the necessary transition to a demand-driven industry with lower waste generation, efficiency, robustness and minimum **energy consumption**. The development and integration of a completely new ICT platform, based on innovative Control and Cognitive system linked to real time monitoring, allows an active control of quality, avoiding the presence of defects or over-cost by directly acting on the process-machine variables optimisation or equipment boundary conditions. The Intelligent Manufacturing Approach (IMA) will work at machine-mould project level to optimise/adapt the production to the specific product and can be extended at factory level to select/plan the appropriated and available production line.

The sensors calibration and quality measurements will be the pre-requisite of Intelligent Sensor Network (ISN) to monitor the real-time production and specific focus will be also devoted to Standardisation issues.

The challenge of MUSIC is to transform a production-rate-dominated manufacturing field into a quality/efficiency-driven and integration-oriented one to exploit the enormous (and still underestimated) potential of HPDC/PIM through collaborative research and technological development, along the value chain with research groups, design, engineering and manufacturing companies and through advances in manufacturing, ICT and model process technologies.''

Chapter 2:

HPDC PROCESS

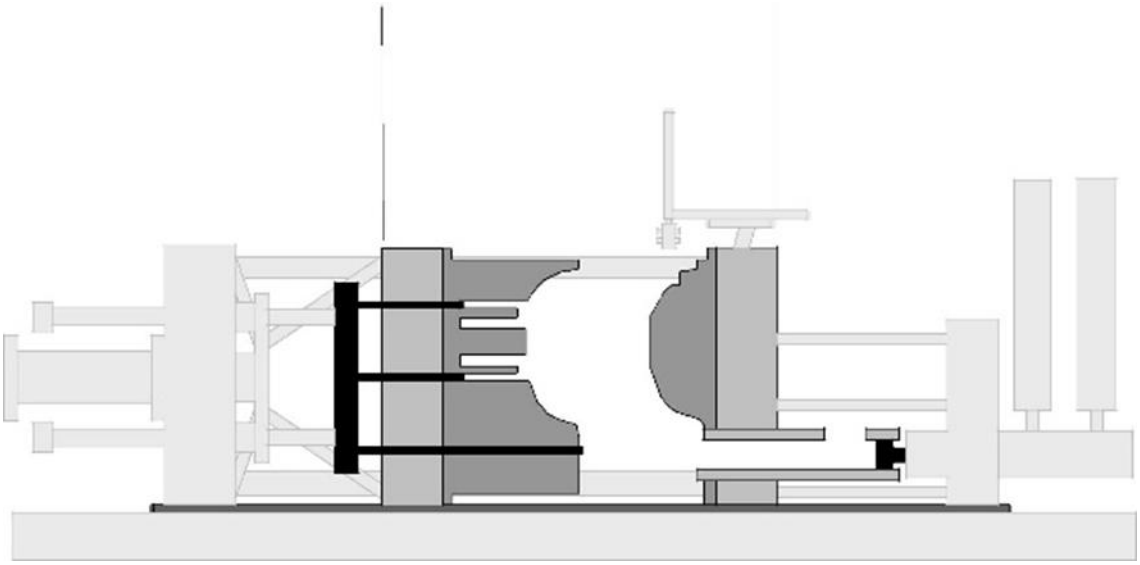

Typical system for High Pressure Die Casting phases [9].

High pressure die casting, HPDC, is a process widely used to manufacture non-ferrous castings for the automotive industry.

With HPDC the molten metal is forced into the die cavity under pressure. Typified by high filling speeds and rapid solidification rates, this casting process can produce shapes which are more detailed than components manufactured using gravity or low pressure die casting methods.

Non-ferrous alloys, mainly aluminium, magnesium and zinc are most commonly cast using this process. HPDC is ideal for high volume thin walled castings due to the fast cycle times, ranging from seconds to several minutes depending on casting size and wall thickness, therefore enabling production in excess of 60 castings per hour from one casting machine.

A production of 100,000–300,000 casting per die is a common series, although some dies fail even after 5000–25,000 cycles. During aluminium die casting, molten aluminium at temperatures 670–710 °C is injected into the mould at velocities between 30 and 100 m/s. The injection pressures are between 50 and 80 MPa.

The important material properties required for HPDC dies are resistance to thermal shock and to softening at elevated temperatures. The most commonly used die materials are H11 and H13 hot work tool steels. The longevity of the die is directly related to the casting temperature of the molten metal, thermal gradients in the die and the exposure frequency to the high metal temperature.

HPDC it is used for almost 70% of aluminium components manufactured today many aluminium components for the automotive industry are cast using this method, due to the high productivity and near net shape production. Large components such as gearbox housings and engine blocks are typical examples where casting weight can be in excess of 15 kg.

2.1 HIGH PRESSURE DIE-CASTING TECHNOLOGY

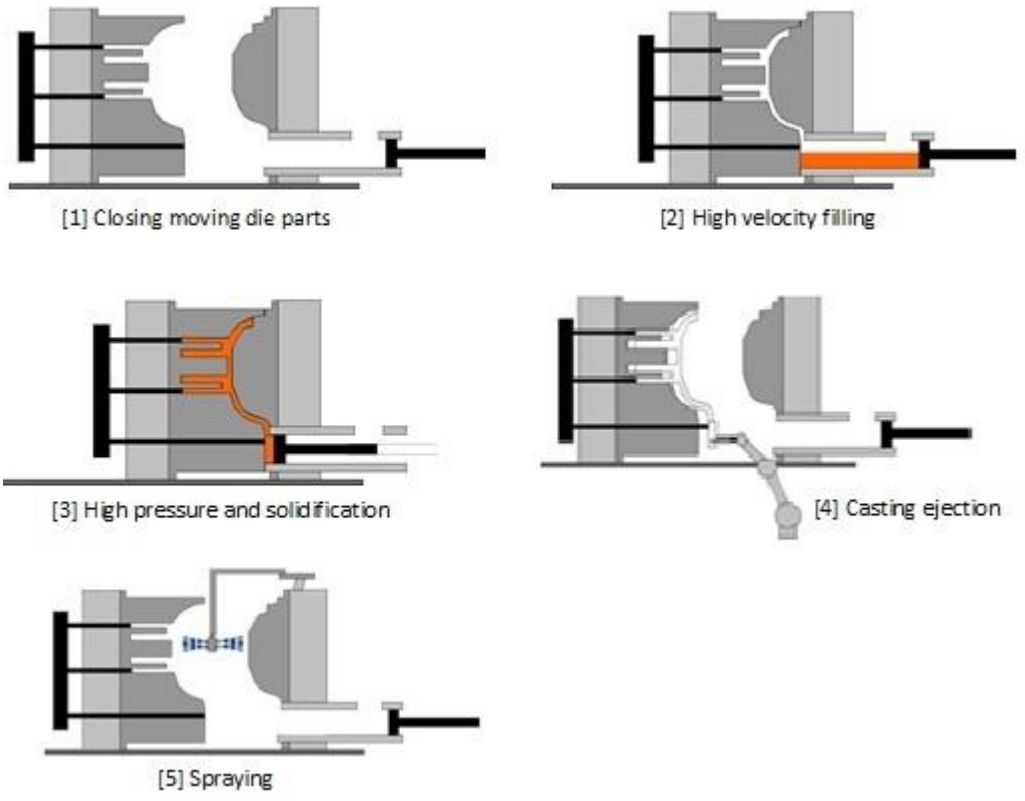

Fig 2.1 HPDC phases [9].

In Fig. 2.1 are showed the different phases of the HPDC process, as can be seen molten aluminium is poured into the shots sleeve and then injected into the die cavity by a plunger under pressure.

The purpose of the applied pressure is to reduce the amount of gas porosity, feed shrinkage porosity, and increase dimensional accuracy of the part. The die is usually internally cooled to increase the rate of solidification. After solidification the die opens and the casting is separated from the die by hydraulic ejector pins.

With HPDC, the die surface is rapidly heated when the molten aluminium is injection into the die cavity. After the casting solidifies, it is ejected and then removed from the die. The die surface is then cooled by the die-lube spray (mix of oil and water), used to both lubricate and cool the surface of the die. For HPDC there is no insulating die coat layer between the casting and the die, which is commonly used for gravity and low pressure

permanent mould casting. Therefore, the molten aluminium makes more direct contact with the die surface, encouraging a fast solidification time due to the high heat transfer coefficient between the die surface and the casting. As there is little insulation between the die surface and the molten metal, the heat transfer coefficient between the die and casting along with the peak die surface temperature are much greater than seen with other casting methods

2.2 HPDC PRODUCTS

High-pressure die-casting is a process widely used to manufacture non-ferrous castings for the automotive industry. The main classes of HPDC products are reported in Figure 2.2. It can be observed that 83.7% of the HPDC foundries focus on automotive applications (with a similar percentage for SMEs and IND), followed by Electronics (30.2%), Mechanical Engineering (27.9%), and Architecture and Design (9.3%). In the "Other" category, mainly applications. for mechanics and engineering were mentioned in the survey. SME and IND's meaning is small-medium enterprises and large industries respectively [10].

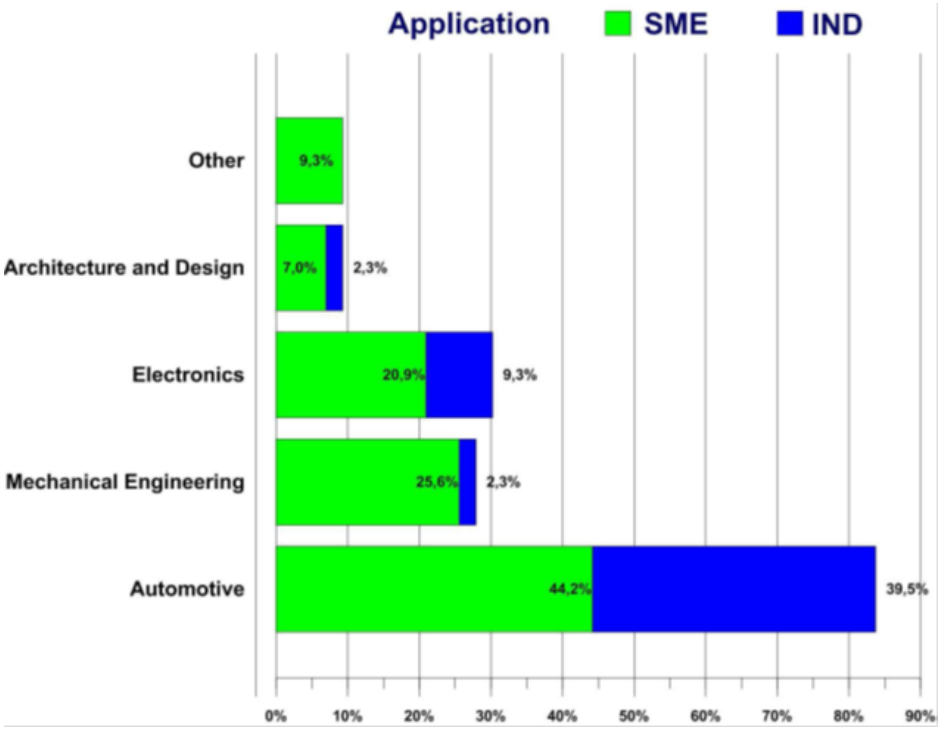

Figure 2.2 Final applications of castings produced by HPDC foundries, divided into SMEs and IND [10]

2.3 DAMAGE OF THE DIE IN HPDC PROCESS

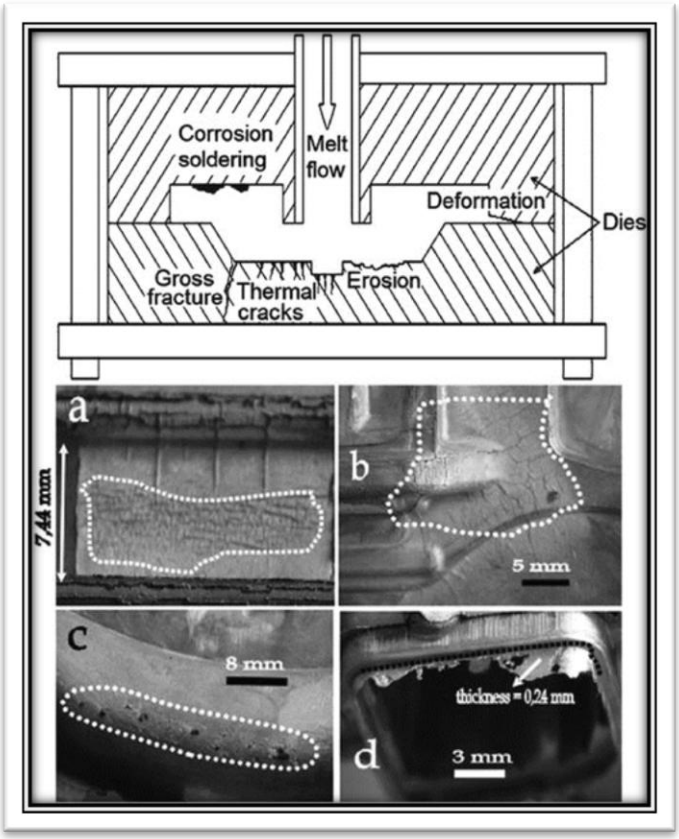

Figure 2.3 Principal Damage of the Die in HPDC Process.

Since the cost of the die covers about 20% of the total production cost in aluminium alloy die-casting, the damage of the dies for HPDC, is a matter which is subject to numerous studies.

The main reasons are essentially two: the spread of this type of process, about 70% of total production, and the maintenance and the initial cost of the die. For these reasons, it has been tried to improve the quality, and in particular the duration of the dies, in order to prevent several costs about maintenance and downtime.

Aluminium die-casting dies fail because of a number of different and simultaneously operating stresses. The stresses are of two basic kinds: the first which are created during the **manufacturing of the die**, and the second which are produced during **exploitation process**. As already said the replacement of a die is expensive in both: money and production time.

In particular during the real exploitation process of die casting, different type of failure take place. The most affecting damage are surface heat checks, which are caused by **thermal fatigue** of die material, and occurs through a process of crack initiation and propagation from the thermal stress fatigue induced on a die surface. These die surface cracks causes the unwanted marks (fins) on the casting surface.

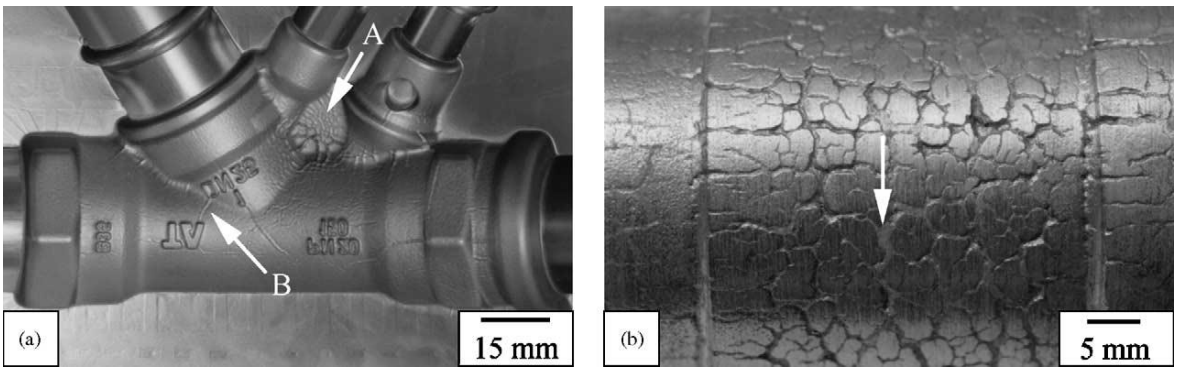

Figure 2.4 Typical macroscopic surface damages observed on worn-out cavity inserts and cores [16].

Furthermore, there are other type of damage like, **corrosion and soldering** due to aluminium oxidation to the die surface; **erosion** due to melt flow; **catastrophic failures** due to thermal shocks; and **heating of die material**, which causes instability of the mechanical properties.

Visual inspection of damaged mould allowed identifying the most common failure mechanisms and most of all are connected to each other's.

A brief presentation of these phenomena is listed below:

Die soldering:

When molten aluminium comes into contact with the ferrous die material, the iron and the aluminium atoms diffuse into each other, resulting in the formation of a series of intermetallic phases over the die. Initially, iron and aluminium react to form binary iron-aluminium intermetallic phases. Subsequently, these phases react with the molten aluminium to further form ternary iron-aluminium-silicon intermetallic phases.

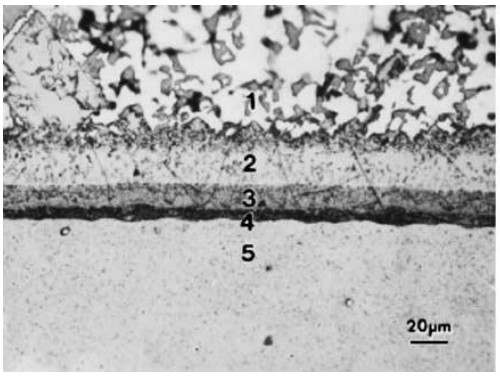

Fig. 2.4 Intermetallic layers formed after dipping H13 steel [11].

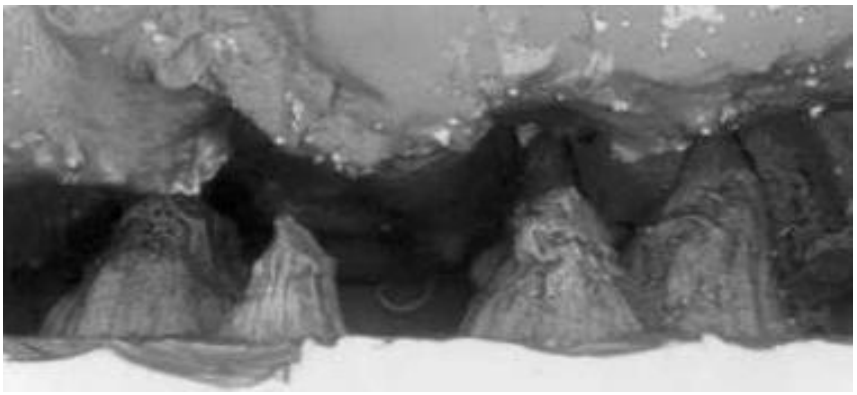

Fig. 2.5 Pyramid-shaped intermetallic phase at the soldering interface [11].

The resulting formation of a layer of the cast alloy that occurs on the interface is called soldering. The distinction between corrosion and soldering has its roots in the die-casting engineering practice. The term corrosion emphasizes the undesirable removal of the die material due to a chemical deterioration of the die surface, while soldering refers to the effect of adhesion (sticking) of cast material to the die surface.

Die soldering can be divide in two categories: *metallurgical-chemical* or *mechanical*.

Mechanical soldering sticking of the melt to the die happens after a few shots. Sticking is not related to any metallurgical-chemical reaction because there is not time/temperature to form intermetallic layers, but could be related either to high pressure or to an error in the design of the mould.

Metallurgical-chemical soldering interactions: dissolution of the die material iron into the melt or to the cast alloy elements diffusing into the die. As result, intermetallic layers are formed on the die surface. Chemical interactions between the die and the melt are

possible only when any protective skin layer (including iron oxide film and lubricant, or coating) is removed by erosion.

In detail, the mechanism of soldering consists in several steps as shown in Figure 2.6. After a local coating failure (Figure 2.7), the molten aluminium attacks the grain boundaries, and loosens up the hard grains and martensitic plates giving rise to pitting on the die surface.

The formation of the iron-aluminium intermetallic phases (such as FeAl, FeAl2, Fe2Al5 and FeAl3) occurs inside the pits and around the broken grains close to the die surface.

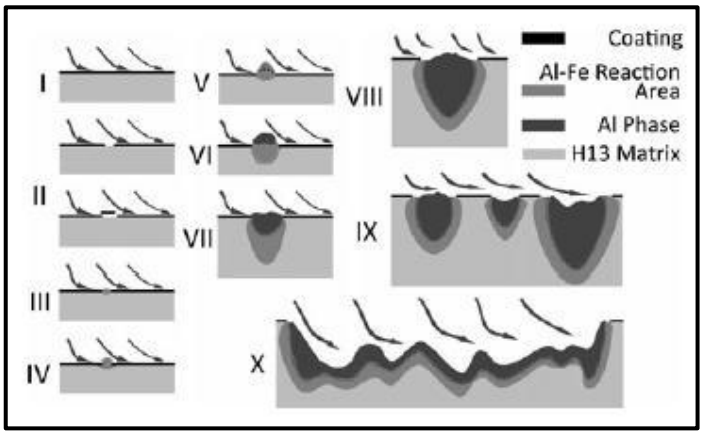

Fig. 2.6 Sketched steps of soldering process [12].

At this point, it should be noted that the solidus temperatures of the binary Fe_xAl_y intermetallic phases are well above 700°C, i.e. much higher than typical die-casting temperatures. Hence such intermetallic sub-layers will remain in solid state throughout the casting operation. Subsequently, the ternary α-(Al, Fe, Si) phase grows with pyramidal shape (Figure 3.2) on the pits over the η-Fe2Al5 and the pits expand laterally and in depth.

When the aluminium concentration in the die surface layer reaches a value sufficient to form a eutectic Al-rich phase and the surface temperature is high enough to re-melt it, the molten aluminium sticks resulting in the beginning of soldering. The intermetallic layers grow and the neighboring pits merge to form a consecutive zigzag shape. After that, the closing of the gaps between the adjacent pits occurs, the chemical reaction mechanism becomes very slow, and silicon precipitates at the grain boundaries of the η-Fe2Al5 phase and at the intersection boundaries between the binary and ternary intermetallic layers.

Irrespective of the process conditions (time, temperature and die surface area), the ratio of the intermetallic layer thickness and the soldered aluminium is ca. 1:5.

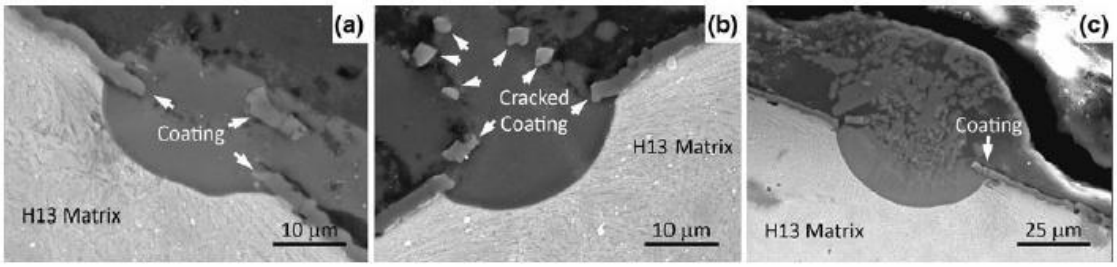

Fig. 2.7 SEM images of the reaction areas: (a) coating broken by lateral growth in soldering area, (b) coating cracked and migrated away, and (c) coating washed-out [12].

Washout:

The term washout (literally *failure*), in the field of casting, and in particular in the case of die casting, indicates a type of damage that developed on the dies. This type of failure is defined as a set of damage that can occur simultaneously, but which have fully different behaviors.

Corrosive wear results from the fact that tool steel and other metal are in some degree dissolvable in liquid aluminium and the high pouring temperatures may cause oxidation of the die surface. Despite this type of behavior, in literature, is often associated to the *die soldering*, it is not entirely true. In fact there are different types of damages due to the effect of corrosion. It is important to clarify the two main phenomena.

The *high temperature corrosion* (or oxidation) is the formation of an iron oxide layer with no chemical reaction and is beneficial to protect the die from damage.

The *chemical* (or electrochemical) *corrosion* is closely related with die soldering, and it could have also influence on thermal fatigue or erosion because of the changes of mechanical properties of the corroded die.

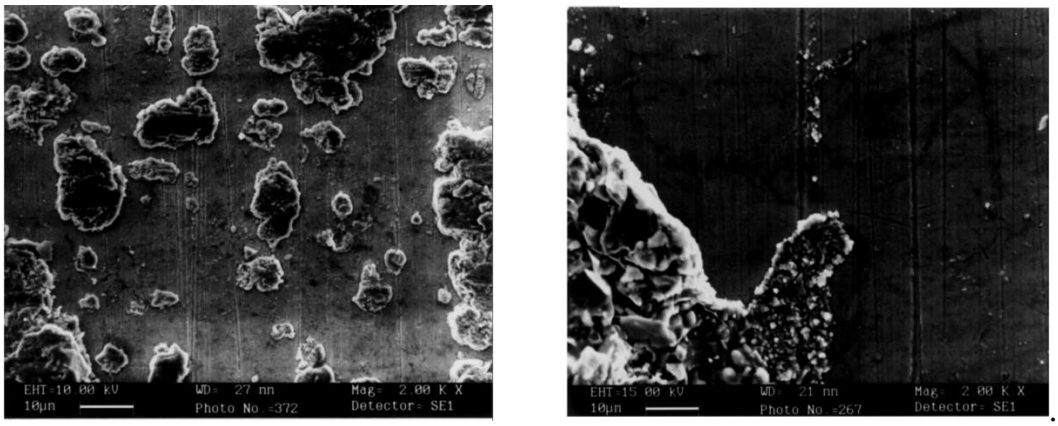

Fig. 2.8 SEM Fractographs taken from tested pins after 94 casting (a) and after 50 casting (b) [13].

Erosive wear is defined as the gradual physical removal of material from the die substrate with every liquid aluminium impingement. This takes place as a result of the motion of the aluminium melt.

Three basic erosion mechanisms have been proposed:

Liquid-impingement erosion that creates pits on the eroded sample surfaces, mostly affected by droplet or jet sizes and impact velocities, die material properties, die working temperature, angle of attack, amount of hard particles in the alloy melt (chemistry and impurities).

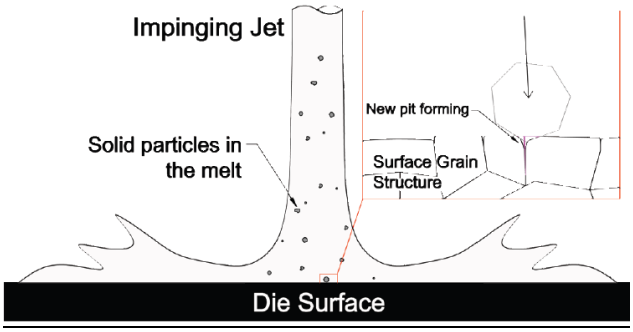

Fig 2.9 Representation of a high angle impinging jet of molten aluminum, and (Inset) pit formation through erosive wear and local deformation [14].

Cavitation, which is the result of the formation and collapse of bubbles (cavities) in a fluid due to local pressure fluctuations that comes from the flow characteristics and from casting metal vapor pressure.

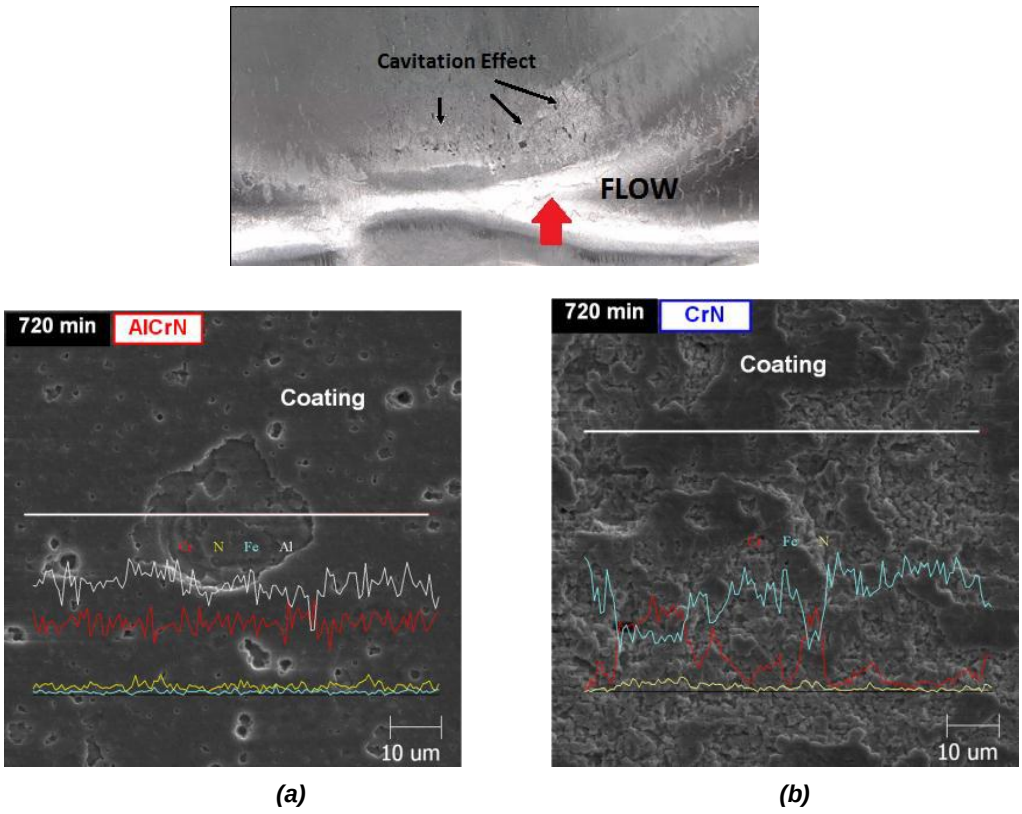

Fig 2.10 Wear mechanisms (a) AlCrN and (b) CrN after 720 minutes of cavitation erosion testing. [15].

And *solid erosion*, which is caused by the impact of solidified particles (Si particles, oxidation particles, and impurity or intermetallic particles) during filling.

Thermal fatigue:

As mentioned previously, the last type of damage described here, is considered the most affecting. It is called thermal fatigue because the material is subjected to real alternating cycles of heating and cooling phases, therefore the stresses to which is submitted the steel of the dies, can be considered fatigue, considered as the original meaning of the word.

Two are the different types of cracks that form due to these stresses *heat checks* and *corner cracks*. In addition to notice them on the die surface, their presence can be seen on the cast causing the unwanted marks (fins) on the casting surface.

Heat checks are normally observed on the flat die surface, where normally stress concentration does not take place. Because of the large thermal gradients, during heating, the die steel surface is under compression and it is in tension during cooling. This leads to die surface cracks, which are popularly known as 'heat checks'. The direction of cracking depends on which component of strain is dominant, but could exist a point in the die where there are two directions of maximum strain because of symmetry, thus the cracking can occur in both directions. This phenomenon deteriorates the surface but can also initiate crack propagation, leading to gross failure of the die.

An example of thermal fatigue cracks in a large transmission die is shown in figure 2.12 and 2.13.

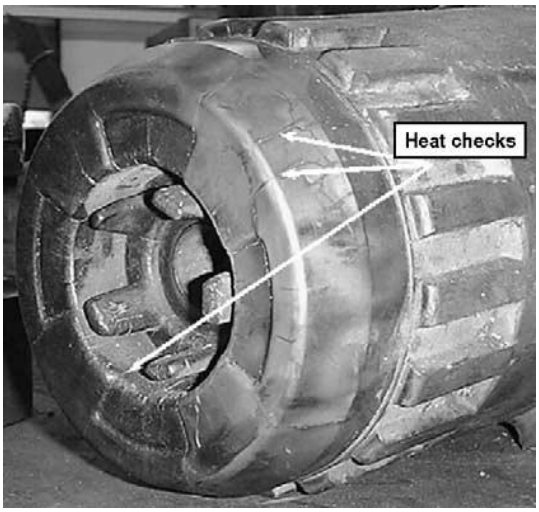

Fig 2.12 Large transmission die affected by heat checks. [17].

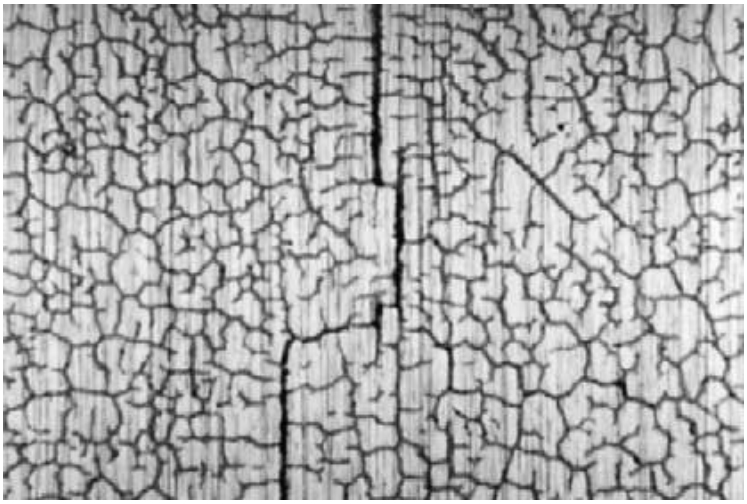

Fig 2.13 An example of heat checking. [17].

Corner cracks the type that, in most of the laboratory tests, are observed more often, may appear in corners that are more susceptible to this type of damage, in particular in presence of sharp edges or abrupt transitions. During the cyclic strain, cracks can appears in two different directions [17], perpendicular to the edge, because of cyclic strain in direction 1, and along the edge because of cyclic strain in direction 2 (fig 2.14 (a),(b)).

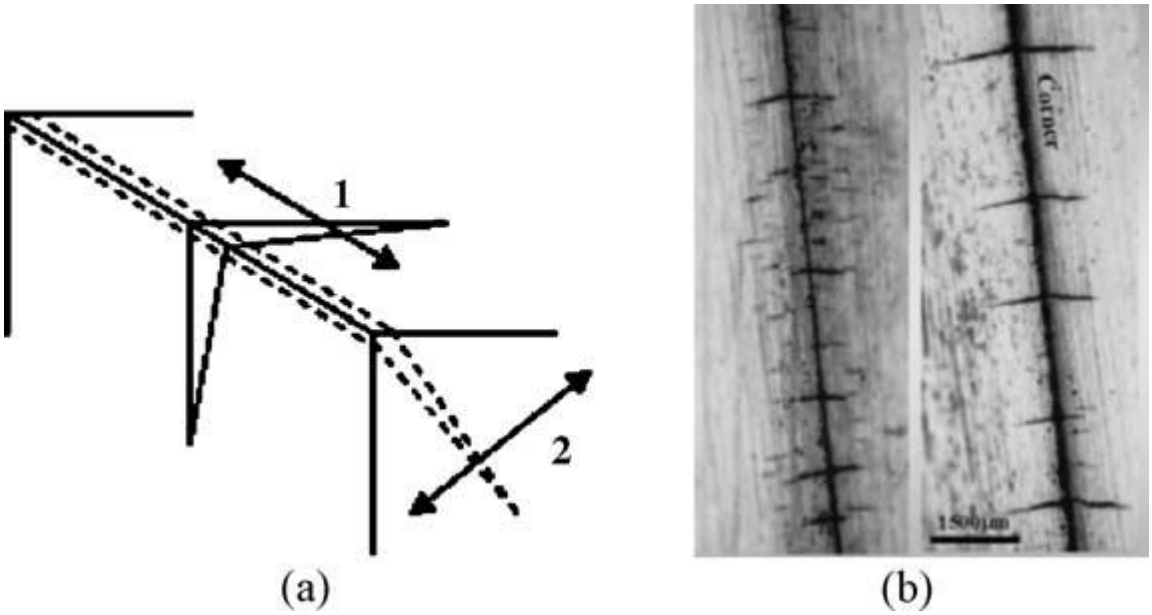

Fig 2.14 (a) Schematic of crack direction and stress direction and (b) corner cracking [17].

The damage due to thermal fatigue, again is considered the most critical, therefore will be analyzed and discussed in detail in the following chapters. As the subject of this analysis, will be detailed theoretical studies, from the literature, and also discussed some practical experiments for the analysis of this phenomenon.

Chapter 3:

WEAR MECHANISM IN HPDC DIES STUDIED:

3.1 THERMAL FATIGUE

Low cycle fatigue (LCF) has been described as a progressive failure phenomenon brought about by the cyclic application of strains that extends into the plastic range to produce failure in about 105 cycles or less. High cycle fatigue is caused when elastic strain exceeds plastic strain, resulting in a failure in more than 105 cycles. *Thermal fatigue* is categorized as low cycle fatigue. Often the strains produced during thermal cycling are not high, yet plastic range is reached due to decrease in yield strength at elevated temperature. It must be observed that for equal values of plastic strain range the number of cycles to failure is much less for thermally cycled specimen. This result shows that although the mechanical low cycle fatigue phenomenon and thermal low cycle fatigue phenomenon are very similar, the use of mechanical low cycle fatigue results for prediction of

thermal fatigue life must be undertaken with care as they significantly over-predict the cycle to failure [45].

Many methods have been used to evaluate the thermal fatigue resistance. Previous work used direct flame impingement on a surface. However, the combustion conditions could introduce an arbitrary environment, which may influence the cracking mechanism. High frequency heating and electrical resistance heating systems are generally expensive to construct and may not represent the rapid heating and cooling experienced in die casting. An effective way of simulating thermal fatigue conditions as well as die-molten metal contact is to use liquid metal bath heating followed by water quenching [45].

3.1.1 NATURE EXPLANATION OF THE FAILURE

The formation of thermal cracks can be divided into three stages: nucleation, initial growth, and proceeded crack growth which produces surface destruction or surface delamination of the degraded material [42].

The crack nucleation is associated with the accumulation of the local plastic strain in the surface material, which is typical for low cycle fatigue (LCF) [43]. This could in turn produce sharp surface corners i.e. weak regions in which crack nucleation could occur. The initial growth of the thermal fatigue cracks is facilitated by oxidation of the cracked surfaces by increasing the volume of the oxidized layer. Proceeded growth is facilitated by filling of cracks with cast material, by oxidation, and softening of the tool material due to tempering or aging of surface layer [43].

Nucleation and initial crack growth.

During the *hot* phase of die casting cycle a high *compressive* stresses are produced in the surface material. These stresses are additionally increased by a filling pressure of the die. Generally a compressive stresses are suppressing the crack nucleation and crack growth, which is favorable, if no local plastic deformation would occur. Instead a local plastic deformation occurs as a consequence of exceeding local material yield strength at working temperature, which is especially expressed on locations with notch effects, stress concentrators, sharp transitions and large changes in the mass of the tool.

During the *cold* phase of die casting cycle a high *tensile* stresses are produced on the surface material, which are increased by the plastic deformation of the surface material. These stresses exceed the local yield strength and sometimes ultimate tensile strength of the surface material at working temperature. At cyclic loading (repetition of these loads) a low cycle fatigue occurs, which produces nucleation and initial crack growth.

Crack growth promoted by crack oxidation.

The crack growth is facilitated by *oxidation* of the working surface and surface of the crack (Fig. 3.1a). Iron atoms from the steel surface layer diffuse to the surface and to the oxygen. Vacancies in the steel surface layer are filled with alloying elements (Ni and Mo) (Fig. 3.1b). On the surface of tools and cracks a layer of iron oxides is generally formed, due to the presence of air oxygen and high temperature environment. Additionally oxides of aluminium and silicon are present, which are the result of reaction between air oxygen and aluminium alloy. At the oxide side of the boundary between the oxide layer and hot work tool steel a chromium oxides are laid (Fig. 3.1b).

The negative influence of the oxide layer is its low thermal expansion, bigger volume and fragility. The presence of nitrogen and aluminium alloy inside the cracks, increases the tension at the crack tip (during the cold phase of the cycle), causing the growth of cracks (Fig. 3.1c)

Tensile stresses during cold phase of the cycle, causes local crack formation in the oxide layer and in the crack filling (Fig. 3.1c). This causes crack opening due to fragility of oxide layer and the difference in thermal expansion between the oxide layer and subsurface steel. These cracks act as the channels for introducing the aluminium alloy and air oxygen into the crack. Air oxygen in high temperature environment is causing the oxidation of the crack [42].

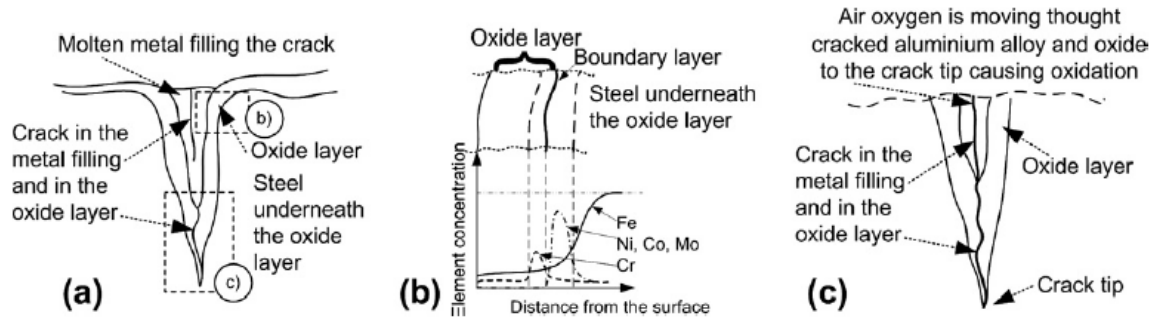

Fig 3.1 Mechanism of crack growth promoted by oxidation [42].

Crack growth promoted by thermal softening

During aluminium die-casting process, the dies operate at temperatures around secondary hardening or even at higher temperatures. Under such operating conditions, almost all steels present a general softening trend. In some conditions a hardening is observed in early cycling, but very soon softening prevails. Three softening stages are observed: rapid softening controlled by a dislocation density reduction, a quasi-stationary softening governed by carbide evolution, and a drastic stress reduction, due to gross cracking. Depending on the type of steel, a strain rate and exposure time also influence on softening. The undesired softening also aggravates material yield strength. This in turn causes rapid progression of the crack length up to the layer of unaffected material [42].

From an accurate measurement of the die surface temperature, the thermal fluctuations could be used to determine the stress fluctuations on the die surface. The stress fluctuations could then be applied to a fatigue prediction model, the results of which could be compared to actual die surface damage [46].

A common approach for estimating the *peak temperature* of the die surface is proposed by Hattel [46]. The theory presumes that the molten aluminium and the die can be treated as semi-infinite bodies and that there is perfect contact between the two, thus neglecting thermal resistance at the interface.

A consequence of the first assumption is that the predicted temperature is independent of time, which clearly it is not. However, the method provides a reasonable estimation of the die surface temperature at the instant in which the molten aluminium first makes contact. This temperature approximates the peak cycle temperature. Figure 3.2 illustrates the

predicted temperature variation between domain 1, representing the molten aluminium, and domain 2, representing the die.

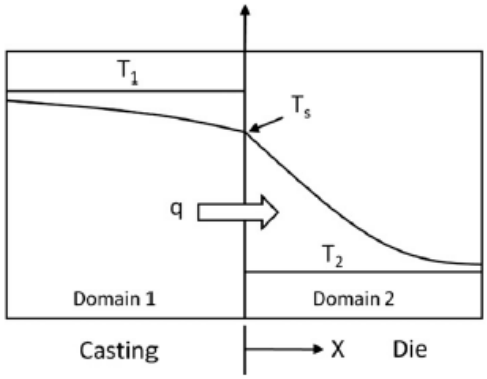

Fig 3.2 Analytical solution for the two domains, i.e. the casting and the die [46].

The peak temperature calculated at the interface between the two domains is the *Riemann temperature* T_S given by [46]:

$$T_S = \frac{\beta_1 T_1 + \beta_2 T_2}{\beta_1 + \beta_2} \qquad 3.1$$

Where $\beta = \sqrt{k\rho C_\rho}$ is the mould cooling capacity, k is the thermal conductivity, ρ is the density, C_ρ is the specific heat capacity.

Considering the first cycle, that means when the die is started from cold (23°C), the peak measured die surface temperature is about equal to the corresponding Riemann temperature. For other cycles, however, the Riemann temperature underestimated the peak cycle temperature. Most of the thermal fatigue theories are based on this case, in which a bar is fixed at its ends between two immovable plates, so that the length of the bar must remain constant. This bar is assumed to be gradually cooled and heated. In this case, cracking will take place only when there is plastic yielding in both cooling and heating cycles, which leads to accumulation of plastic strain in every cycle. The constraint to thermal expansion is due to thermal gradient between surface and core of material and therefore, the thermal strain does not completely convert into mechanical stress. When the surface of the die is heated, a part of thermal strain converts into mechanical stress because of thermal gradient, and the remaining appears on the surface as it is.

3.1.2 FACTORS AFFECTING THERMAL FATIGUE AND HIGH TEMPERATURE MECHANICAL FATIGUE

During the study of thermal fatigue it showed that there are some parameters that influence the effect, increasing or decreasing, the impact on the materials. They can be divided into categories depending on what element of the analysis are going to affect.

The most important are of course the material properties: thermal expansion coefficient, thermal conductivity, yield stress, ultimate strain, Young modulus, resistance to tempering. Also during the experimental part it was highlighted how fundamental and how they can change the progress of the test. For example due to the repeated temperature fluctuations on the die, it must be dimensionally stable, have high hot yield strength, good resistance to high temperature softening and good thermal conductivity [46]. Furthermore higher thermal conductivity of steels enables quicker transmission of heat from the die surface to the core of the die. This lowers the thermal gradients i.e. thermal stresses and has the beneficial influence on the prolongation of the tool lifetime[42]. The negative influence of the oxide layer is its low thermal expansion between the oxide layer and subsurface steel, the bigger volume and fragility.
The extreme thermal fatigue resistance of materials like *Anviloy1150*, *Mo-785* results from the combination of high thermal conductivity, small thermal expansion, and very high melting point temperature (this will result in very high softening resistance at the tested temperature)[44].

The other category of affecting parameters is related to the die surface temperature and gradient during cycle: depends on casting temperature, cooling channels temperature, spraying, mould design.

Finally Stress concentrators: due to the mould cavity geometry (corners) as discussed, but also at microscopic level (surface finishing) and also residual stresses.

Regarding High Temperature Fatigue, apart from the parameters that affect fatigue such as the stress, material properties, and stress concentrators it is affected by temperature.
In a HTMF test temperature and strain change simultaneously and independently. The changes in strain arise from a combination of thermal and mechanical effects. Since the

thermal strains are not associated with loading, it is customary to subtract the thermal strain to give the mechanical strain. It is also possible to define various paths in terms of temperature and strain[50].

A schematic of the stress/strain response in a so-called bi-thermal is shown in Figure 3.3 in which the total (mechanical + thermal) strain is shown for purpose of clarity.

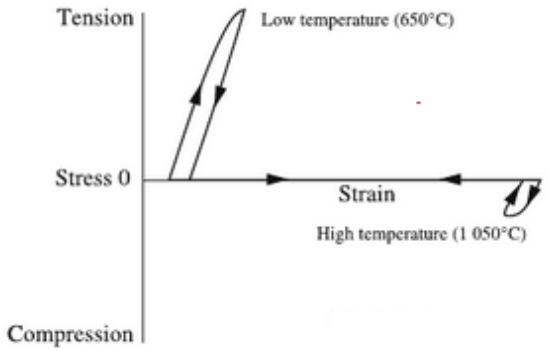

Fig 3.3 Illustration of a Thermo-mechanical cycle [50].

According to literature the effects of high temperature in properties that can affect fatigue are the following:

- The tensile strength is reduced but elongation increases.
- Young modulus reduced: Less stress for the same deformation. It has to be kept in mind that Low Cycle Fatigue (what concerns this study) is ruled by deformation and not by stress like in High Cycle Fatigue.
- Oxidation: thermal fatigue is generated by an intergranular cracking in the surface. Oxidation is an intergranular effect as well. Its influence increases with time.
  Clearly oxides that form at high temperatures are easily cracked by the slip bands that form at the lower temperatures.
- Creep: Viscous behaviour at high temperature. Deformation increases for a constant stress Fatigue resistance reduction and fatigue limit disappears. Creep temperature for these steels is around 580ºC, not being probably an influencing effect.

3.1.3 EXISTING TEST PROCEDURES AND PROTOCOLS

Several authors have conducted research regarding the behavior of a specimen subject to thermal fatigue. The starting point of any study are definitely the *E606* and *E2368* standards [1, 2], which describe both the analysis for strain controlled thermomechanical fatigue testing, and for normal strain-controlled fatigue testing. Using these starting guidelines some studies have been developed using different test rig to evaluate the effect of stress caused by both mechanical and thermal stresses.

One of the most innovative work on how to test an element subjected to thermal stresses, and which describes the development of a test rig has been developed by some authors in the University of Ljubljana [40].

The laboratory test rig (equipment) for their evaluation must be capable of carrying out such tests at various temperatures and have the capability, at the same testing temperature, to generate various temperature (stress) fields in order to better evaluate the usage of materials for a specific application. The test rig developed enables generation of high thermal stress with well-defined thermal boundary conditions which allows the study of the temperature and thermal stress distribution in order to better evaluate the thermal shock or fatigue resistance of the tested material[40].

The main idea was that the specimens would be rapidly heated to the maximum holding temperature and then the surface would be quenched with water. It was estimated that the cracks would form earlier than in 1000 cycles (for tool steel); this would shorten the testing time of a given specimen. This advantage becomes crucial in the analysis of cyclical stress, because they may need periods of very long experimentation.

Circular and hollow shaped specimen were applied for testing, using a thermocouple inside welded system. The outer testing part of the specimen was placed in a cooling chamber (Fig 3.4). The cooling and emptying process was optimized by a pair of magnetic computer controlled valves. One valve controlled water quench and the other controlled the air compression to empty cooling chamber.

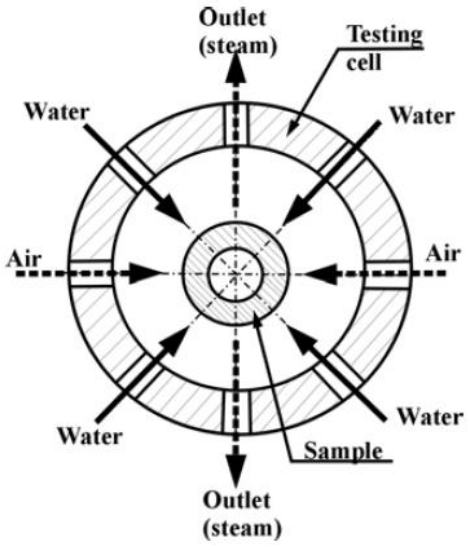

Fig 3.4 The cooling chamber with water quenched sample [40].

The setup of test rig, without working jaws is shown in Figure 3.5(a) and its positioning in the load cell is shown in Figure 3.5(b).

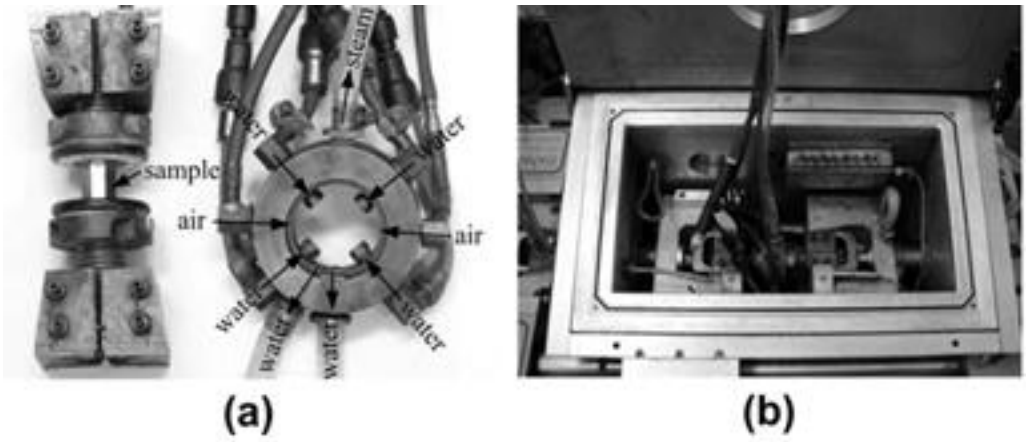

Fig 3.5 (a) Testing device with specimen, (b) Inserted test rig in the load cell [40].

At the end it was showed that the test was efficient and repeatable. In particular with a combination of simultaneously controlled cooling and resistance heating of the specimen, greater thermal gradients in relatively thin specimen surface layer were achieved, while the remaining depth of the specimen kept approximately the same value. This reduced the number of cycles needed for crack nucleation and resulted in faster crack growth.

With the possibility of generation various thermal gradient, the test can also simulate various thermal loading conditions in an applicative environment.

If we go more specifically to evaluate the procedures developed in the analysis of the damage in case of die-casting dies it is possible to refer to the analysis of the *D. Klobc˘ar, Kosec, B. Kosec, J. Tušek* on damage of dies caused by thermo fatigue cracking [41, 42].

In these works it was tried to develop an optimal geometry for the specimens used in thermal fatigue analysis, the development of the optimized test specimen geometry is represented (Fig. 3.6).

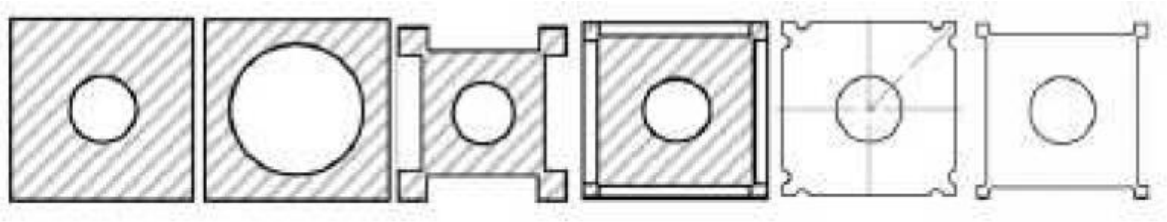

Fig 3.6 Evolution of the specimen geometry through the optimal one [41].

The aim of the *optimized geometry* is to accelerate thermal fatigue testing on immersion test apparatus. The immersion test apparatus [42] is shown in Figure 3.7 (a). It enables a controlled thermal fatigue testing at conditions similar to aluminium alloy die-casting. Thermal fatigue loading is achieved by cyclic movement of specimens between baths of molten aluminium thought the air into the bath of water-based lubricant. Nevertheless, the test specimens are not subjected to pressure and aluminium flows, unlike the die during die-casting.

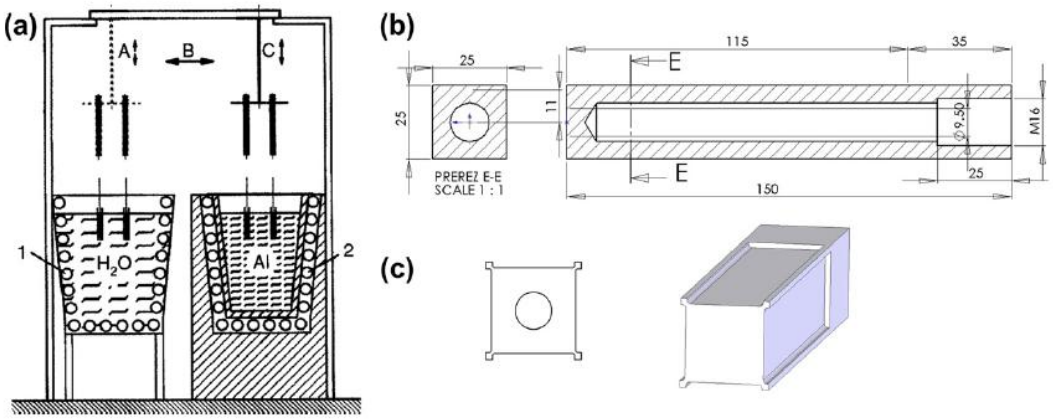

Fig 3.7 (a) Schematic of immersion test apparatus, (b) schematic of classic thermal fatigue test specimen, and (c) cross section of optimal test specimen [42].

The duration of thermal fatigue testing cycle is 21 s. The test specimens must be immersed in water-based lubricant which prevents sticking of aluminium to the test specimens and generates thermal gradients in the test specimen during cooling. Then specimens must be moved thought the air at lower temperature into the bath of molten aluminium alloy at around 700°C. After few second of immersion in this bath, the specimens must be air cooled for a brief time while moving to the bath of water-based lubricant. The test specimens are internally constantly cooled with water.

Figure 3.7(b) shows 150 mm long classical test specimen with 9.5 mm axial hole 140 mm deep and its cross section. A tube, connected to the cooling circuit, must be inserted into the specimen hole. Cooling water at temperature 20°C is brought to the bottom of the specimen and flows upwards between the tube and the specimens inner wall to cool the specimen.

This effect of cooling produces high temperature gradients between outer and inner surface of the specimen. Temperature measurement can be performed using thermocouples, which are inserted to diameter holes, drilled to the different depths (Figure 3.8). These holes are positioned at edges of samples 1, 3 and 4 mm from the specimen edge [43].

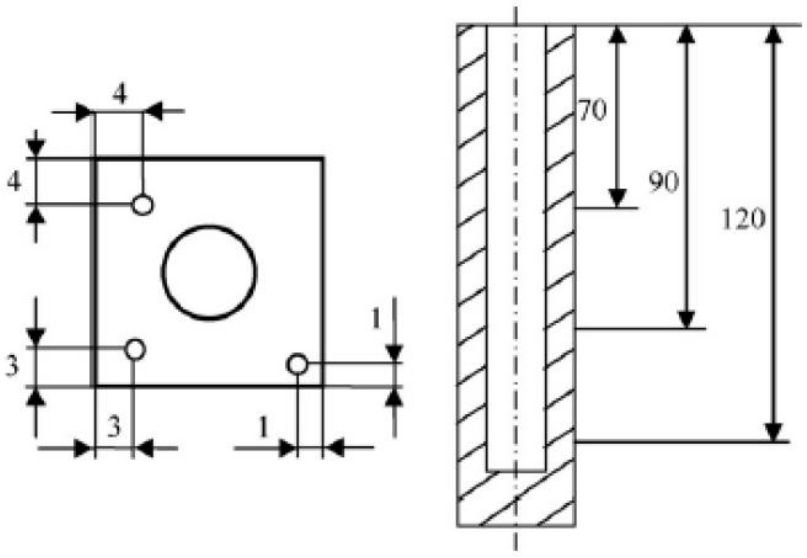

Fig 3.8 Reference positions and depths of holes in the non-optimized geometry specimen for the thermocouples insertion [43].

The test specimens are subjected to a series of thermal fatigue cycles [42]. The edges of test specimens should be visually inspected every n cycles, for example 4000 cycles, in order to find surface cracks.

Thermal stresses during the immersion test are the consequence of thermal gradients between the surface and the center of the test specimen. The highest thermal gradients will be obtained right after immersion of test samples into a hot aluminium alloy or a cold water-based emulsion. After a few seconds immersion, the thermal conditions stabilize, i.e. thermal gradients drop and consequently also the thermal stresses. During the immersion of samples in a hot aluminium alloy the surface stresses will be *compressive,* while during the immersion in cold water- based emulsion the surface stresses will become *tensile*.

For what concerns the outcomes of the immersion test, temperature transients at different locations of test specimen can be measured and used in computation of transient stresses performed by finite elements. After completion of a certain number of cycles, the specimen edge surfaces can be examined visually.

Other analyses after the immersion test are the observation of the hardness profile in direction from edge to the center of the specimen. Moreover, two concepts are used for the evaluation of thermal fatigue resistance of die materials, i.e. total crack area and average maximum crack length [44].

Total crack area takes into account of all cracks contribution. Therefore, if a die's total crack area reaches a certain limit, the whole die fails.

The area of a crack is defined by the square of crack length and the total crack area is the multiplication of the areas of all cracks.

Average maximum crack length is based on the assumption that if a single crack is big enough, the whole die is unusable. It represents the average length of the longest crack of each of four corners.

In conclusion, the developed test for the analysis of the thermal fatigue appear to be all very similar, the parameters that can change are the size and geometry of the specimen, the cooling and heating system or the type of bath. In some tests the specimen can be placed in rotation on its axis to strip the adhered metal from the specimen surface[45].

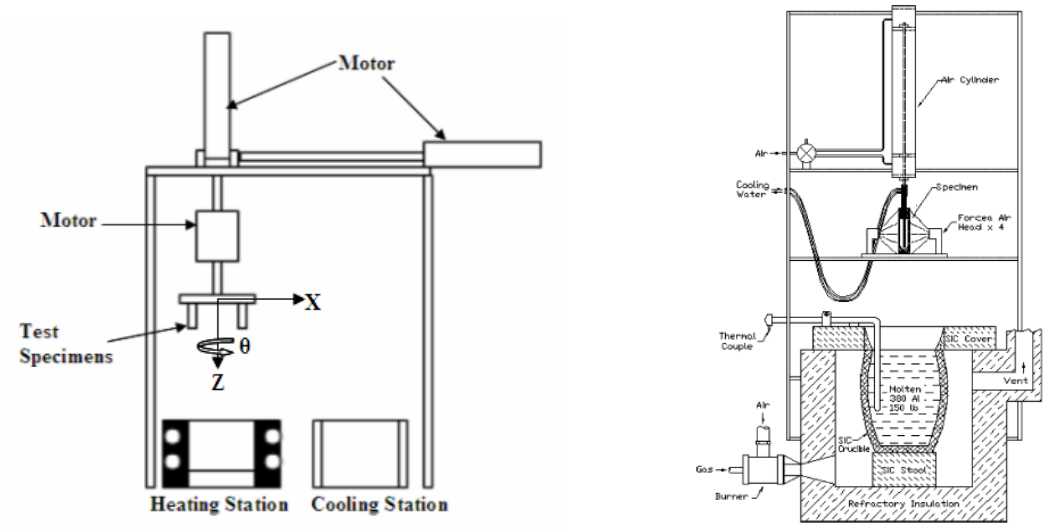

Fig 3.9 Different Thermal fatigue testing equipment and specimen [45, 44].

3.1.4 SOME RESULTS FROM BIBLIOGRAPHY

The concepts seen before are used as guidelines to interpreted the results and so the behavior of the material trough thermal fatigue. The test was performed on *pins* of different material positioned in the gate runner inside the die. Usually inside the dies not only exists a phenomenon of damage, as described in the introduction chapter, it is possible to have to study the effect of two or more phenomena that act simultaneously. For example, some studies have demonstrated there is no intrinsic relationship between thermal fatigue, soldering, and washout, as shown in the graph 3.1, result from a work of analysis of both damage and their behavior for different material and [44].

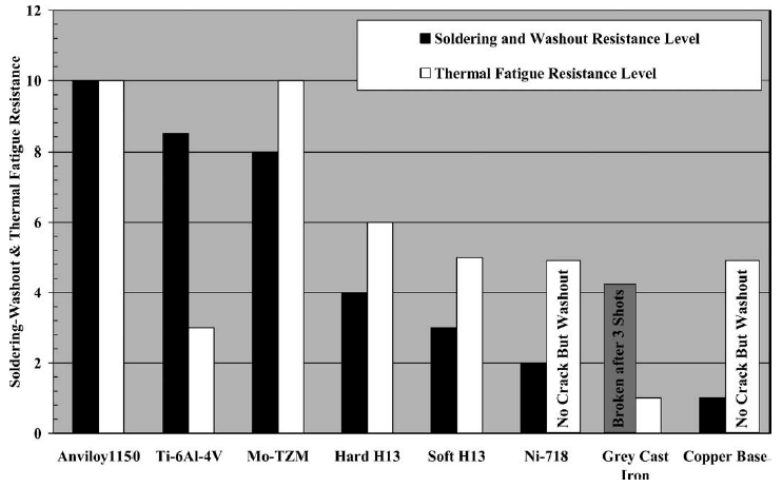

Graph. 3.1 Soldering-washout and thermal fatigue resistance ranking (10: best; 1: worst) [44].

Washout is a long-term process and obvious washout is not likely to occur before the formation of the soldering because the damage of erosion-enhanced corrosion mainly caused by the diffusion of atoms needs time. Thermal fatigue will lead to cracking on the die surface. The crack will increase the roughness of the die surface. The increased surface roughness will increase the tendency of soldering and washout[44].

If it considers only the case of thermal fatigue phenomenon, studied using an immersion test it is result, through an FE analysis, that the highest temperature gradients between outer and inner surface are reached shortly after immersing the specimen in the molten aluminium. One shall expect that the thermal fatigue cracks will appear at the specimen surface due to higher temperature and due to the material strength decrease at higher temperatures. When the specimen outer surface is at higher temperature than the core material, the stresses at the outer surface are compressive, and vice versa when the outer surface temperature is lower than that of core material [43], as shown in graphic 3.2.

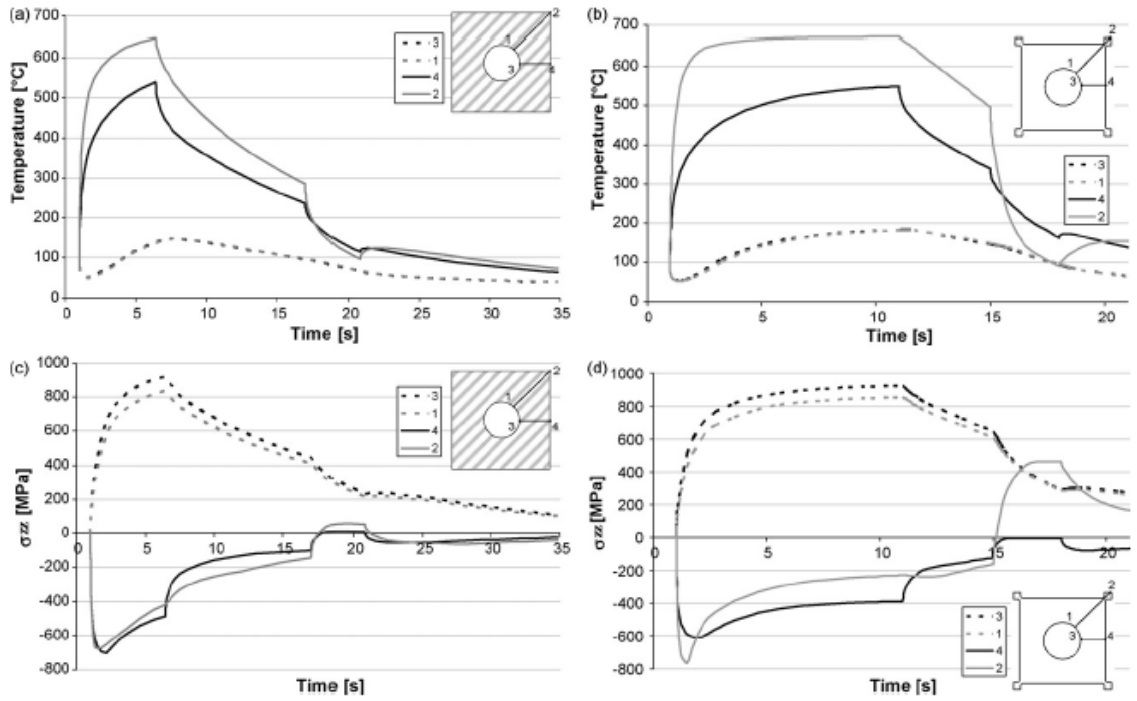

Graph. 3.2 The results of FE computations: (a) temperature and (b) axial stress at different locations of test specimen throughout the cycle [43].

Also in this work, showed that the tool steel, in particular H13 achieved good results demonstrating small cracks, small crack density, and small hardness drop. H13 steel, heat treated without protective atmosphere, experienced small number of very long cracks and substantial hardness drop. The crack length equals the depth of decarburized layer. H11 steel experienced slightly longer cracks and higher hardness drop than H13. At high pressure die-casting tool life can be increased by using high strength materials, with high thermal stability of mechanical properties at operating temperatures.

Tools for die casting of non-ferrous metals usually fail due to thermal fatigue cracking. At steels with lower yield strength and lower hardness a smaller number of longer cracks appear. A die casting die life can be increased with the use of tougher, harder and ductile materials, which must be resistant to tempering or aging during usage[42].

When the die is stopped, heat rapidly lost. Therefore, to slow the rate of heat loss from the die, internal water cooling should be switched off when the die is stopped for a short period of time. The stress analysis which compared the standard to the interrupted die cycle indicates that frequently stopping and cooling the die to room temperature, will result in more widespread and deeper cracking on the die surface [46].

Finally, One of the important decisions in numerical modeling of thermal fatigue cracking is to decide on which criterion should be used to model cracking. Some of the researchers have used elastic and plastic strains to predict thermal fatigue life, whereas others consider residual stress as important[45].

From the results obtained in the different studies analyzed, it is possible giving guidelines, based the theory that the in-service tool life could be prolonged with decrease of thermal gradients, i.e. loading stresses during die-casting, for an optimal design of the dies.

There are several ways to achieve this goal [41]:

- Designing die geometry, sharp corners, notches, and quick changes in toughness should be avoid and all transitions should be made with the biggest radius possible;
- During die manufacturing, a great care must be taken to enter the least amount of residual stresses;
- The die must be evenly cooled down by additional cooling channels to prevent local overheating, which could worsen the mechanical properties of die material;
- The die must be preheated to an optimum temperature in order to decrease temperature gradients and consequently stresses to minimum;
- The material of the die should be dimensionally stable, have high hot yield strength, good resistance to high temperature softening and good thermal conductivity [46];
- The temperature of molten alloy should be lowered;
- The injection velocities should be lowered to decrease temperature gradients and erosion of surface material.

3.2 EROSION

One of the objectives of this study is to investigate erosive wear on die surfaces where high molten metal flow velocities exist and to develop erosive wear models that quantify the effect of process parameters on erosive wear in die casting dies. This exposition outlines the details and discusses preliminary results of this experimental-numerical investigation of the effect of process parameters on erosive wear in die casting.

It is important to know the results obtained up to it by following the literature. Several authors have attempted in the analysis of the damage caused by erosion, with excellent results relating in particular to the production by HPDC. Wear phenomena are widely observed in H-series [52] die steel the most commonly used die material due to this severe mechanical and thermal loading. It was found that one of the major wear mechanisms leading to premature die failure is erosion or washout, that is a result of the high velocities with which the molten metal impinges parts of the die cavity causing steel to be washed away with the melt. Most die casting dies have complicated geometrical features, such as cores, pins, ribs, and corners, which are especially prone to erosive wear. This erosive wear reduces the ability of the die to maintain dimensional tolerances and often requires rebuilding of regions of the die that have suffered extensive washout.

3.2.1 DIFFERENT EROSION WEAR MECHANISMS

A few publications have outlined the likely causes of erosion in die casting dies from empirical observations. *Barton* [32], for example, classified erosive wear in die casting dies as being of four significant types:

Gate erosion

After a die has been in service for a long time, a gate is larger than it was initially. As expected, this change is most noticeable with castings that have long shallow gates. *Barton* attributed gate erosion to the repeated abrasion and regeneration of the amorphous oxide film, which is created on the die whenever it is in contact with the molten metal. This action takes place only at the gate because it is only here that the metal velocity is

sufficient to allow fluid metal to flow in contact with the die surface. Furthermore Industrial experience reported in the past has indicated that core pins or die inserts exposed to the liquid metal attack in front of the gates exhibit the highest level of erosive wear and soldering.

Washout

This particular phenomenon can be also called as solid particle erosion, in fact, take place in system subjected to solid material flow. It is a most common type of erosion that occurs when a metal stream or jet impinges directly on the cavity surface (e.g. a core or pin) at a short distance from the gate. Barton surmised that washout was primarily caused by the localized heating that occurs due to impinging jets. This causes severe localized thermal stresses, which result in a shearing of the oxide layer on the die thereby causing erosion. Washout is the most common type of die erosion and also the most significant in relation to die performance.

Cavitation erosion

At high speeds common in die casting, cavitation bubbles are generated in the flow [33, 34]. When they collapse at the die surface, large forces are generated and produce die erosion. *Davis and Murray* [35] reported that cavitation was a common cause of erosion in the die casting of zinc alloys because of the high gate velocities (40 to 60 m/s) required to produce high quality castings. It is, however, not as significant in aluminum casting because of lower velocities. Cavitation was observed to occur, depending on the ration between the film thickness and the sliding speed[36]. The better cavitation erosion behavior of the quenched and tempered steel sample in relation to the annealed sample could be attributed to the higher mechanical properties of tempered martensite. Another important mechanical property for cavitation erosion resistance is the resilience of the material. In general, it is observed that high resilience leads to high cavitation erosion resistance [38].

Erosion caused by flow separation

Another cause of erosive wear, reported by *Smith* [37], was by flow separation at some point where due to a change in direction the molten metal separates from the die surface.

This type of erosion does not, however, appear to be very common although different theories have been suggested to explain the mechanisms involved [32, 37].

3.2.2 EXISTING TEST PROCEDURES AND PROTOCOLS

To describe the most appropriate conditions for the effect of erosion testing of building materials, you can refer directly to the G76 rules [6]. This type of standard describes in detail what are the key points to be taken into account during analysis of a material which has damage caused by erosion. Allowing through this analysis to create a predictive method by knowing the factors to which the system is subjected.

In particular the method described in the *G76* standard covers the determination of material loss by gas-entrained solid particle impingement erosion with jet-nozzle type erosion equipment. This test method may be used in the laboratory to measure the solid particle erosion of different materials and has been used as a screening test for ranking solid particle erosion rates of materials in simulated service environments (24, 25). Actual erosion service involves particle sizes, velocities, attack angles, environments, etc., that will vary over a wide range. Hence, any single laboratory test may not be sufficient to evaluate expected service performance. The test method describes one well characterized procedure for solid particle impingement erosion measurement for which interlaboratory test results are available.

One of the tests conducted that is very reliable, considering the case in the present Treaty processed, that is, the damage of the steels used for the dies, is done by *K. Venkatesan and R. Shivpuri* called "*Experimental and Numerical Investigation of the Effect of Process Parameters on the Erosive Wear of Die Casting Dies*" [19].
In this work, in order to evaluate different materials or surface coatings, "a multiple-pin flat plate die" with six test pins was designed and fabricated for the experiments as shown in Fig. 3.10.

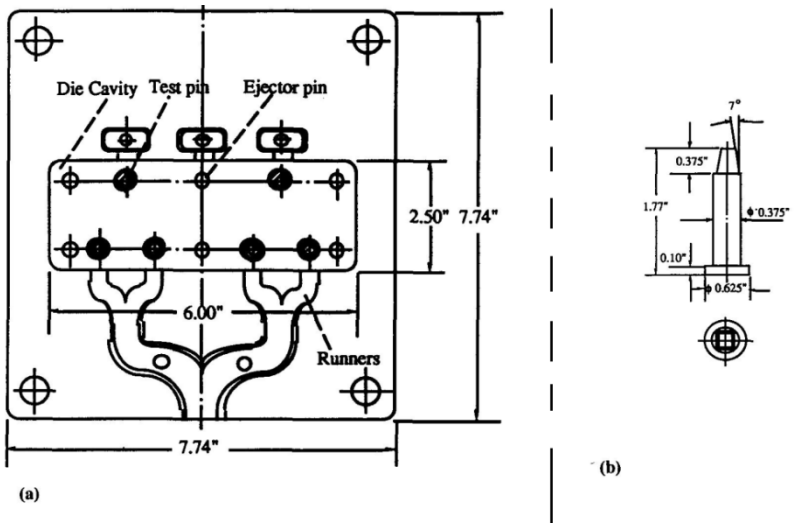

Fig 3.10 Dimensioned drawing of the multiple pin die [19].

Only the top edge of the pin shown in Fig. 3.10(b) is within the die cavity and is exposed to the molten metal. One of the reasons for choosing the multiple-pin design was the ease of assembly, disassembly, and measurement. In addition, a multiple-pin design allows the testing of several pins simultaneously thus providing multiple test sites for comparative evaluations.

The flat cavity (plate) design also allows for the study of the effect of filling and solidification on die wear because of its geometrical simplicity. In addition, the test pins can be rotated or their shape changed, permitting the study of the effect of the angle of attack and surface geometry on wear.

Because wear is a gradual loss of material, tests could be very long term (>100,000 shots) and costly. In order to accelerate the wear effects and to allow for quantifiable erosive wear in a reasonable number of shots, an operating procedure was developed to provide an extreme environment on the test pin so that quantifiable wear loss can occur in a reasonable number of shots. One of the operating conditions chosen to accelerate the erosive wear rate is the use o f a pyramidal test pin design with sharp comers (Fig. 3.10). These sharp pin comers will easily erode, solder, and exhibit heat checking along the edge within a reasonable time frame. To further accelerate the erosive wear, a hypereutectic aluminum alloy, A390, with a high silicon content was used for the tests. Furthermore, because the silicon is very hard, A390 is more aggressive than other aluminum die casting alloys, which results in a higher abrasive wear rate for the die surface.

Two major performance measurements selected for wear quantification were the pin weight loss and the edge profile change. The profiles of the pin edges facing the gate were measured by a comparator using 20x magnification and are used in this study to quantify the effects of process parameters.

Two basic orientations of the test pins in the die were tested. In this design, the pin orientation is such that the molten metal from the gate first strikes the edge of the pin. This is clear in Fig. 3.11, which shows a schematic of this pin layout in the die cavity and the pin geometry, indicating regions of the pin most prone to washout.

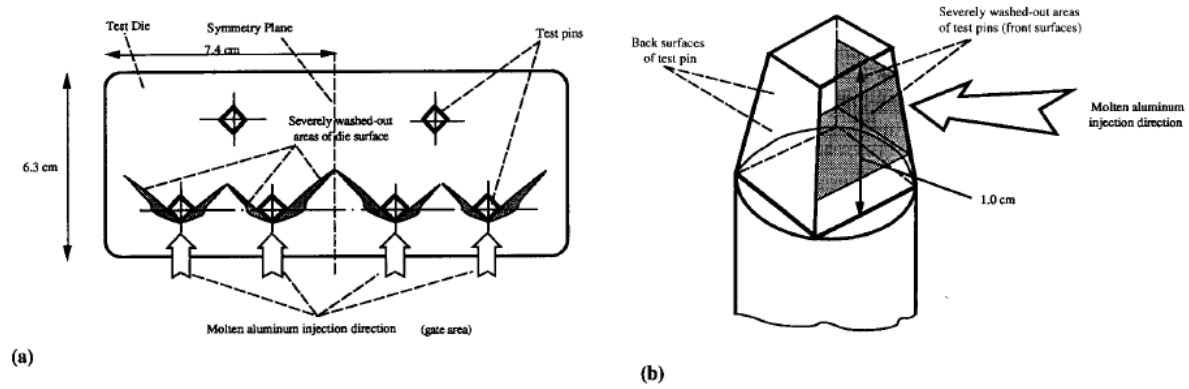

Fig 3.11 Schematic of a cross section of the die geometry of the original pin layout indicating regions of the pin (b) most prone to washout [19].

To evaluate the effect of die geometrical features (specifically the effect of impact angle of the molten metal) on die erosive wear, *Chu and Shivpuri* [26] and *Venkatesan and Shivpuri* used a modified design and layout of pins in the six pin erosive test die, as shown in Fig. 3.12a.

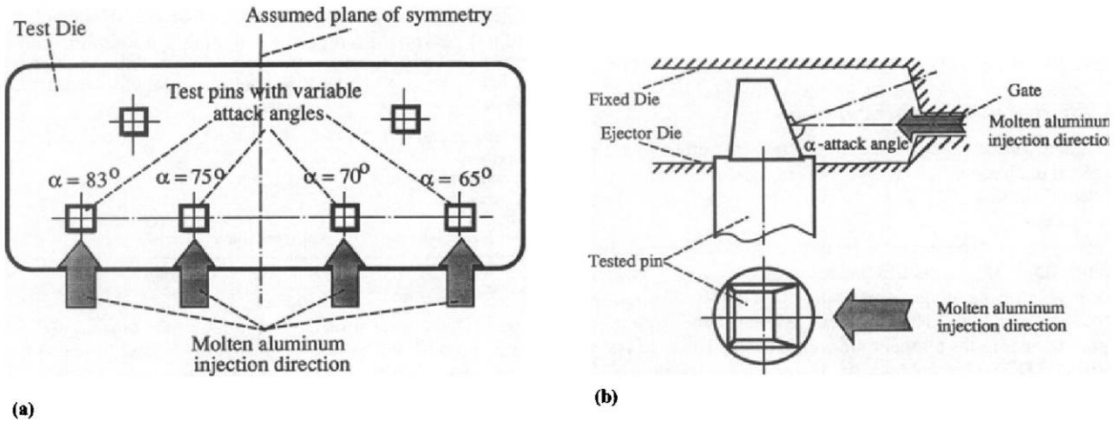

Fig 3.12 Schematic of the orientation of test pins in the test die for the angle of attack layout. The location of pins with differing front edge angle α in the die is shown in(a)

Unlike the original pin layout, the side of the pin (instead of an edge) is directly in front of the molten metal from the gate. The front edge angles for which experiments have been performed at present are 83, 75, 70, and 65 degrees as shown in Fig. 3.12(a). Thus the angle at which the molten metal impinges on the pin is different for each pin thereby providing a means to evaluate the effect of angle of attack under similar experimental conditions.

Other types of tests have been studied by several authors, always with the same objective of creating a model that could relate the erosion rate with the parameters of the working system. The types of tests can be divided mainly into two categories, those in which the eroding is in the form of solid particles, and those in which the eroding is a liquid material flow, also called liquid impingement test.

For the first category, solid particles test, the authors *J.R. Laguna-Camacho, L.A. Cruz-Mendoza, J.C. Anzelmetti-Zaragoza, A. Marquina-Chávez, M. Vite-Torres, J. Martínez-Trinida,* in *"Solid particle erosion on coatings employed to protect die casting molds"* [27] rely on the standard initially expressed by conducting a standard test with a very similar to the one described in the G76 instrumentation. In this study, the performance of coatings that were subjected to solid particle erosion tests was evaluated. These coatings can be used to protect die casting dies. The main interest of this research project was to find possible alternatives to increase the wear resistance of these mechanical components.

An erosion test rig standard was designed and built to perform the tests (Fig 3.13). The abrasive particle used was angular silicon carbide (SiC) with a particle size of 420–450 µm. Tests were carried out using different impact angles (30°, 45°, 60◦ and 90°) with a particle velocity of 24±2 m/s and an abrasive flow rate of 0.7±0.5 g/min. The particle velocity and the abrasive flow rate were low in all of the tests to reduce the interaction between the incident particles and the rebounding particles in the system.

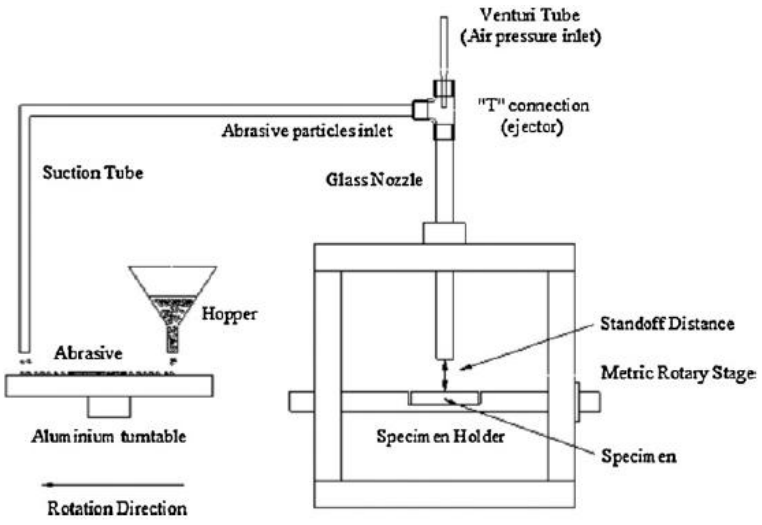

Fig 3.13 Schematic diagram of the erosion rig developed [27].

Four types of materials were analyzed, two with coating and two without. In order to understand which is the rate difference between the treated material and untreated one. The wear mechanisms identified were pitting and ploughing action at low impact angles ($\alpha \leq 45°$) due to sliding component commonly observed at these incident angles whereas bigger craters, radial cracks and a more roughened surfaces were seen at angles near or at 90°. In addition, it was observed that the damaged area was extended in all of the cases at 30° and 45° reducing considerably at 60° and 90°. The wear scars were characterized by an elliptical shape at 30° and 45°, which is a characteristic feature when the specimen are impacted at low-incident angles ($\alpha \leq 45°$) whereas a roughly circular was seen at 60° and 90°.

Another work developed study on erosion caused by solid particles it was taken on by the authors *A. Mohammed, M.B. Marshall, R. Lewis*, in "*Development of a Method for Assessing Erosive Wear Damage on Dies used in Aluminium Casting*"[28].

The feature of this work was investigate the erosion effects of the aluminium particles in both flat and cylindrical specimens made from H13 steel (typically used for die manufacture). Also unlike the previous one, the flow of eroding, was composed of the aluminum balls (3mm diameter – based on aluminium droplet size calculations), and not an aluminum powder flow.

It was used a standard test rig (Fig. 3.14) where the frame was placed in a shot blaster which was used to fire aluminium balls at the specimens.

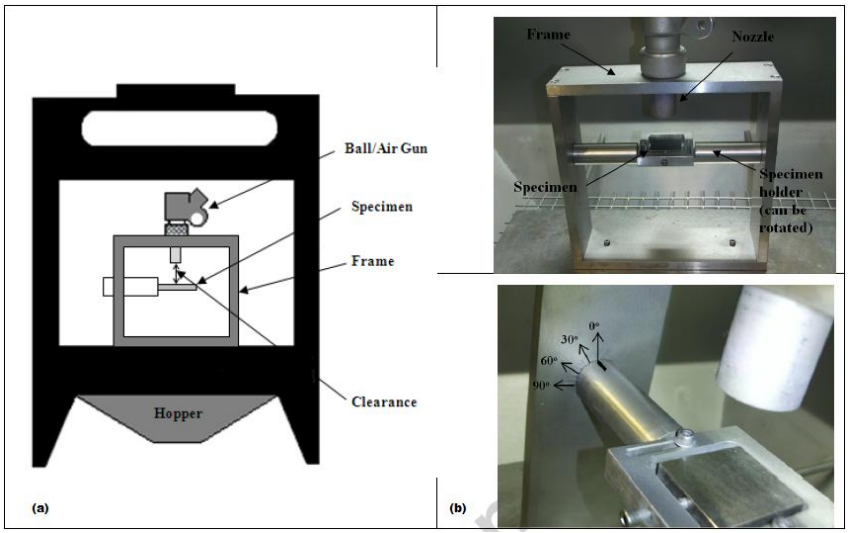

Fig 3.14 Test Arrangement: (a) Schematic of Overall Test Set-up (with cylindrical specimen mounted); (b) Test Surface Mounting Frame [28].

Different velocities were used and the it was designed for be rotated to set different erodent impact angles.

Flat specimens were tested at different angles and cylindrical specimens were tested central to the flow of aluminium and in an eccentric position to cover a range of possible aluminium/die impact scenarios. It was concluded that the test method was a suitable approach to use.

Initial studies using the rig indicated that with a continuous flow of balls the wear was taking a long time to accumulate. An investigation with a high speed video set-up to determine the impact rate showed that a very large number of balls would be needed to keep the impact rate high so it was decided to try a pulsed approach, i.e., fire all the balls in the machine, then stop and allow them to recollect and then re-fire.

The objectives of the work just described were to set-up the test approach; decide what the best erodent is and how to apply it in a representative way; determine the best counterface to use to mimic the varying geometry found in a die; then carry out wear tests to assess wear behavior with time while varying parameters such as erodent contact angle and velocity, and develop test methodologies that can be used in the future to assess the effect on wear of potential die coatings and treatments.

One of the tests that belong to the other category, that of the liquid material flow has been developed by the author *Shuji Hattori* in the work "*Effects of Impact Velocity and Droplet Size on Liquid Impingement Erosion*" [29]. In this paper it takes into account the effect of the liquid impingement (Fig. 2.9).

Liquid impingement erosion has been originally of practical concern chiefly for low-pressure steam turbine blades, and for aircraft and missiles subject to rain erosion. The erosion rate, as always was defined as the mass loss per unit area per unit mass of water impinging.

The parameters remarkably influencing the liquid impingement erosion are impact velocity and droplet size [29]. A guideline used for this experiment and for the analysis in general was published by JSME (Japan Society of Mechanical Engineers) in 2005 [30]. However, the effect of impact velocity was not clearly understood especially for the threshold velocity, below which erosion rate is zero or negligible small. On the other hand, several researches have been conducted on the effect of droplet size. Some researchers found a strong increase in erosion with droplet size and the others found a weak dependence. In this study, effect of impact velocity on liquid impingement erosion was studied for pipe steels of low carbon steel, stainless steel and alloy steel .

The test rig used for this kind of experiment was quite different from the others described before.

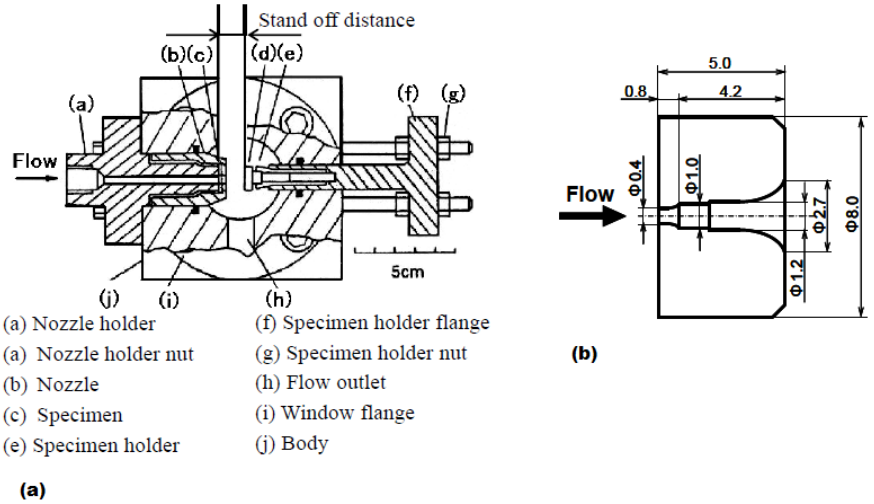

Fig 3.15 Test Arrangement: (a)Cavitation Chamber; (b) Nozzle Shape [29]

Fig. 3.15(a) shows the cavitation liquid jet chamber which is specified in the ASTM G134-95 standard [31]. Liquid impingement erosion tests were carried out using this test chamber. The chamber was full of air. A liquid jet issuing from the nozzle impinges on the test specimen. The test liquid was tap water kept at 35 ± 2 degree Celsius.
Fig. 3.15(b) shows the nozzle shape used for the test. The nozzle shape is different from that specified in the ASTM standard, but it was clarified that the erosion test results by the cavitation jet method are almost the same in spite of the difference in nozzle shape.
The erosion mechanism by liquid impingement proceeds due to fatigue. That is, asperities appear by plastic deformation at the crystal grain boundaries and the areas produce high stress concentrations, resulting fatigue crack initiation and material removal. The volume loss per droplet increases with the 5th power of droplet diameter, and a new formulation of volume loss per droplet was proposed in terms of impact velocity and droplet diameter.

3.2.3 MOST AFFECTING PARAMETERS

Taking over the analysis carried out previously by other authors, it was analyzed what can actually be the most influencing parameters during the HPDC process, related to damage by erosion. The literature has shown that the main factors are metal velocity, impact angle and metal temperatures. These are described in detail in this section, referring to the pins on tests, previously described [19].

Wear models can be developed from experimental data obtained from erosive wear tests if the values of important process parameters at the erosive wear pins and different locations in the die cavity are known during the filling and solidification stages for different choices of process conditions. These values of flow and thermal parameters are very difficult to measure during a die casting operation. Because erosive wear takes place primarily during the filling stage, the most important requirement of a die casting process simulation model for this study is the fluid flow modeling during mold filling. The modeling of the filling of a mold cavity in die casting is, however, very difficult. This is because fluid flow during this stage is highly transient, inertia dominated, and often turbulent with Reynolds numbers in excess of 10000 due to flow of high velocity metal through rapidly changing geometry

in the runner-gate system or in the casting cavity. Thus any model used for evaluation of the effect of process parameters must be capable of handling momentum dominated flow, jetting, and the complex free surfaces commonly seen in die casting.

The analysis nearly described, showed that the most affecting parameters on the erosion rate of a component subject to liquid impingement or a pulverized solid material flow, are three: Metal velocity, Impact angle and Metal Temperature.

It has been tried to present them using the guidelines in the report of *K. Venkatesan and R. Shivpuri* [19].

Effect of Metal Velocity

In order to quantify the effects of process parameters on erosive wear, the edge profiles of the "original pin layout pins" were used as a quantitative measure of erosive wear. The profiles of the pin edges facing the gate were measured by a comparator using 20x magnification. The profiles were drawn before and after the experiment, and a square grid was placed along the pin edge traced before the experiment. Wear was then measured in terms of the length of grids.

Using the FLOW - 3D based numerical model, a numerical simulation of the filling of the original pin layout was obtained [19].

Velocity profiles of different pins from these original pin layout simulations were obtained and correlated with the experimentally obtained edge wear profile. This was done by plotting the component of the velocity normal to the pin obtained from these simulations, as a function of the distance along the pin edge that is directly in front of the molten metal. The wear ratio is plotted against the velocity ratio at the nodal points where the velocities are obtained. The ratios at different locations are evaluated by dividing the value at the location by the highest value along the pin edge. A positive correlation exists between wear and velocity distribution along the pin edge thereby indicating that the metal velocity is a primary mechanism of erosive wear. This correlation between velocity and erosive wear along the length of the pin was obtained for a particular velocity. Experiments are will be conducted and presented in this paper to evaluate the erosive wear for a range of alumina flow velocities. Since the impact velocities on the surface of the pin are likely to be very similar to the gate velocity because of jetting, the experiments, done in this work,

will provide a further quantification of the effect of impact velocity on erosive wear in die casting. Preliminary results indicate that the wear profiles on pins for different velocities are similar to those reported in this paper.

The results from the study on the pins were reported in Graph 3.3, were is showed the correlation between die wear profile distributions and velocity profile distributions along an edge of a wear pin. The wear and velocity ratios indicate the ratio of the wear and velocity at a location to the maximum

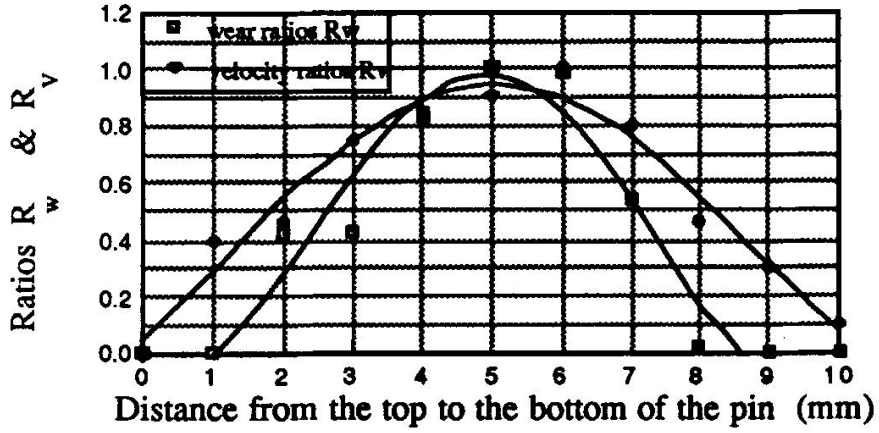

Graph 3.3 Correlation between die Wear Profile distributions and Velocity Profile distributions [19].

Effect of Angle of Metal Impact

Preliminary results of the effect of the attack angle of molten metal on the erosive wear rate of die pins is shown in the graph 3.4. The erosive wear rate defined by the weight loss of the pins after 1000 shots is plotted against the attack angle of the molten metal (angle α in Fig. 3.12(b)). As shown, the maximum wear rate occurs at an impact angle of approximately 72° degree. Previous studies have indicated that for impact of pure liquid, the impact angle at which maximum wear occurs is 90° [20]. For solid impact, the tangential component contributes to erosive wear, and the impact angle at which maximum wear takes place is 45° [21]. These results indicate that the aluminum metal is not completely molten, but is partially solidified. This is typical of die casting operations where large heat losses in the ladle, sleeve, and runner-gate system result in partially solidified melt during filling.

Experimental determination of the wear profiles of the specimen face for the angle of attack will also be determined in this work. These wear profiles and weight loss profiles will be compared with the velocity distributions already obtained to study further the effect of the "angle of metal impact" and molten metal velocity at impact on die erosive wear. The experiments will be repeated for a range of velocities and temperatures to study further the effect of the "angle of metal attack" for different process conditions. Previous results obtained from pin experiment show that the trend of erosion rate and impact angle can be described as the one in the Graph 3.4

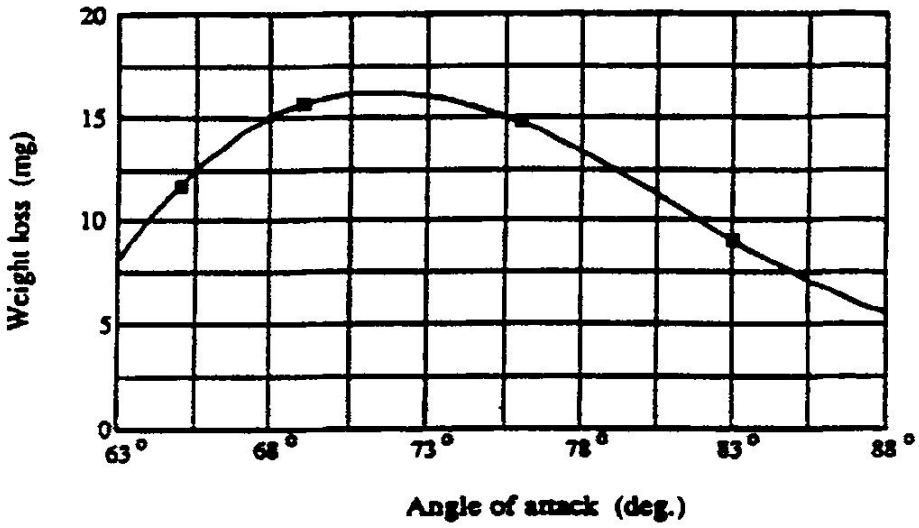

Graph 3.4 Dependence of Erosive Wear Rate on impact Angles of molten aluminum alloy [19].

Effect of Metal Temperature

Studies were also conducted to determine the effect of molten metal temperature on erosive wear of wear pins under production conditions. Preliminary results of this study are taken from the report of *K. Venkatesan and R. Shivpuri* [19] and shown here.

Erosive wear experiments, described before, on pins of dies, were initially conducted with aluminum alloy A390 at two different temperatures: 150° and 50° superheat. Both temperatures fall within typical die casting operational windows. The edge wear profiles of H-13 pins for both the temperatures are shown in Graph 3.5. As report, the wear profiles, although qualitatively similar, are quantitatively quite different. The wear seen at the lower temperature is much greater than that seen at a higher temperature.

Table 3.1 shows the ratio of the total weight loss to the initial weight of pins for the H13 at these temperatures.

Material	H-13 weight loss, mg/g
Low temperature (50 °C superheat)	0.519
High temperature (150 °C superheat)	0.306

Note: The weight loss of the pins is measured after 1000 shots.

Tab 3.1 Dependence of Erosive Wear rate H13 test pins on the temperature of molten aluminium alloy [19].

The erosive wear rate is much higher at the lower temperature for the sets of pins. Although it would appear that the percentage weight loss is small, remember that only a small part of the pin is exposed to the erosive wear action of molten metal.

This is the opposite not only of the results obtained by *Malm and Tidlund* [22] and *Yu and Shivpuri* [23] but also those that will be presented later in the experimental discussion; in fact all these authors observed an increase in the wear with an increase in the temperature. These dip tests, however, consider merely the effect of metal diffusion or corrosion and do not take into account the effect of physical impact and high velocities. As the temperature decreases, the solid fraction and consequently the amount of solid particles in the melt increases. The impact of more solid particles on the pins at the same velocity thus causes greater wear at the lower temperature. Although the die is likely to be cooler at a lower temperature thereby reducing metal diffusion, the increased wear due to the impact of more solid particles appears to be more significant to the overall wear.

These results thus show that the most significant driver of die erosion is the impact of high velocity solid particles on the die. That is why the experimental part will analyze this particular phenomenon, also experiments will be conducted for more temperatures to quantify further the effect of temperature on erosive wear, using solid alumina.

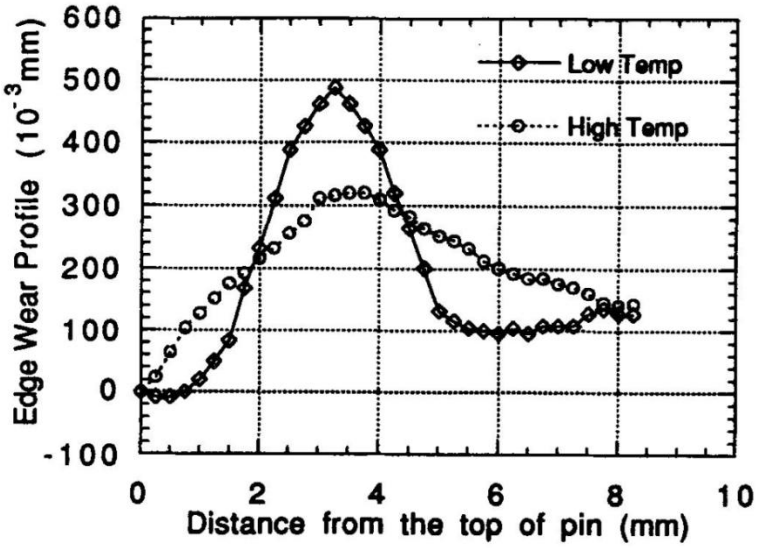

Graph 3.5 Dependence of edge wear profiles of H- 13 test pins on the temperature of molten aluminum alloy [19].

3.2.4 SOME RESULTS FROM BIBLIOGRAPHY

As shown, the metal temperature, metal velocity, and angle of metal impact have a significant impact on die erosive wear. The results reported here are preliminary and taken from the literature. A series of experiments will be conducted based on a "design of experiments" approach to complete the literature part of the effect of process parameters on erosive wear in die casting. The metal velocity, metal temperature, angle of metal impact, die material hardness, will all be varied in each set of experiments to obtain comprehensive wear models for a range of conditions. The ultimate aim of such a wear model is to predict the erosive wear in an actual die casting die, given the process conditions, using numerical simulations to obtain the values of parameters, such as velocity, temperature, etc. at various locations of the die.

If it are analyze the results related to the trend of impact angle and erosion rate, all authors of the preceding work related to this type of analysis are in agreement that the peak wear occurs at 30°[28], where a higher damaged zone was observed[27].

In particular in all of the cases, the size of the wear scars increased at low impact angles (30° and 45°) and is reduced at 60° and 90°. An elliptical shape was seen at 30° and 45° whereas a roughly circular shape was observed at 60° and 90° [27]. This result can be

explained by the impact geometry, which modified the orientation of the specimen when it is positioned at different impact angles.

It is assumed that the sliding component at this incident angle makes the difference to reach a higher wear damage. On the other side, a more roughened surface, characterized by a slightly darker area with a more pronounced pitting, smeared wear debris and inserted abrasive particles are observed at 90°. The different flow behavior than the corner you can see in Fig. 3.16.

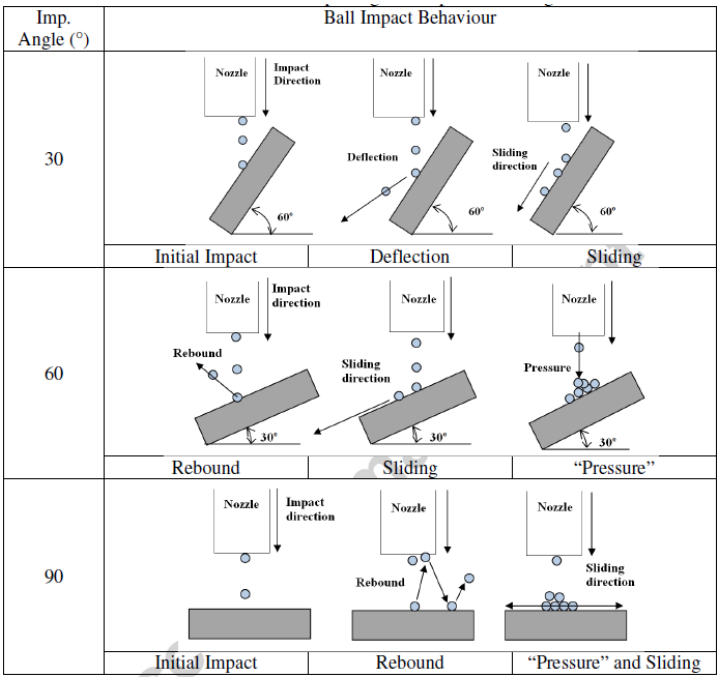

Fig. 3.16 Ball Impact Behavior against Flat Specimens at a Range of impact Angles [28].

This is not surprising; the wear rate at this angle is much higher than the other two angles, and damage leading to material loss would have occurred much quicker as the balls are sliding and cutting the specimen rather than impacting and forming craters (see surface images in Figure 3.17.

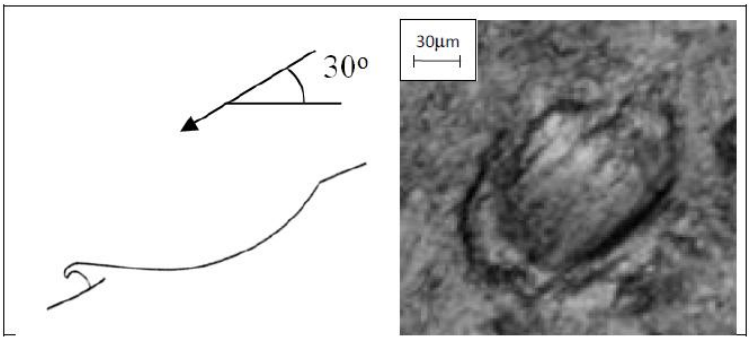

Fig. 3.17 Typical Example of a Cutting Wear Feature from a 60° Impact Test [28].

If is requested a graphically comparison between the behavior of the erosion rate to know the behavior of the materials when they are subjected to erosion tests, could be used the one illustrated in graph. 3.6 [39],

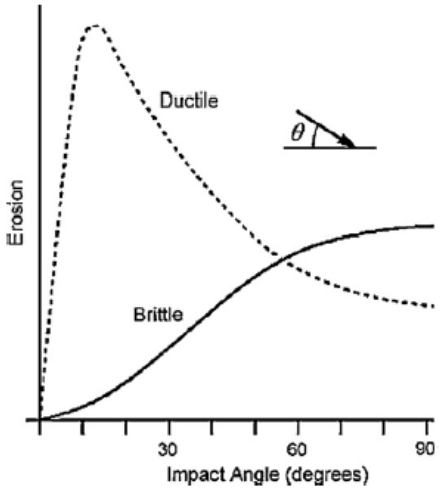

Graph 3.6 Erosive wear rates for ductile and brittle materials versus impact angle [39].

From this graph is also possible understand the difference between a brittle and a ductile material. Verified relation, for example when the content of titanium and aluminium(ductile materials) was significant to have this behavior. On the other hand, CrN coating displayed a brittle type behavior which it was related to its high hardness and low fracture toughness [27].

Similar results are reported by *A. Mohammed, M.B. Marshall, R. Lewis* [28], as shown in graph 3.7, the steady state erosion rate versus impact angle behavior follows the trends observed in previous work.

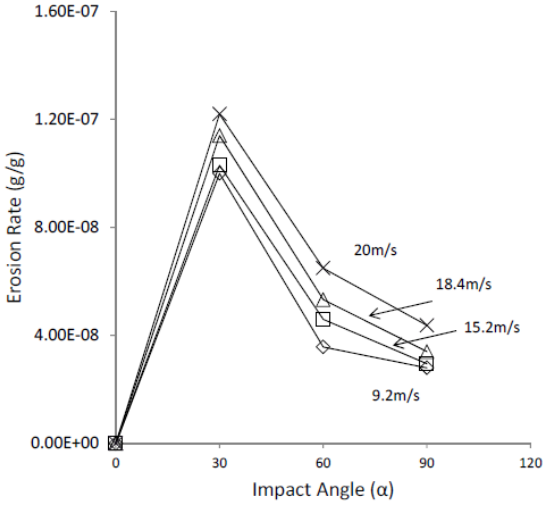

Graph 3.7 Specimen Impact Angle against Steady State Erosion Rate for Impact Velocities [28].

Directly linked to the previous speech, are the values of mass lost that provide the value of the degree of erosion of a specimen. Has been highlighted by some authors that the wear damage is proportional to the elapsed time [27]. It has been observed commonly in other erosion studies. It shows that steel without coating was the material with the highest mass loss whereas coating and aluminium materials exhibited the lowest wear damage at 30° and 45°, respectively.

Also important is the influence that the speed of the erodent flow on the specimen. as demonstrated above, this value is one of the most affecting. However it has been shown that does not have a dominant influence as well as the impact angle, in fact, as can be seen in Graph 3.5[28], the velocity waveform compared to erosion rate is similar for the different impact angles.

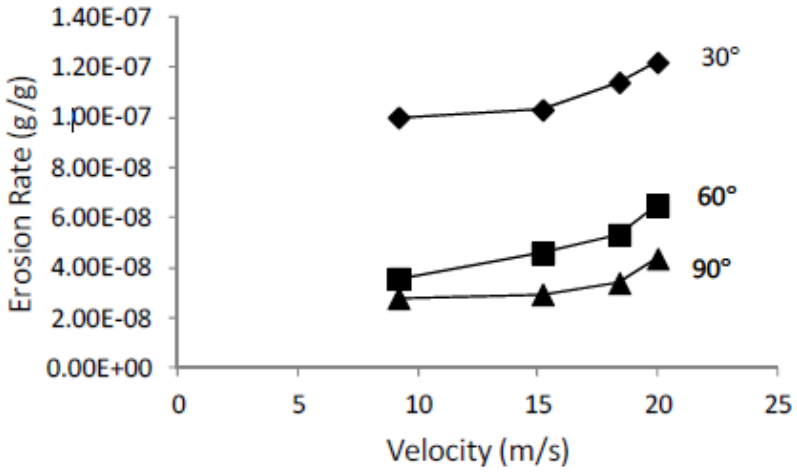

Graph 3.8 Steady State Erosion Rate against Impact Velocity [28].

The rate of increase does not match those observed in previous tests. This may be because in most erosion work the erodent is much harder than the counterface, whereas here it was the opposite. As a result, at higher speeds greater erodent damage resulted from the impact and surface damage did not increase as much[28].

These comparisons show that the computed velocity profile at the edge of experimental die used for the wear study matches closely with the measured wear profile indicating metal velocity to be a primary mechanism for core pin and, consequently, die washout.

Chapter 4:

MATERIALS AND METHODS

4.1 HIGH TEMPERATURE MECHANICAL FATIGUE TEST

In general, Strain-controlled fatigue is a phenomenon that is influenced by the same variables that influence force-controlled fatigue. The nature of strain-controlled fatigue imposes distinctive requirements on fatigue testing methods. In particular, cyclic total strain should be measured and cyclic plastic strain should be determined. Furthermore, either of these strains typically is used to establish cyclic limits; total strain usually is controlled throughout the cycle. The uniqueness of this analysis and the results it yields are the determination of cyclic stresses and strains at any time during the tests. Differences in strain histories other than constant-amplitude alter fatigue life as compared with the constant amplitude results (for example, periodic overstrains and block or spectrum histories). Likewise, the presence of nonzero mean strains and varying environmental

conditions may alter fatigue life as compared with the constant-amplitude, fully reversed fatigue tests. Care must be exercised in analyzing and interpreting data for such cases. In the case of variable amplitude or spectrum strain histories, cycle counting can be performed with different methods.

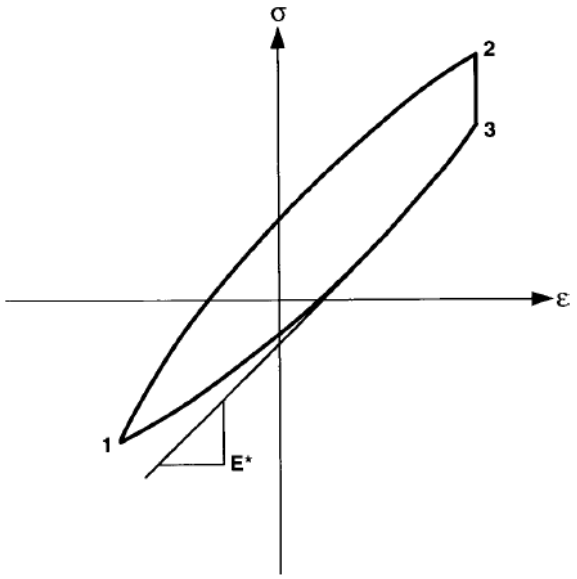

Fig 4.1 Analyses of a Total Strain versus Stress Hystersis Loop Containing a Hold Period [1].

The description just exposed is generally true for all the fatigue analysis; in the specific case developed in his project, in addition to mechanical stress is measured also the influence of temperature.

The test that has been carried out can be defined as *High Temperature Mechanical Fatigue Test*, that is, an analysis of components under cyclic stress and subject even at high temperature. It is not correct to define as a thermal fatigue test, as the cyclical stress placed upon the material are mechanical tension, but it is possible to take the thermo-mechanical fatigue testing ASTM standard E2368 and E606 [1], [2] as a guideline to describe it. Because there are many points in common between the two experiments it is possible to state that even the standard key points can be used in both analysis.

The strain-controlled thermo-mechanical fatigue (TMF) test is often used to investigate the effects of simultaneously varying thermal and mechanical loadings under idealized conditions, where cyclic theoretically uniform temperature and strain fields are externally imposed and controlled throughout the gage section of the specimen. A "thermomechanical" fatigue cycle is defined as a condition where uniform temperature and

strain fields over the specimen gage section are simultaneously varied and independently controlled.

In the utilization of structural materials in elevated temperature environments, components that are susceptible to fatigue damage may experience some form of simultaneously varying thermal and mechanical forces throughout a given cycle.

These conditions are often of critical concern because they combine temperature dependent and cycle dependent (fatigue) damage mechanisms with varying severity relating to the phase relationship between cyclic temperature and cyclic mechanical strain.

During the analysis the behavior of both stress can assume two configurations, in-phase, a cycle where the maximum value of temperature and the maximum value of mechanical strain occur at the same time, or out-phase, cycle where the maximum value of temperature leads the maximum value of mechanical strain by a time value equal to 1⁄2 the cycle period, an example is shown in figure 4.2.

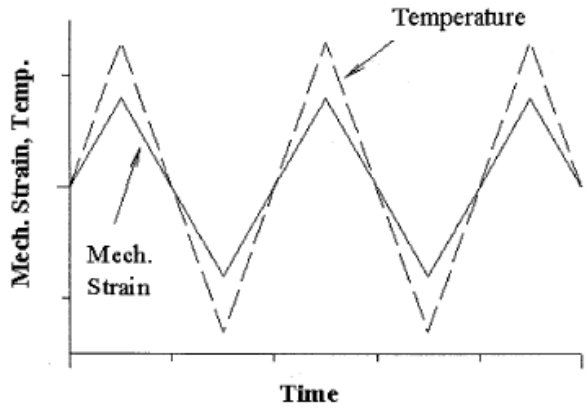

(a) In-phase TMF test (ϕ=0)

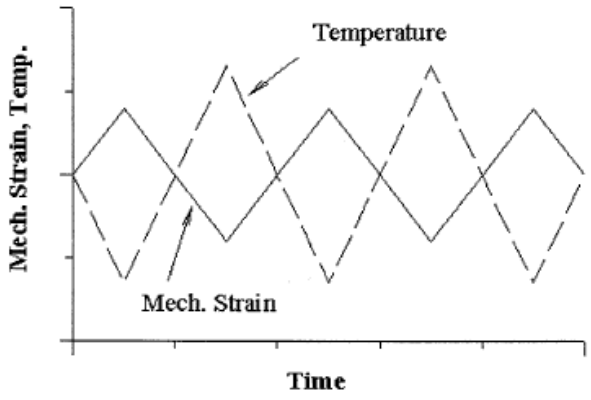

(b) Out-of-phase TMF test (ϕ=180)

Fig 4.2 Schematics of Mechanical Strain and Temperature for In- and Out-of-Phase TMF Tests [2].

Such effects can be found to influence the evolution of microstructure, micromechanisms of degradation and a variety of other phenomenological processes that ultimately affect cyclic life.

The test system shall be able to independently control both temperature and total strain. In addition it shall be capable of adding the measured thermal strain to the desired mechanical strain to obtain the total strain needed for the independent control.

Fixtures used for gripping specimens shall be made from a material that can withstand prolonged usage, particularly at high temperatures. The design of the fixtures largely depends upon the design of the specimen. Typically, a combination of hydraulically-actuated collet grips and smooth shank specimens provide good alignment and high lateral stiffness.

Specimen heating can be accomplished by various techniques including induction, direct resistance, radiant, or forced air heating. In all such cases, active specimen cooling (for example, forced air) can be used to achieve desired cooling rates provided that the temperature related specifications in standard are satisfied.

All specimen designs shall be restricted to those featuring uniform axial gage sections, as these specimen designs offer a reasonable continuum volume for testing. Tubular specimens are preferred to solid specimen designs because they will tend to facilitate thermal cycling due to lower material mass and will reduce the potential for unwanted radial temperature gradients during thermal cycling.

The specimen used in the actual analysis is similar to that shown in Fig. 4.3, with threaded ends, even if this kind of samples with typically tend require more effort than those with smooth shank ends to meet the alignment criteria; for this reason, smooth shank specimens are preferred over specimens with threaded ends.

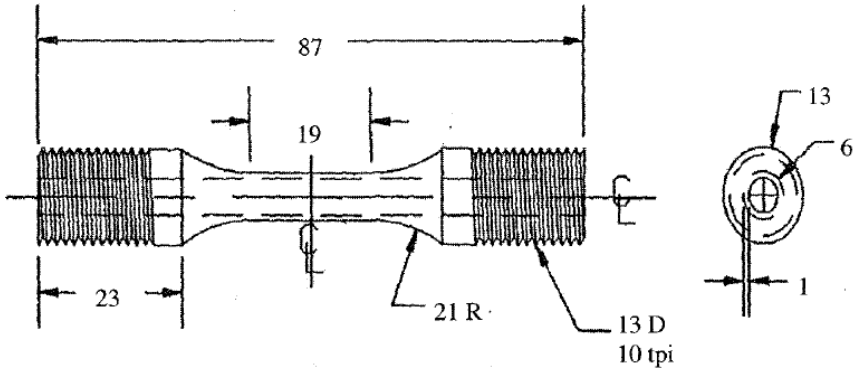

Fig 4.3 Samples of Thin-Walled Tubular Specimens for TMF Testing, Cylindrical threaded shank [2].

4.1.1 DESCRIPTION OF TEST DEVICE AND PROCEDURE

The tests that were performed, as previously said may be denominated as High Temperature Fatigue tests. They were carried out at the research center Tekniker IK4. The research center is a leader in the field of tribology, it counts several laboratories and a lot of developments regarding the analysis of contact behavior between different materials. In particular, the work has been done in the workshop of the tribology unit, which has several devices for the experimentation of materials under different conditions.

The first step to define the experiments carried out is the description of the materials used and the test device.

One objective of MUSIC project was the analysis of the behavior of steel usually used for HPDC dies. Hence, it was tried to use materials that are mainly and currently adopted for the creation of dies, i.e. chromium-molybdenum hot work tool steels. In this category the most common are the H13 and H11, designated in this way according to AISI standard. These types of steel are commonly used for the creation of dies, given their characteristics and their resistance.

H13 tool steel is a versatile chromium-molybdenum hot work steel that is widely used in hot work and cold work tooling applications. The hot hardness (hot strength) of H13 resists thermal fatigue cracking which occurs as a result of cyclic heating and cooling cycles in hot work tooling applications. Because of its excellent combination of high toughness and resistance to thermal fatigue cracking (also known as heat checking) H13 is used for more hot work tooling applications than any other tool steel. Because of its high toughness and very good stability in heat treatment, H13 is also used in a variety of cold work tooling applications. In these applications, H13 provides better hardenability (through hardening in large section thicknesses) and better wear resistance than common alloy steels such as 4140. Typical applications include inserts, cores, and cavities for die casting dies, die casting shot sleeves, hot forging dies, extrusion dies, and plastic mold cavities and components that require high toughness.

H11 hot work tool steel is a 5% chromium hot work steel that is characterized by excellent impact toughness. It contains less vanadium than the widely-used H13 hot work tool steel. This provides for the higher toughness, with some reduction in wear resistance and temper resistance. H11 hot work tool steel is a deep-hardening, air-hardening steel that exhibits minimal size change during heat treatment. It has good resistance to thermal fatigue cracking (heat checking) and excellent resistance to gross cracking and thermal shock when water cooled in service. H11 hot work tool steel is recommended for hot tooling applications where maximum resistance to cracking is required. Such applications include hot punches, die casting dies, forging dies, hot shear blades, hot gripper dies, and extrusion tooling.

Steel		Si	Cr	Mo	V	Mn	HARDNESS
H13	Nominal	1.00	5.10	1.35	0.90	0.40	43 HRC
	Measured	0.91	4.85	1.33	0.96	0.35	
H11	Nominal	1.00	5.10	1.35	0.40	0.40	43 HRC
	Measured	0.99	4.90	1.20	0.31	0.40	

Tab. 4.1. Measured (by optical emission spectrometer) and nominal (according to AISI) chemical compositions (wt.%) of H13 and H11 steels used in the study.

To comply with the rules that describe the performance of this type of tests, it has been used standard specimens with threaded ends both for H11 and H13, which dimensions are described in Fig 4.4a.

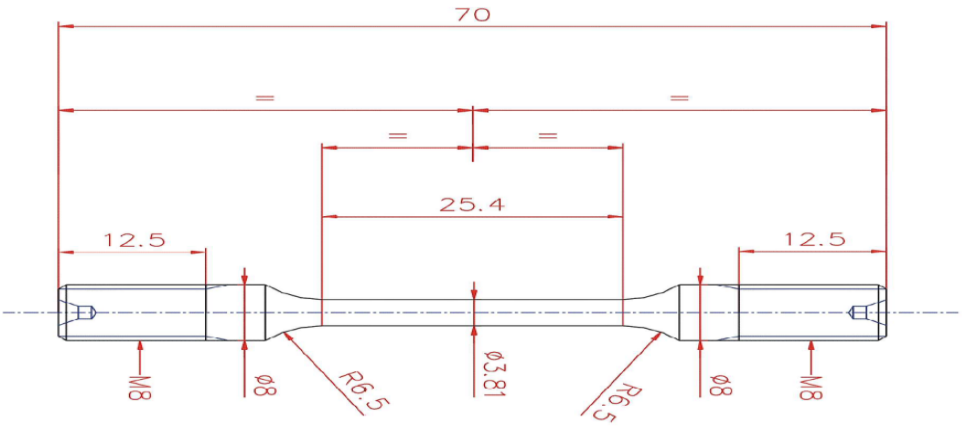

Fig 4.4a Samples of Thin-Walled Tubular Specimens used for the Tests in Tekniker.

Fig 4.4b Samples of Thin-Walled Tubular Specimens used for the Tests in Tekniker.

The specimens used for the analysis must be treated before it can be tested. The preparation of the samples consist of cleaning all the parts from residual, by the use of an ultrasound machine, which acts through a water container where is immersed the bowl with the specimens. The cleaning process takes five minutes, and is done before in a bath of ether, which ensures thorough cleaning of the specimen; and then another five minutes in a bath of acetone, that remove all the residual of ether on the sample. This process is widely used for the cleaning of many components before the testing.

The machine used during the test is called ***25kN SSRT Furnace Loading Unit*** that have been designed and manufactured by *CORMET Oy*. The system also include the 25kN SSRT Titanium Autoclave which is another valuable tool for the analysis of materials at higher pressures.

The general specifications of the Furnace machine are given in Table 4.2

Specification	Value
Max design / operation pressure	Ambient / ambient
Max design / operation temperature	800°C / 800°C
Volume	0.0008 m^2
Material	Nimonic 80A, aluminium oxide

Tab. 4.2 Specification Value provided from Cormet Oy.

The available equipment for conducting the tests consist of a motor controlled in speed and load. The motor is connected to a software that allows to program the desired operating conditions. The load limit of the cell is 25 kN, the speed is adjustable between $1.67x10^{-9}$ µm/s and 32.8 µm/s. The furnace can reach a temperature of 800°C. Warming up is advisable to approach the desired temperature slowly to prevent thermal deformation damaging equipment.

The schematization of the machine and of all its components is represented in figure 4.5; are also indicated the various connections between the control device, and a detail of the load cell of the test specimen.

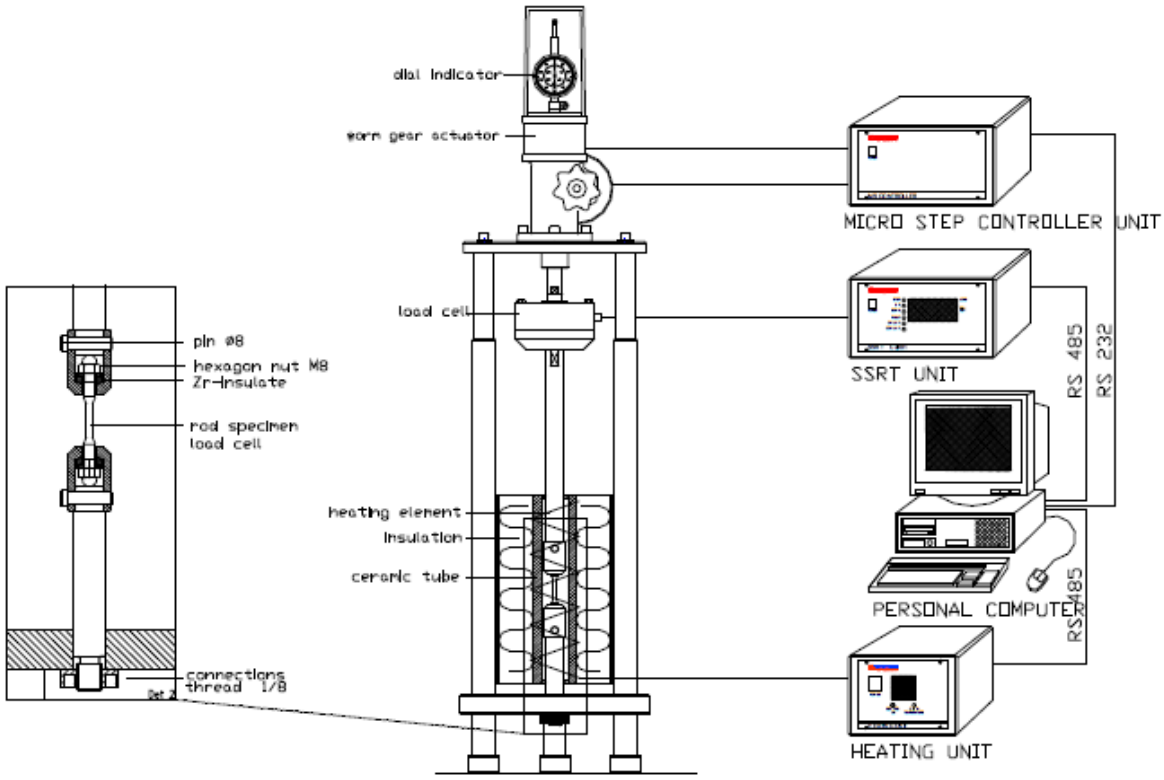

Fig 4.5 Loading device with furnace [3].

Computer controls step motor and gear box that is loading the specimen. The displacement rate or load rate will be specified in computer software by the operator. The load measurement value from load cell will be displayed in the computer software.

The computer saves both the displacement and load data automatically. The data will be available for further handling in ASCII format.

The SSRT instrument fulfills the requirements presented in *ASTM Practice G129* [4].

When constant load feature is used, the load cell response is used as a feedback signal to the computer software that controls the motor. In other words, computer software controls the displacement so that the load cell measurement value is equal to the load set point that has been specified by the operator.

Low frequency cyclic fatigue test can also be performed with the instrument. The cyclic loading can be performed either under load or strain control. The shape of the loading can be either of trapeze (a special case: saw tooth) or sinusoidal type. The maximum frequency depends on the amplitude but a reasonable f_{max} is about 0.02 Hz. Maximum load during cyclic loading is 10 kN.

A tube furnace will be integrated in the loading system construction. The furnace is feed with nitrogen, CO_2 and SO_2 as furnace gases. There will be panel mounted inlet ball valves and rotameters for all three gases mounted on a panel that is attached to the loading device body. Gas line(s) will be led to lower part of the furnace. There will be three union fittings for OD 6 mm tube / hose for inlet gases in the gas panel. The furnace will not be completely gas tight. There will be covering plates on the top and bottom of the furnace to prevent convention through the furnace. It is possible to use gases to make stress-corrosion cracking, but during the experiment it was only used the resistance heating furnace, not gases.

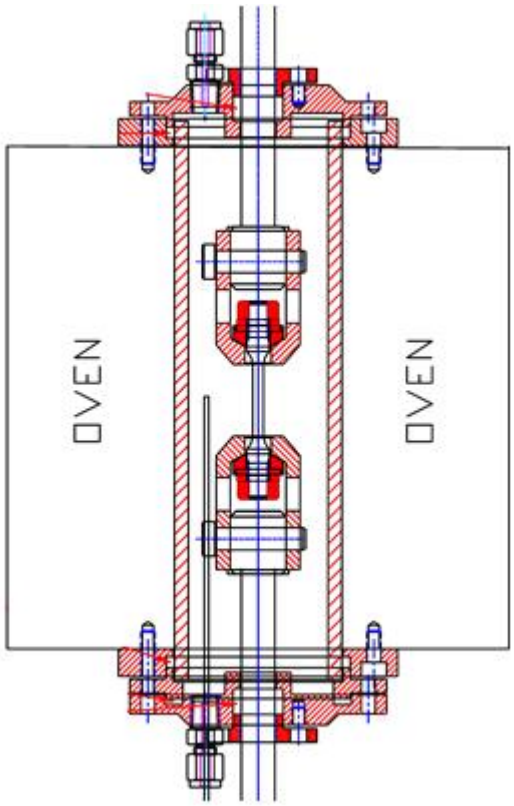

Fig 4.6 Furnace System scheme [3].

As mentioned above, the operation of the oven is conditioned by the gradient of heating, it must not be too high to prevent malfunctions or damage to the system. For the tests conducted it was decided to fix a heating gradient of 40°C / h, which makes the process of analyzing longer but ensures a successful experiment.

The last critical step to describe the device is the installation of the specimen; the installation is crucial because it can lead to measurement error derived from the incorrect mounting of the component.

The round tensile type is installed to specimen holders using electrically isolating parts between the specimen holders and the specimen.

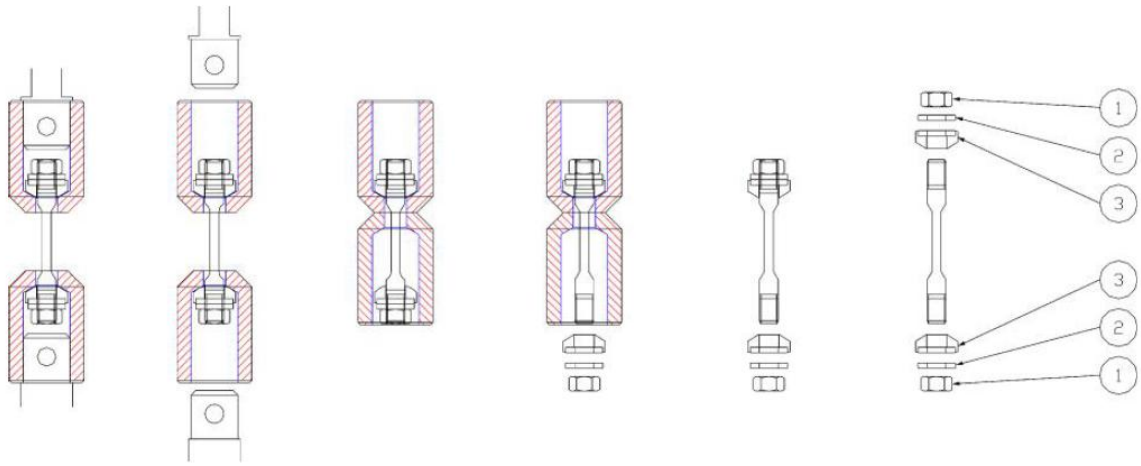

1	Nut M8, Nimonic 80A	3	Nimonic 80A cup with a magnesia stabilized zirconium oxide ceramic washer
2	Special washer, Nimonic 80A		

Fig 4.7 Round tensile specimen Installation [3].

Referring to Fig. 4.7 following steps should be used:

1. Install part 3 to one side of specimen;
2. Install part 2 to specimen, same side as step 1;
3. Install part 1 to specimen, same side as steps 1-2. Apply anti-seize compound to thread;
4. Insert the specimen through both specimen holders;
5. Repeat steps 1-3 to the other side of the specimen.

The specimen is installed to the specimen holders first, while oven is up. The specimen holders are installed to the ends of the *pullrod* and lower rod with pins. *Pullrod* is driven

up (with software) to make space for the holders. After holders are in place, the pullrod is driven down to install pins. After the pins are in place, it is possible to preload specimen with thumbnut at the end of lower rod and driving pullrod up. Finally, the oven is lowered down, and the six thumb-screws are installed.

4.1.2 SETTING-UP TESTS

Like in all the experimental studies, before starting with the actual testing valid for the purposes of analysis it is convenient to perform various tests that can be considered setting tests. This kind of preliminary tests are necessary to understand the behavior of the machine and the material tested, so it is necessary to provide an adequate number of specimens for the whole study.

Before make any kind of test, however, it is necessary understand the operation of the machine used for the first time; because of it was important to thoroughly study the use of software that relates the user with the loading and heating devices.

The device has a software, through which it is possible do different operations, using the manual control or set a loading control process. Tests that can be performed with this equipment is extensive: a constant load, constant strain rate, with constant load increased, with varying cyclic deformation or cyclic loading.

The kind of stress that we want to apply will depend on the study planned on the test sample. Programming test is performed by software SSRT, particularly with the control unit "Loading unit control" that can be seen in Figure 4.8.

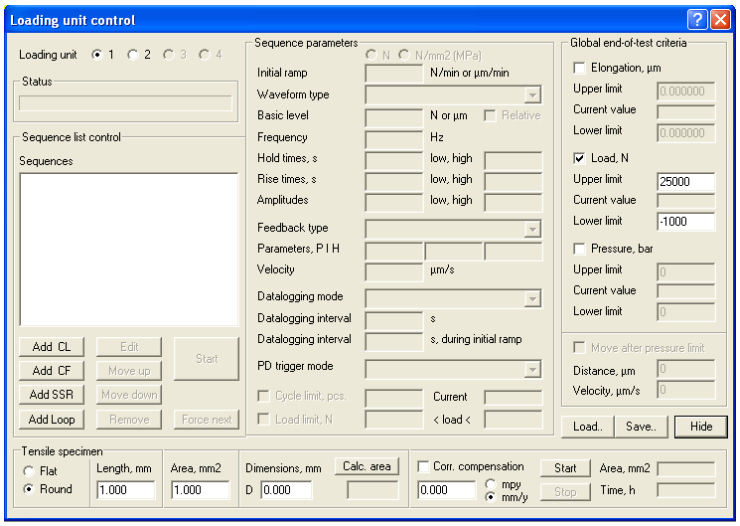

Fig 4.8 Loading Unit Control [3].

The Loading Unit control allows to schedule and run tests with different conditions, and with different types of stress described before and shorten such as CL, CF, SSR and LOOP.

The parameters entered in this part determine the success of the test, it is therefore essential study them before, in order to obtain optimal data for every type of test. In this window all necessary for performing the test parameters are set.

The three types of tests that can be performed and combined with each other are:

- Constant load: With this sequence, initially a ramp runs from the current load value to the desired value (Basic level) and then will maintain the constant force throughout the test. The parameters to be set are "Basic level", "Initial ramp", "Velocity", "P", "H" and "Datalogging interval".
- Cyclic Fatigue: variable load cycles between two limits are created. The parameters to be set are "Basic level", "Initial ramp", "Velocity", "P", "H", "Datalogging interval", "Frequency", "Amplitude" and "Wave form". If a test is performed with trapezoidal wave is necessary to set "holding time" and "rise time". It is also possible to set the maximum number of cycles performed.
- SSR (Slow Strain Rate) is simply a trial to defined speed. The user must establish what timely ramp speed would, given the expected total strain at break and the desired assay time. The parameters to set are the strain rate "Velocity", "P", "H" and "Datalogging interval".

The other tool provided by the software essential to the work is **The Movement Controller** (Fig 4.9), that makes instant operations, and allows to control the load and the position of the device. It is essential for getting started, and also check the real test conditions (positions and load).

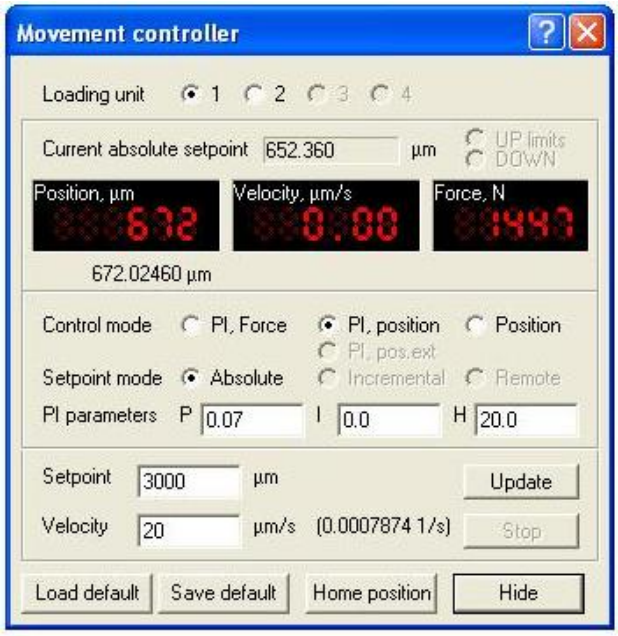

Fig 4.9 Movement Controller [3].

After understanding the operation of the software and have identified what are the basic parameters to be find in order to make the best results it is possible begin to make preliminary tests. Preliminary tests are used to understand the behavior of the machine in relation to the material to be studied and the analysis required. In particular by doing several attempts it is possible to get the analytical values of the parameters identified before.

The main parameters that influence on the performance of a fatigue test on this device system are listed below with a description of what specification they influence, also the optimal range values obtained through various attempts. It is important to note at this point that the entered values are relative and optimal for the type of study performed, while it is not guaranteed that during a different type of analysis the ranges are the same.

Let's start with **FREQUENCY** that influence the course of the cycles.

- If too high → NOT COSTANT PEAK, not repeatable, wrong cycle shape
- If too low → VERY LONG TEST

***OPTIMUM RANGE*: (0,010÷0,014) Hz**

Than **VELOCITY** that has a big influence on the course of the motor and cycles.

- If too high → NOT COSTANT PEAK

  → PROBLEMS WITH MOTOR
- If too low → VERY LONG TEST

***OPTIMUM RANGE*: (27÷31) µm/s**

The **AMPLITUDE** has a big effect on the position and deformation of the specimen.

- If too high → PLASTIC REGION
- If too low → WRONG ELONGATION

OPTIMUM RANGE: see the load cycles, and characteristic of the material.

To investigate this particular parameter it was performed a test called **Slow Strain Rate Test** (SSRT), it is a standard method of testing of materials, often metals, in which the specimen is subjected to elongation at a constant rate. The load is varied to maintain the constant extension rate. While extended, the material is exposed to an environment (temperature, specific fluid, etc.). The method evaluates the corrosion behavior of the material in the given environment, often the environmental effects on the material fracture or stress-corrosion cracking susceptibility.

The important characteristic of these tests is that the strain rate is low, for example extension rates selected in the range from 10^{-8} to 10^{-3} s^{-1}. The selection of the strain rate is very important because the susceptibility to cracking may not be evident from result of tests at too low or too high strain rate. For numerous material-environment systems, strain rates in range 10^{-5}- 10^{-6} s^{-1} are used; however, the observed absence of cracking at a given

strain rate should not be taken as a proof of immunity to cracking. There are known cases wherein the susceptibility to stress-corrosion cracking only became evident at strain rates as low as 10^{-8} or 10^{-9} s^{-1}. Graph 4.1 is a typical trend of SSR test.

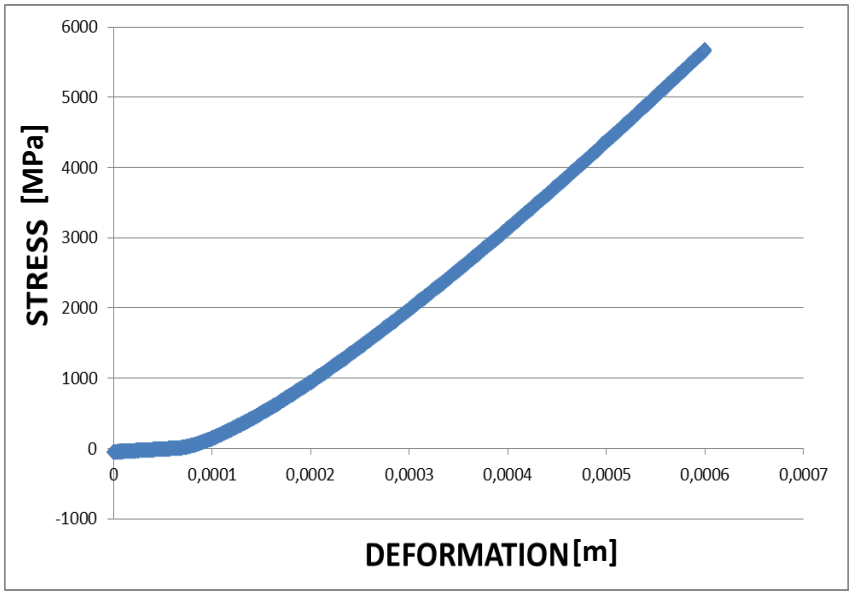

Graph. 4.1 Slow Strain Rate Test.

This particular test is done to verify the stiffness of the structure, and if it coincides with that calculated, using the relative Young's modulus. The test was stopped before the breaking of the specimen, to collect information on the behaviour under stress. Below you can see the formula used that express the difference between the deformation of the specimen and the structure.

$$\Delta L_{tot} = \Delta L_{struc} + \Delta L_{sp} \quad 4.1$$

$$\Delta L_{tot} = \varepsilon_{r2} - \varepsilon_{r1} \quad 4.2$$

$$\Delta L_{sp} = \frac{(\sigma_2 - \sigma_1) * l_{start,sp}}{E\,[f(T°)]} \quad 4.3$$

$$\text{Stifness}_{\text{struc}} = \frac{\Delta F}{\Delta L_{tot} - \Delta L_{sp}} \quad 4.4$$

Finally, thanks to the results we managed to have the value of the **AMPLITUDE** to put inside the software.

P / I / H PARAMETERS were the most difficult values to find, that have a direct effect on the movement of the device have been found in attempts

- **P:** used to calculate correction from difference of set point and process value.
- **I:** used to calculate cumulative correction value.
- **H:** Hysteresis term
- ***OPTIMUM VALUES:*** **P=(0,49÷0,52) / I=0 /H=5**

In order to find the last parameter it was performed a test that was really similar to the actual analysis test, a CYCLE FATIGUE TEST, that can be called preliminary because it provides the values of upper and lower limits of the cycles. It is carried out in order to calibrate parameters that will not bring the specimen to a of plastic deformation region, or to a very low level. The parameter found is the Basic Level that indicates the load level from which to perform the analysis cyclical, that is, the lower limit of the cycle.

The **BASIC LEVEL** that influences the elastic or plastic behaviour of the specimens.

- If too high → SPECIMEN IN A PLASTIC REGION,

  → WRONG DEFORMATION
- If too low → DEVICE PROBLEM WITH NUT UNSCREWING

Another test done before proceeding with the actual study of the behavior of the specimen subjected to HTMF is to ensure the correct trend of the Young's Modulus.

The first step was to create a curve to determine the modulus of Young of the two steels (H11, H13), on the basis of the data found on the internet and on the literature through the manuals of the materials. After collecting all these data have been created, using a spreadsheet, first a graph (graph 4.2), and then a table that given the temperature as input, would provide the value of the module as output data.

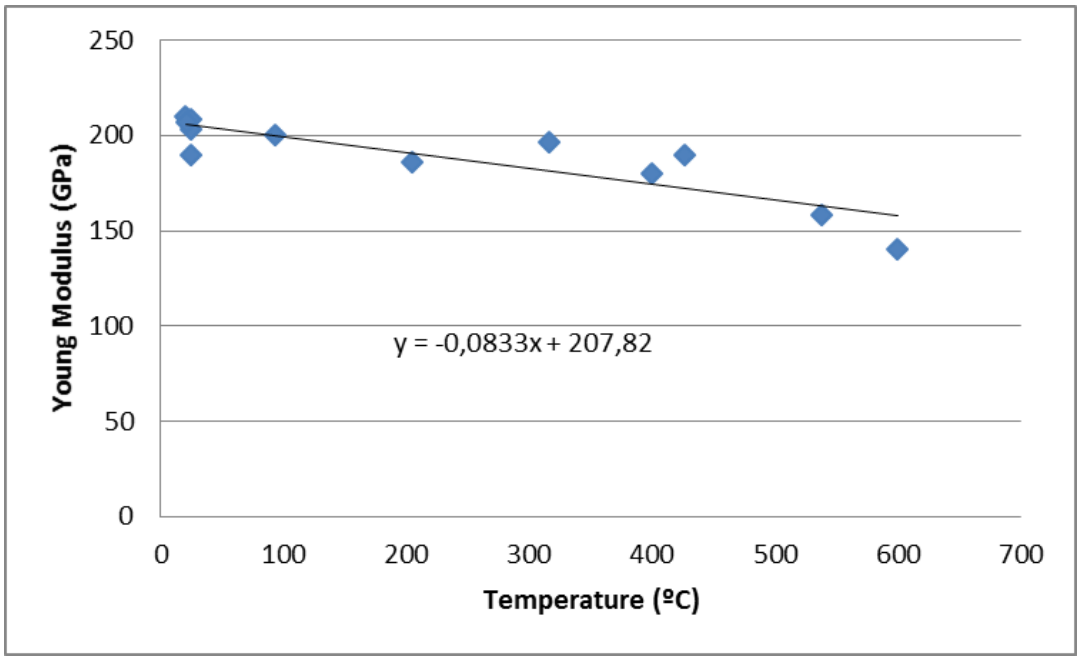

Graph. 4.2 Young's Modulus vs Temperature.

Finally, in order to understand possible differences of both steels at their fatigue behavior at high temperatures, tensile tests were performed at 300, 400 and 500ºC. The key properties selected for the evaluation were the yield strength, yield strain, maximum stress, final elongation, and young modulus (slope).

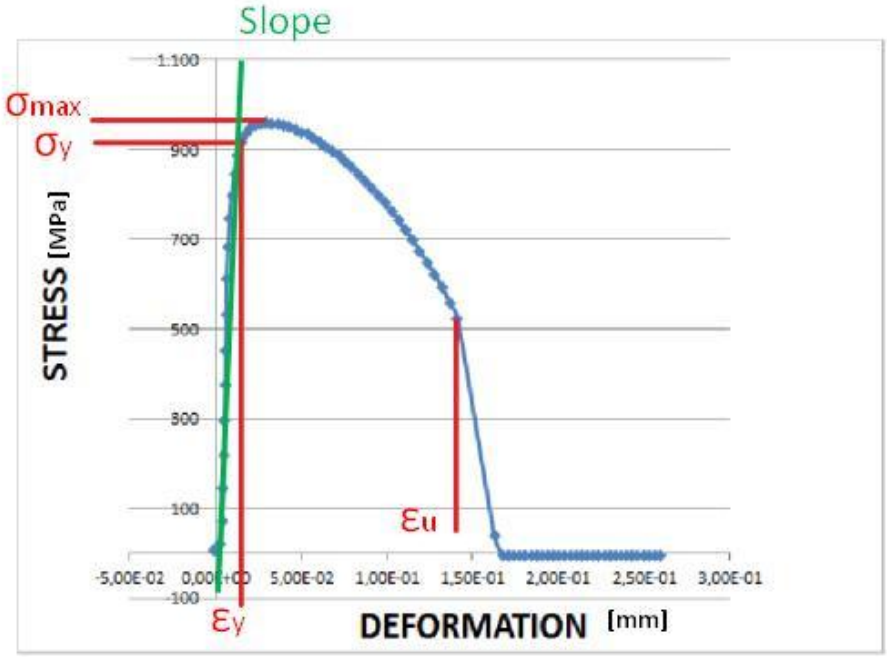

Graph. 4.3 Tensile test key properties evaluated.

According to literature [5] the effects of high temperature in properties that can affect fatigue are the following:

- The tensile strength is reduced but elongation increases
- Young modulus reduced: Less stress for the same deformation. It has to be kept in mind that Low Cycle Fatigue (what concerns this study) is ruled by deformation and not by stress like in High Cycle Fatigue.
- Oxidation: thermal fatigue is generated by an intergranular cracking in the surface. Oxidation is an intergranular effect as well. Its influence increases with time.
- Creep: Viscous behavior at high temperature. Deformation increases for a constant stress Fatigue resistance reduction and fatigue limit disappears. Creep temperature for these steels is around 580ºC, not being probably an influencing effect.

The tensile tests performed showed the results of graph. 4.4 a, b. The theory was confirmed, reducing the tensile stress, increasing the elongation and reducing the Young Modulus with temperature. The differences between H13 and H11 were not important, consequence probably of being both heat treated to the same hardness. H13 is able to be heat treated to a higher hardness than the H11.

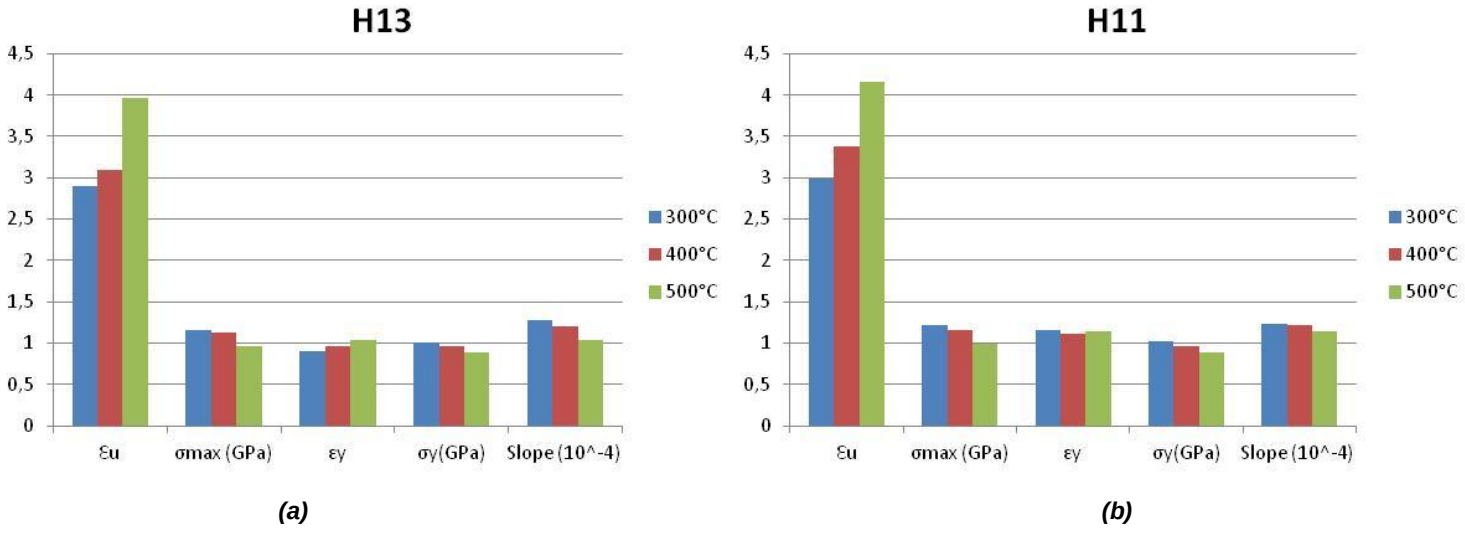

Graph. 4.4. Results of H13 (a) and H11 (b) samples tensile tests at 300, 400 and 500ºC

High temperature tensile tests shown before in graphic 4.5 are important to understand the mechanical behavior of materials, but dedicated fatigue tests are necessary to support the thermal stress calculation in order to have a reliable thermal cracks appearance prediction.

The tests performed on the two steels H11 and H13 didn't show a big different between the two steels, what is reasonable regarding their equal Hardness.

The influence of the temperature have a combined effect that has been explained in the tensile tests part. At lower temperatures, the Young Modulus is higher for the same strain, at 300ºC we are applying higher stress, but it also would have higher maximum stress but on the other side lower maximum elongation. As a good correlation, the relation between the stress and cycles to failure was found and can be described as shown in the next figure. This equation would be valid for a martensitic steel at 43HRC hardness:

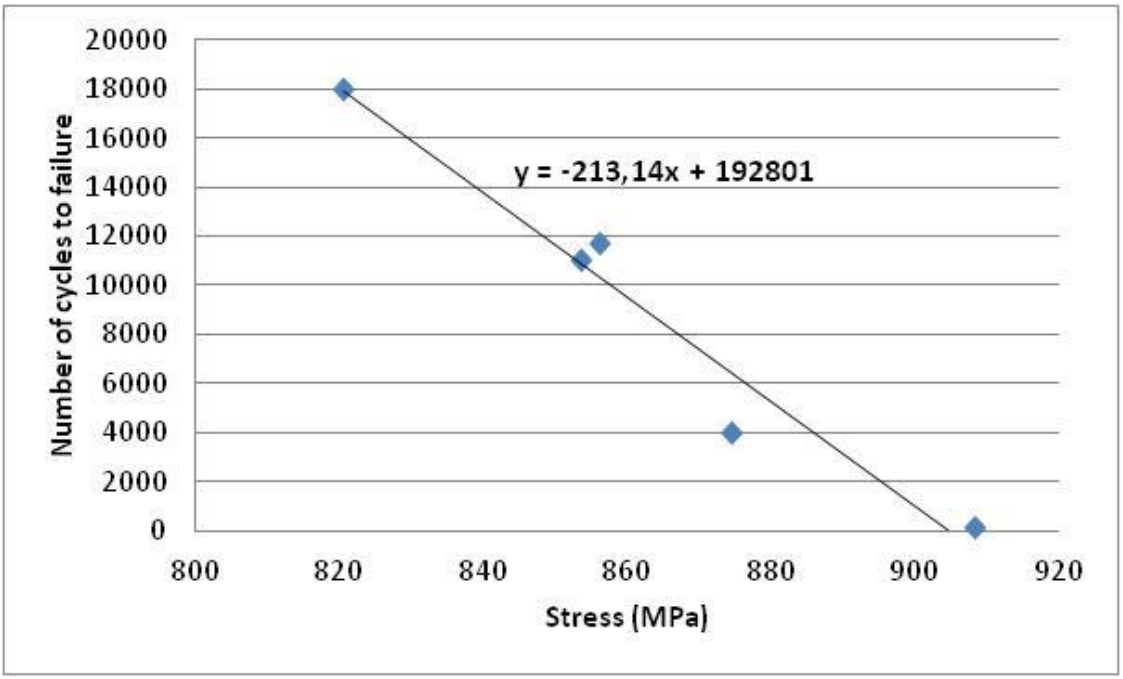

Graph. 4.5 Cycles to failure for different stress level.

This equation will be further validated making more fatigue tests as well with the results of Thermal Fatigue Machine.

Having done all the preliminary testing necessary to understand both the behavior of the machine (stiffness, limit values and parameters) and the material (Young's module, maximum stress and strain etc..) it is possible to proceed with the characterization of the specimens subjected to HTMF.

The type of analysis that has been chosen to perform involves the study of the behavior of the test specimen described before of two different material H11 and H13, subjected to a fatigue load and high temperature. Specifically the number of cycles must be relatively low to obtain a of low-cycle fatigue stress. Set the objective, the evolution of the experiment will be marked by some different tests that were necessary to achieve the best behavior of the specimen tested. The main difficulties have been encountered in finding the values of the parameters described in the previous paragraph. In fact, it was noted that sometimes, inserting different values of parameters the experiment trend was erroneous. Therefore it can be said that the design of the experiment will be adjusted by the parameters found during the tests. The parameters will be inserted in the dialog box described previously (Fig. 4.8).

The **FIRST** test was carried out to 500˚C and the furnace has a temperature gradient of 40˚C/h, so for reaching the input temperature it has required more than 12 hours. Therefore, in order to analyze the behaviour of the cycles only at high temperature, it is placed a *Constant Load* of the same duration as the heating time. It is also important to highlight that the test was done under *Strain Control*.

The parameters used for the experiment are described in Table 4.3, divided into *Constant Load* and *Cyclic Fatigue*.

Constant Load						
Initial Ramp	**Basic Level**	**Velocity**	**Duration Limit**			
60 N/min	600 N	1 µm/s	750 min			
Cyclic Fatigue						
Initial Ramp	**Waveform Type**	**Basic Level**	**Frequency**	**Amplitude**	**P / I / H**	**Velocity**
50 µm/min	Sinus	550 µm	0,013 Hz	500 µm/s	0,52 / 0 / 5	31 µm/s

Tab. 4.3 Parameter used during the FIRST HTMF test.

As the first one, the **SECOND** test was held at 500˚C, so it took the same time to reach the required temperature and because of this has the same initial Constant Load. In order to improve the results and correct the problems, the test lasted longer, maintaining the desired parameters throughout all the process. As in the previous test the all operations will be under Strain Control.

They were also changed some parameters to allow better performance. the parameters changed are highlighted in the Table 4.4.

Cyclic Fatigue						
Initial Ramp	**Waveform Type**	**Basic Level**	**Frequency**	**Amplitude**	**P / I / H**	**Velocity**
50 µm/min	Sinus	**350 µm**	**0,014 Hz**	**350 µm/s**	0,52 / 0 / 5	31 µm/s

Tab. 4.4 Parameter used during the SECOND HTMF test.

As can be seen the changes have been made on the parameters that influence the amplitude of the cycle. This, because it has been noted that if the cycle was too wide could bring the specimen in the area of plasticity (if too high), or cause problems with the locking system (if too low).

The **THIRD** test was set using all the solutions that we have learned through experience of the first two. So, as for the second test, we changed some parameters in order to eliminate the previous problems. The Constant Load was kept equal even for this attempt. The changed parameters are highlighted in the Table 4.5.

Cyclic Fatigue						
Initial Ramp	**Waveform Type**	**Basic Level**	**Frequency**	**Amplitude**	**P / I / H**	**Velocity**
50 µm/min	Sinus	**365 µm**	0,014 Hz	**365 µm/s**	0,52 / 0 / 5	31 µm/s

Tab. 4.5 Parameter used during the THIRD HTMF test.

The values that have been changed, are related to the stress amplitude of the cycle. It has been tried to increase this parameter so that the specimen came slightly in the plasticity zone, influencing the number of cycles to failure with the aim of reducing them.

The parameters used in the last tests seem to lead to an optimal behavior of the specimen and to a limited number of cycles to failure. For this reason it was decided to continue the analysis, using both materials to be tested, H11 and H13. Also to avoid problems related to the lowering of the charge it has been introduced a Loop command. The **Loop** sequence will move back the specified amount of sequence, the specified number of times

After conducting tests and bringing the specimens 'til break, it is interesting to analyze the specimen breaks on the fractured surface. To obtain this information the company is equipped with an Olympus microscope SZX16, with SDF PLAPO 0.5XPF. It is a precision microscope, designed for very demanding applications with the ability to resolve 900 line pair/mm. It is also possible to utilize the full zoom range (0.7x–11.5x) with the equipped dual turret. The extendable eye point adjuster provides comfortable posture for users of different heights.

Thanks to the use of this type of instrument, it was possible to analyze the dynamics of rupture of the specimen according to the signs shown on the broken end. The results are reported in the next chapter. The images are of high quality and thanks to the connection to a terminal has been possible to make some screenshots at more depth levels, in order to obtain an image that reflects performance three-dimensional fractured end.

Fig 4.10 Olympus microscope SZX16 [18].

As already said the system allows accurate analysis that can be considered almost letterpress. The user is able to photograph the sample analyzed at different zoom, or layer, from which the software automatically generates a superimposed image and high definition, in figure 4.11 are represented some examples of images reported by the device.

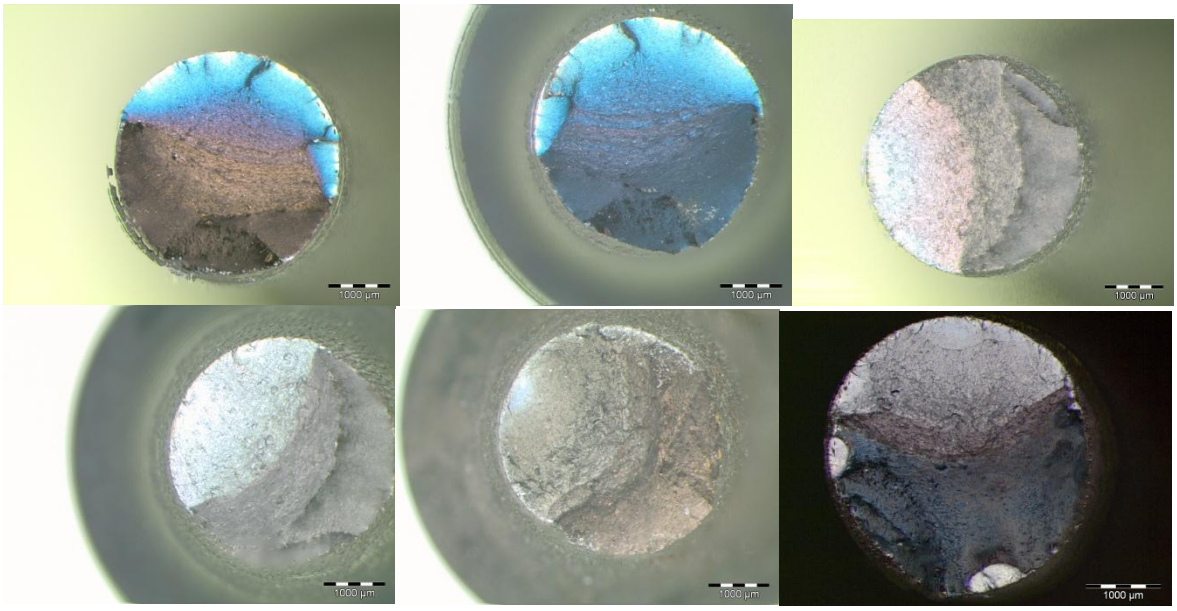

Fig 4.11 Examples of analyzed specimens with the Olympus microscope SZX16.

4.2 EROSION TEST

The erosion tests were carried out using as guideline the ASTM Standard showed in the *paper G76* [6], this reference indicates some key points to consider when testing a material subject to erosion, also declared that deviations from this standard conditions are permitted if described thoroughly.

The erosion damages can be defined as a progressive loss of original material from a solid surface due to mechanical interaction between that surface and a fluid, a multicomponent fluid, or impinging liquid, or solid particles. In particular impingement is a process resulting in a continuing succession of impacts between (liquid or solid) particles and a solid surface.

These particular tests method utilizes a repeated impact erosion approach involving a small nozzle delivering a stream of air containing abrasive particles which impacts the surface of a test specimen. This test method may be used to rank the erosion resistance of materials under the specified conditions of testing.
However, it is important to know that the rate of the erosion and the behavior of materials will depend on many factors concerning the conditions of service applications.
The erosion testing machine, or in general the apparatus for testing may be different, but there are some analysis devices and design characteristics that must be respected; in Fig. 4.12 it is showed a schematic equipment with the main part for an erosion testing machine.

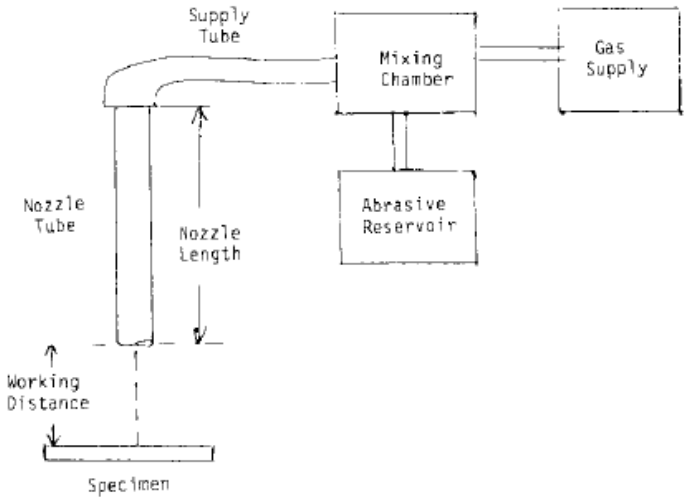

Fig 4.12 Schematic Drawing of Solid Particle Erosion Equipment [6].

As always deviations from this design are permitted; however, adequate system characterization and control of critical parameters are required. Necessary features of the apparatus shall include a means of controlling and adjusting the particle impact velocity, particle flux, and the specimen location and orientation relative to the impinging stream.

Various means can be provided for introducing particles into the gas stream, including a vibrator-controlled hopper or a screw-feed system. It is required that the system provide a uniform particle feed and that it be adjustable to accommodate desired particle flow values.

A method to measure the particle velocity shall be available for use with the erosion equipment. Examples of accepted methods are high-speed photography, rotating double-disk, the one that will be used in our tests, and laser velocimeter. Particle velocity shall be measured at the location to be occupied by the specimen and under the conditions of the test.

Setting all the best test conditions is essential retesting at least a couple of times, in order to get a range of data and verify if the tests are repeatable. After completion of the various tests, the goal of the analysis is to present a report, where, in addition to the main material characteristics of both specimen and erodent, should be presented all the parameters that could change during the test:

- temperature
- discharge velocity
- particles velocity
- time
- impact angle

Finally, in the report it is possible and important to plot, according to the parameters just seen, different types of results, as shown in Fig. 4.13 e 4.14, expressing the different relationship between variables of the equipment. The possibility of changing the values is critical to represent different conditions to which it may be subjected the actual material.

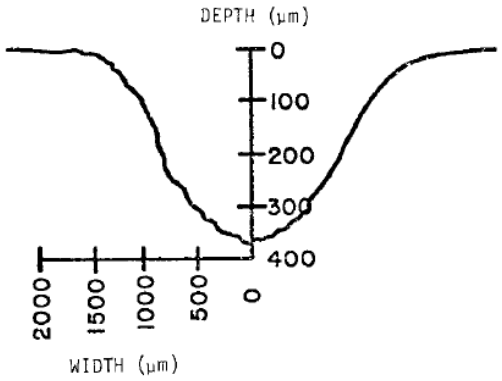

Fig 4.13 Example of Erosion Crater Profile for Steel [6].

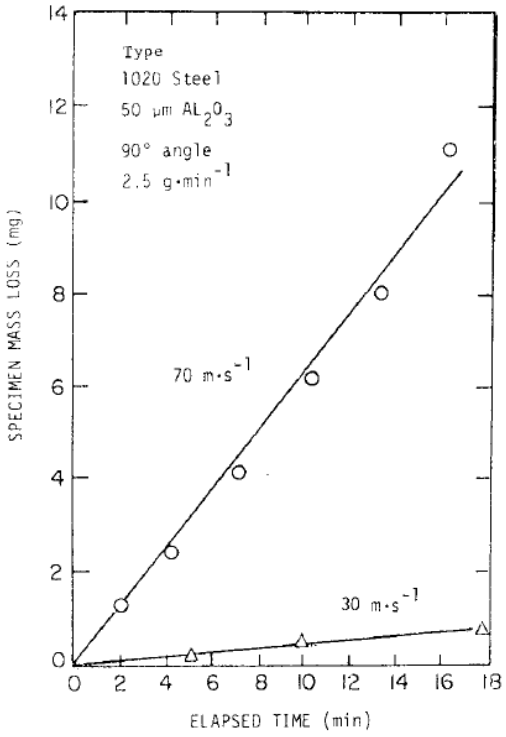

Fig 4.14 Two Example of Erosion versus time for Steel [6].

4.2.1 DESCRIPTION OF TEST DEVICE AND PROCEDURE

The experimental part continues with the actual analysis carried out in the company. As already mentioned the tests were carried out at the research center Tekniker IK4. The research center is a leader in the field of tribology, it counts several laboratories and a lot of developments regarding the analysis of contact behavior between different materials.

For completeness of presentation is necessary first to describe the types of materials used and the type of device for testing.

The main project *MUSIC* was developed for the analysis of the behavior of steel usually used for HPDC dies. Hence, it was tried to use materials that are mainly and currently adopted for the creation of dies, i.e. chromium-molybdenum hot work tool steels. In this category the most common are the H13 and H11, designated in this way according to European standards. Observing the structure that these steels have, were chosen to continue the analysis with two materials that present similar structure and properties, which were easier to access and machining 1.2738 BM and 1.2738 HH.

In order to verify the statement just expressed, and justify the use of a different material in the analysis, pre-tests were carried out in the laboratories of metallography by Tekniker. The analyzes [7] were done on specimens of both materials, in both cases it was found that the structures were very similar, as well as the properties of hardness.

Steel 1.2738		**C**	**Si**	**Mn**	**Ni**	**Cr**	**Mo**	**P**	**S**
BM	Nominal	0.450	0.40	1.60	1.20	2.10	0.25	0.030	0.035
	Measured	.35	0.20	1.30	0.90	1.80	0.15	Max	Max
HH	Nominal	0.26	0.25	1.48	1.05	1.30	0.70	0.015	0.003

Tab. 4.6. Measured (by optical emission spectrometer) and nominal (according to AISI) chemical compositions (wt.%) of 1.2738BM and 1.2738HH steels used in the study.

The first material is the BM (from now on this name will be used for simplicity), which has similar characteristics of H11 and, as you can see in Fig. 4.15, the crystal structure of the grains is very similar.

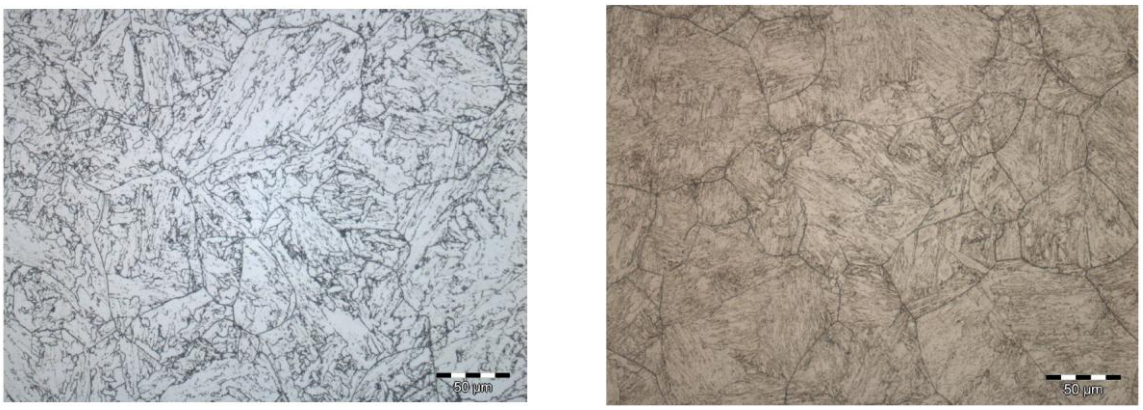

a. ***b.***

Fig 4.15 Similarity between the crystal structure of a. BM, and b. H11[7].

The second material that will be used during the experiments is an HH the steel, which again according to metallographic studies, it results to have a crystal structure very similar to steel H13, as shown in Fig. 4.16.

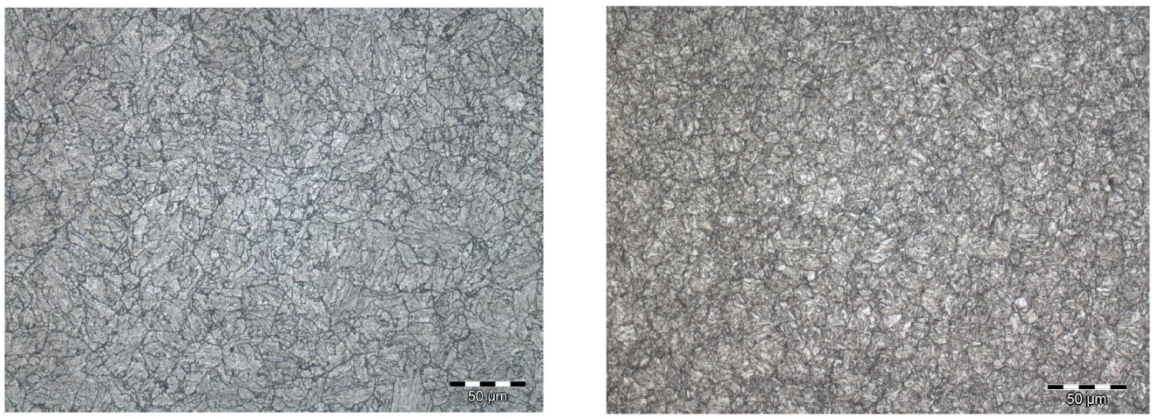

a. ***b.***

Fig 4.16 Similarity between the crystal structure of a. HH, and b. H13 [7].

In Table 4.7 are also showed the hardness values obtained from the same analysis as previously nominated. The values refer to steel BM and HH and are obtained using the standard *S/UNE-EN ISO 6507-1:2006*. It is presented the individual values and the average values, along with the uncertainty values used for the calculation. Finally, the conversion of hardness was carried out following the standard *ISO-18265:2013*.

Specimen	Area	Individual Values	Average Values	Type	HRC Conversion
BM	Superficial	274 – 270 – 270	271±7	HV 10	26.4
HH		287 – 283 – 289	286±7		28.5

Tab. 4.7 Hardness values of BM and HH specimen [7]..

Both steels both can be catalogued as hardened and tempered plastic mould steel. In fact according to online sources, they are mainly used for steel dies in plastic injection. Because of the Ni-addition there is no hardness decrease in the center of large sizes over 400 mm thickness. A special melting technology offers good machinability.

The main applications are large dies (over 400 mm thick ness) for plastic processing, mould carrier frames for the plastic moulds, components for general mechanical engineering and tool manufacture.

The types of specimens available to the experiment were standardized and created especially for the holder of the machine. They have parallelepiped-shaped, and depending on the impact angle, they have different sizes and bevels.

Fig 4.17 Representation of used specimen.

In Fig. 4.17 are presented sketches of the samples, with and without bevels.
The dimensions are directly related to the type of holder, in fact, as will be described in the part of the machine, depending on the impact angle (α) between the erodent flow and the base material, changes the holder type for the experiment.
The specimen size used for this particular type of machine are 25x25x5 mm, for the impact angle of 90° samples, or 25x21x5 mm for the impact angle of 45°/15° samples.

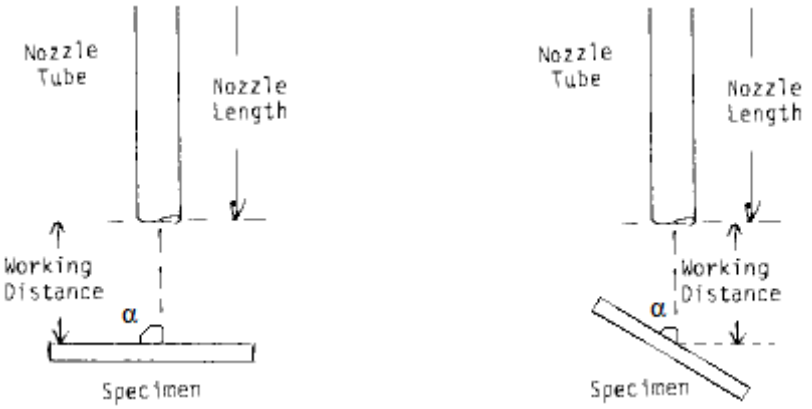

Fig 4.18 Variation of the impact angle for the analysis [6].

Fig. 4.19 show the three different types of specimen respectively used for the analysis at 90°, 45° and 15° degrees.

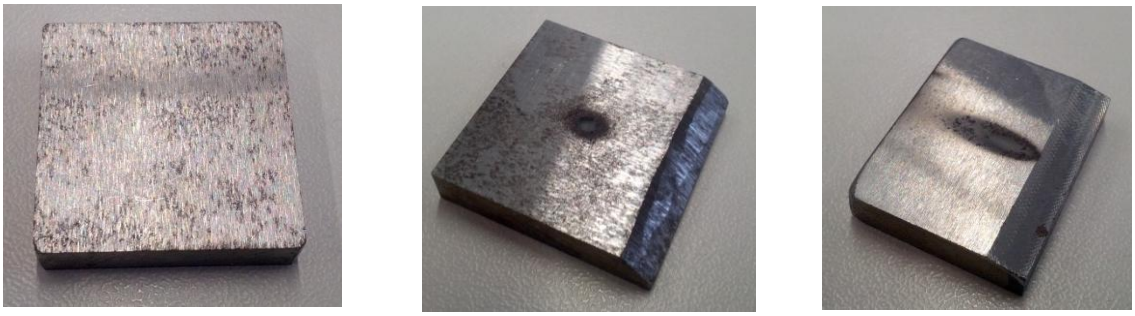

a. ***b.*** ***c.***

Fig 4.19 Actual specimen used during the experiment at α=90°(a), α=45°(b), α=15°(c).

As can be noted from the images the specimen used for the analysis with a flow at 90° is completely flat and without bevels, while the one for the analysis with an angle of 45° has slightly smaller dimensions and a chamfer, and finally the specimen used with the angle of 15° is dimensionally smaller with a bevel.

After treating with a general description of the specimens, the analysis continue with the description of the procedure for the preparation of parallelepipeds to the experiment. First it was necessary to adapt some pieces to the different holder size, using a mechanical grinder, in order to create the bevels and reduce the relative dimensions.

The preparation proceeds with the cleaning of the specimen by the use of an ultrasound machine, which acts through a water container where is immersed the bowl with the specimens. The cleaning process takes five minutes, and is done before in a bath of ether, which ensures thorough cleaning of the specimen, and then another five minutes in a bath of acetone, that remove all the residual of acetone on the sample.

This process is widely used for the cleaning of many components before the testing, especially if it important to measure as a variable the weight loss. Hence to get this weight difference, after cleaning the samples the process continues taking at least 3 weight measurements on each sample. It is used a precision balance that reports as a result a value with at least four decimal numbers, since the difference between the measurements is minimal.

The process for the preparation of the specimen can be considered complete, in Table 4.8 is shown an example of how each sample is catalogued, and with an excel spread sheet is also defined the average of the initial weight obtained by a simple arithmetic mean.

	Specimen n°	weight.1[g]	weight.2[g]	weight.3[g]	Arit. mean[g]
BM Steel	1°	23,4393	23,43937	23,43869	23,43912
	2°	23,48002	23,47962	23,48018	23,47994
	3°	18,88592	18,88604	18,88592	18,88596
HH Steel	1°	23,93469	23,93475	23,93436	23,9346
	2°	23,92485	23,9249	23,92496	23,9249
	3°	18,86056	18,86044	18,86038	18,86046

Tab. 4.8 Example of weight measurement and of arithmetic mean.

The description of the experiment continues with the introduction and description of the other key element in the study of the damage, the erodent. Given the need to study the behaviour of steels in contact with the aluminium, to highlight the best state of contact, it was used as the erodent, an aluminium oxide commonly called ALUMINA.

Fig 4.20 Alumina in the most common form.

Aluminium oxide is a chemical compound of aluminium and oxygen with the chemical formula Al_2O_3. It is the most commonly occurring of several aluminium oxides, and specifically identified as aluminium(III) oxide. It may also be called *Aloxide*, *Aloxite*, or *Alundum* depending on particular forms or applications. It commonly occurs in its crystalline polymorphic phase α-Al_2O_3, in which it composes the mineral corundum, varieties of which form the precious gemstones ruby and sapphire. Al_2O_3 is significant in its use to produce aluminium metal, as an abrasive owing to its hardness, and as a refractory material owing to its high melting point.

During the tests the alumina used was provided by the company and used as a refractory material. The type used had an average particle diameter of 50 µm made of fine and very light flakes. It is hygroscopic and has a tendency to form lump when it absorbs moisture. This element as already seen in the samples of steel, requires a preparation before putting into operation, in fact this type of alumina must be heated previously to 100˚C and maintain at this temperature for at least 24 hours. The furnace should have provision to remove evaporated moisture otherwise it will condense again. This operation is necessary to remove all the moisture that is formed leaving unused material, thus avoiding that the material blocks inside the machine during the discharge phase. If done correctly you will have a steady stream during the experiment.

Fig 4.21 Photomicrograph of 50 µm Al2O3 particles used in testing [6].

The last element useful for the purposes of description of the procedure of the experiment is the type of machine used for testing. As seen in the introduction of the chapter, the devices to perform the analysis of erosion must follow certain standards regarding operating parameters.

The machine used in the company is called ***Air Jet Erosion tester tr-471*** provided by *Ducom tribology*, an Indian company. As reported in the manual the machine can be used to rank the erosion resistance of materials using a repeated impact erosion approach. The method involves using a small nozzle delivering a stream of gas containing abrasive particles that impact the surface of a test specimen. Test parameters such as particle velocity, erodent feed rate, temperature, test duration, and orientation of specimen can be varied. The fields of application are linked to the analysis of the erosion damage and behavior.

This type of device gives some features and benefits:

- Conforms to ATM G76 international test method.
- Specimen, erodent and air are heated up to 400°C.
- Highly controlled and accurate erodent delivery system.
- Erodent feed rate is variable.
- Velocity of impingement is variable.
- Angle of impingement is variable in step of 15°.
- Easy to replace nozzle.
- Erodent velocity, erodent feed rate, temperature, test duration and angle of impingement can be pre-set.

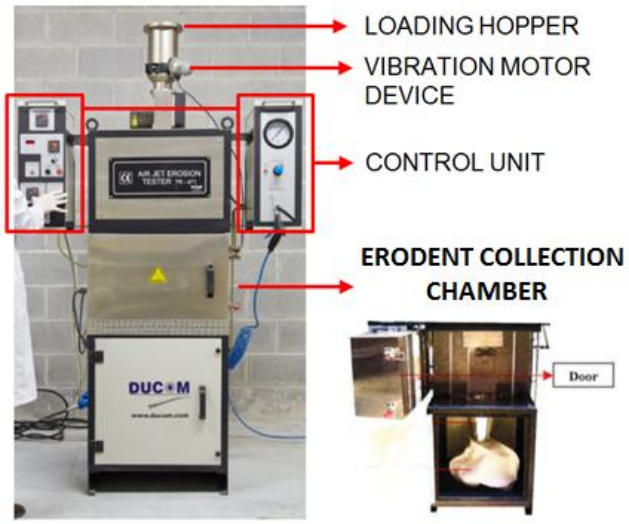

Fig 4.22 Schematic of the machine used for the erosion analysis.

The machine-system, shown schematically in Fig. 4.22, consist of a loading hopper, which has a total capacity of about 3 Kg of erodent. Hopper allows erodent to fall under gravity through throat on to a wheel. The wheel is driven by a motor through timer belt and a motor speed, both controlled by an AC drive. The vibration motor device helps the smooth flow of alumina from the hopper, higher the speed greater is the discharge rate and vice versa. The erodent pass through narrow throat on to wheel, the speed decreased to get very low discharge rate. The discharge is measured by weighing the actual amount of erodent collected for known interval of time, as it will be explained later for the calibration test.

There are two control units, one is an electrical controller box that supplies power to the heaters and measures the temperature of the specimen; besides this presents the values of the discharge frequency, the air temperature and the setting time for the experiment. The other unit is a pneumatic controller box, from here you can control the air direct to the mixing chamber, which pass through an ON & OFF valve, contactor and a pressure regulator. The inlet pressure to mixing chamber is set by turning the knob of pressure regulator, the pressure value is indicated on a gauge fixed above.

Very important component of the system is the mixing chamber, represented in Fig. 4.12, it consist of a heat resistance steel tube, where, on one end is fixed the nozzle holder and on the other end is connected to erodent feeding system seen before. Three plates are fixed on this tube and the ends are connected to terminal of transformer for heating. An heating

resistance steel tube surrounds this tube and is connected to air inlet. The unit is mounted vertically on furnace top.

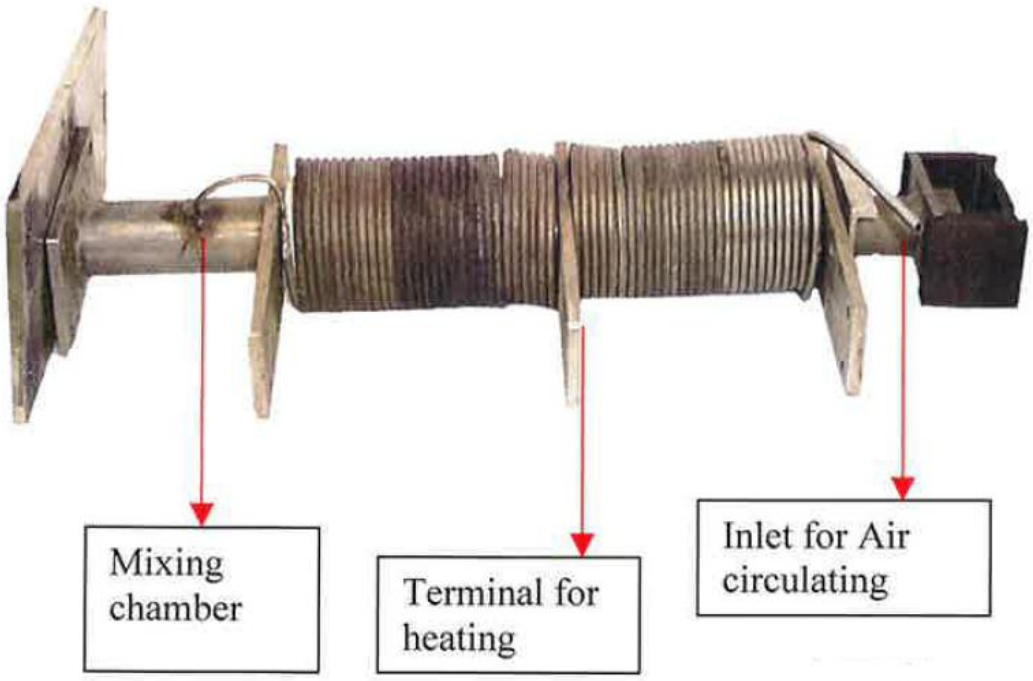

Fig 4.23 Scheme of the mixing chamber system [8].

All the mixing chamber system it is mounted within the Furnace unit, this part accommodates both heater for specimen heating and heater for air, this one in particular is heated by heating the tube through which air is flowing. The mixing chamber is covered by insulated material to prevent heat loss. The heater are mounted at the bottom of the furnace, they are made of two halves, one half remains on fixed portion of furnace and other is fixed to the door. When the door opens, the heather halves separate and the specimen is exposed for easy removal. The outer body of furnace is covered by a steel body, there is a connector for air inlet fixed on left panel, on the top of the furnace is mounted the erodent feeding system and below is placed the erodent collector.

The nozzle is made of tungsten carbide material, having outer diameter of 12 mm, and inner diameter of 1.5± 0.075 mm and a total length of 50 mm. along with machine ceramic nozzle of the same size mentioned before.

Table 4.9 summarizes all the technical specifications of the machine described above.

Sl No	Part detail	Range
1	Nozzle bore diameter	1.5 mm
2	Working height from floor	650mm
3	Hopper height from floor	2210mm
4	Nozzle height from floor	1010mm
5	Electrical controller height from floor	1570mm
6	Pneumatic controller height from floor	1570mm
7	Erodent specification	50micron, Al_2O_3
8	Hopper capacity	3kg
9	Erodent discharge rate	1 to 5 gm/min
10	Temperature	Ambient to 400°C
11	Erodent Velocity	30 to 100 m/sec
12	Angle of incidence	15°,30°,45°,60°,75° & 90°
13	Sample size	25 x 25 x 5mm
14	Erodent motor speed	Minimum speed 1rpm
		Maximum speed 70 rpm
15	Pulley ratio	1:3
16	Over all size of the machine L x W x H	1250x110x2210mm
17	Weight of the machine	kg
18	Floor size L x W	1500x1500mm

Tab. 4.9 Mechanical specifications.

4.2.2 CALIBRATION TESTS

After describing the main elements of the experiment and their main characteristics, before starting the actual test, it is important to introduce few operations designated as calibration procedures. This type of operations are performed each time that the machine is used for a new type of analysis or experiment. Procedures are described in the manual provided by the builders of the device, and then adapted to the company's standards for acceptable but most relevant repeatable results, and are done in order to ensure proper operation of the machine. Performing the calibration test is essential, so that once obtained the results, they are guaranteed and acceptable.

The manufacturers ***Air Jet Erosion tester tr-471*** of have planned three types of calibration operations:

- DISCHARGE RATE
- PARTICLES VELOCITY
- TEMPERATURE

The first operation is performed to analyze the amount discharged during a given period. The determination of the erodent **discharge rate** is done by collecting the erodent coming out of wheel in a container without passing air pressure for a given duration, which in this case it was chosen of **5 minutes.**
In order to obtain accurate results it was decided to follow the procedure given in the manual of the machine:

Weigh an empty bag or a empty container, the container used is a packet supplied by the company, that after few measurements done with the same precision balance used before, appear to have the average weight of 0.73g.

Fasten the container to the nozzle of the machine, .he packet was ensured at the exit of the nozzle using a fastening system.

Activate the system with a determined frequency of discharge, thanks to the control unit of the machine, it was possible to fix a frequency value different for each test, in order to obtain a wider range of results. The frequency chosen value were: 2, 3, 4, 5, 7.5 [Hz].

These values have been chosen relatively small and with small dispersion, so that the final analysis had comparable results.

Extract the container and weigh it again, after finishing the process, weighing the container extracted, it was possible to obtain the gross weight (packet plus discharged alumina) of the sample, using the precision balance.

Analyze the difference of weight for know the quantity of alumina discharged, after entering the results obtained from different measurements in a spread sheet, it is easily obtainable the net weight of the alumina discharged using the values difference. Therefore is obtained the quantity of erodent discharged in a given period.

Repeat the same operation with different frequencies, as said before to obtain a curve of values, it is necessary to test the discharge rate at different frequencies, and it is also important to perform at least two measurements for each frequency to get a mean of the corresponding value.

Finally to obtain the average amount of alumina discharged at a given frequency for one minute, is done simply the ratio of the value obtained and the duration of the experiment (5 min.). It is thus obtained a curve plotted in Graph. 4.5 that has, as abscissa values of frequency of the motor, and as ordinate values the amount of alumina discharged expressed in 1 minute. Tab. 4.10 shows the weights obtained during the analysis relating to frequencies, and the difference between net and gross weights.

Hz	Weight.1 gross [g]	Weight.2 gross [g]	Packet weight [g]	Weight.1 net [g]	Weight.2 net [g]	Aver. Weight [g]	Discharge rate [g/min]
2	4,769	5,385	0,73	4,039	4,655	4,35	0,87
3	10,459	9,99	0,73	9,729	9,26	9,49	1,90
4	14,337	14,191	0,73	13,607	13,461	13,53	2,71
5	16,536	17,696	0,73	15,806	16,966	16,39	3,28
7,5	25,64	26,594	0,73	24,91	25,864	25,39	5,08

Tab. 4.10 Discharge Rate analysis values.

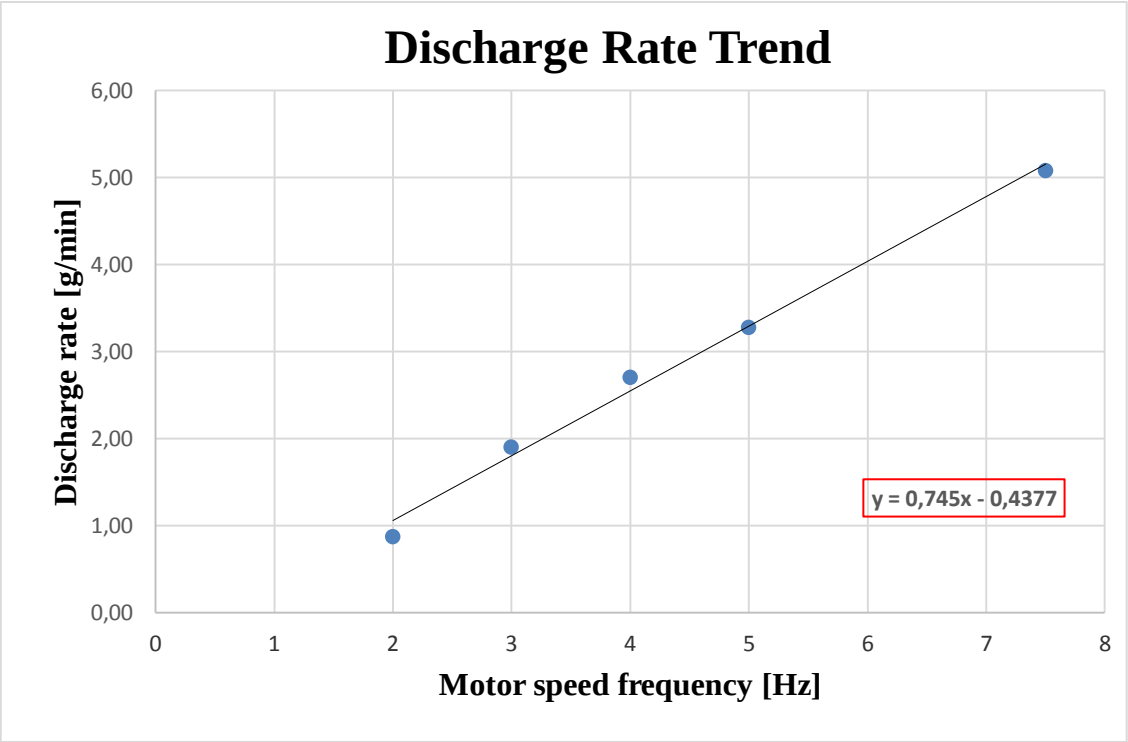

Graph. 4.5 Discharge Rate Trend.

In the chart above can be seen the measurements represented by the blue dots, obtained during the experimental part, while the black line is a tendency line calculated by the software. The equation that identifies this trend line, is *y=0.745x-0.4377* and expresses a linear dependence in the behavior of the machine.

This increasing trend is desirable to repeat the experiments, in fact as can be guessed, at higher frequency (speed) of the motor correspond a higher discharge rate.

It becomes clear from the data results that the calibration was successful, therefore it is guaranteed the correct operation of discharging of the machine.

The second operation necessary for the calibration of the device is the analysis of the speed of the particles of erodent within the system. As described previously, the parameter **particles flow velocity** is variable and is operator's choice. This choice is made according to the speed required, and varies by changing the corresponding value of air pressure through the pneumatic control unit. It must be verified that to a greater pressure corresponds a greater velocity of the particles.

Also in this case it was decided to follow the procedure given by the manufacturers, and in this particular case the calibration of the velocity is made with the help of an outside system.

The system, fig 4.24, consist of rotating part and a controller unit. The motor part it is made of two different flanges with a common hub, the bigger flange has a side that is held inside the motor, and the other end is fixed to a smaller disc with two holes. As the disc rotates the holes exactly go below the nozzle to allow a small quantity of erodent to pass through it and strikes on the bottom flange, the gap between two flanges is maintained at 30mm. The double disc system is clamped on a holder driven by an external motor. The holder has a T shape which easily slide into special bracket on mixing chamber. The motor speed used for the rotating system is 10.000 rpm.

The controller unit starts the motor and could be set manually in order to achieve the desired speed.

a. *b.*

Fig 4.13 Double disc system for particles velocity measurement: a. Rotating part. b. Controller unit.

Apply a thin layer of permanent ink on top surface of the lower disc, it will be the area subject to erosion of the flow.

Ensure the motor device into the mixing chamber, aligned with the noozle axis, operation described previously, which allows the smooth passage of the particle flow.

Close the front door, switch on the electronic control box and set:

D.S (discharge speed)= 10Hz
T.D (time duration)= 4 min,
M.S (motor speed)= 8000rpm.

These are the standard values indicated for the operation of calibration to set on the Electrical Controller Unit. These values remain the same for all the tests, the parameter that will change will be the air pressure and therefore the speed of the particles.

Activate the system, (start motor) and run for the set time.

Switch off motor, open the door and clean the motor system, it is really important to clean the system, in order to obtain more accurate measurements.

Draw a straight line at the edge of the erodent mark (min, max) on the disc, in this operation it is essential to use a ruler to delimit the sign of erosion on the disc. Fig. 4:25 schematically shows the procedure for measuring the angle A°.

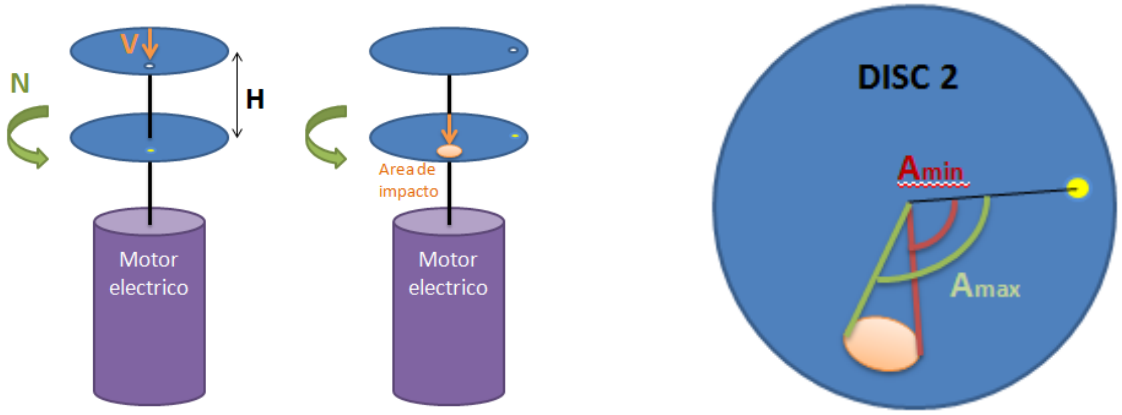

Fig 4.25 Measurement Scheme of the angle A°.

Calculate the velocity using the equation:

$$(V) = [(H) \cdot (N)] \cdot (1/A) \qquad 4.5$$

V= Velocity of the particles [m/s];

H= Distance between two disc, that is a costant parameter **0.03** [m];

N= Revolutions per second of the double disc system. [rpm/60];

A= Angular displacement in radiant, (angle of incidence/ 360°) [rad].

During the calibration operation, the motor speed is set at **8000** rpm, hence the only parameter to detect for the equation just presented is the angle of incidence A°.

After remove the paint, repeat the same operation with different pressure, it was decided to calibrate the device with four pressure values, well distributed, and representing a minimum and a maximum particles velocity.

The values used were 0.15, 0.3, 0.8, 1.5 [kg/cm^2].

For each measurement were performed two tests, to avoid mistakes and to make the results more acceptable. The obtained values, including the values for the corresponding velocity, calculated with Eq. 4.5, are reported in Table 4.11.

Pressure [kg/cm^2]	Angle min 1 [deg]	Angle min 2 [deg]	Angle max 1 [deg]	Angle max 2 [deg]	Media 1 [deg]	Media 2 [deg]	Media Tot	Particles velocity [m/s]
0,15	48	33	67	66	57,5	49,5	53,5	26,91588785
0,3	28	21	52	21	40	21	30,5	47,21311475
0,8	17	11	37	33	27	22	24,5	58,7755102
1,5	9	7	29	24	19	15,5	17,25	83,47826087

Tab. 4.11 Particles velocity analysis values.

Plotting the results, it is obtained a curve plotted in Graph. 4.2 that has, as abscissa values of pressure of inlet air, and as ordinate values the values of the particles velocity. The blue dots indicate the values from the experimental part, the black line is a tendency line calculated using a spread sheet.

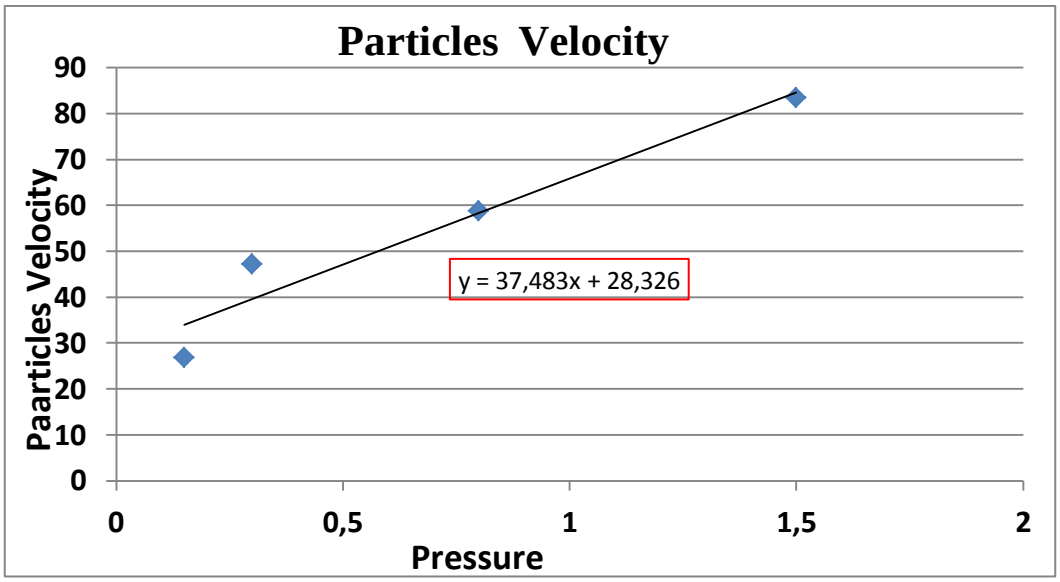

Graph. 4.6 Particles Velocity Trend.

From the graph it can be noted that the calibration was successful because at higher values of pressure, match greater values of velocity. Although there is a certain scattering between the experimental values and the trend line, it can be considered a linear relationship between pressure and velocity.

Thanks to this type of graph and the trend line, we were able to identify two fundamental values for the following tests. In fact, as will be explained in the next paragraphs, the analysis of erosion on the samples, must be performed at maximum and minimum values of the particles velocity. .

The chosen values are identified by the red lines present in the image 4.26, and are 0.2 and 1.5 [kg/cm^2].

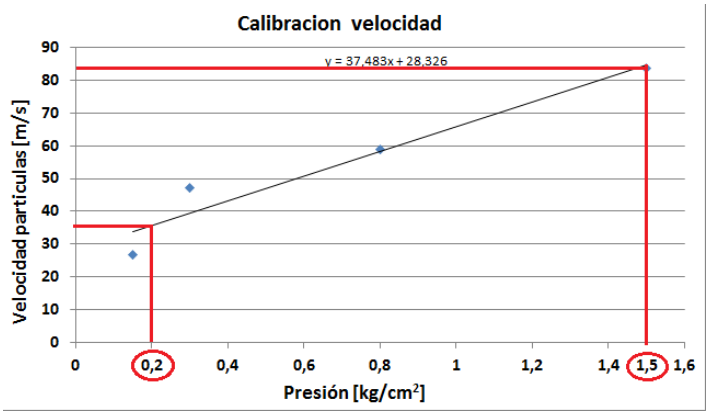

Fig 4.26 Particles Velocity trend with chosen values for the analysis.

The last calibration operation is related to the temperature variations and the heating unit. As previously described, the system has the possibility of heating the specimen at high temperatures in order to verify the behavior of this in different conditions. Before starting the test it is important to ensure that the heating unit bring the sample at the set temperature. Therefore to calibrate accurately, the test requires a heating plate as an external system, and a reference thermocouple, that were provided by the company.

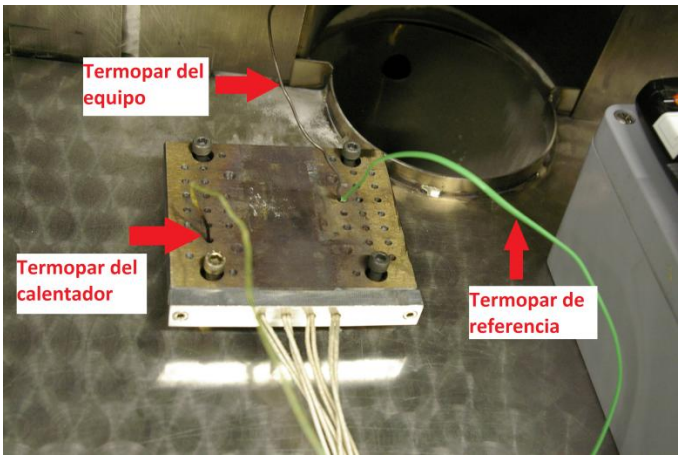

Fig 4.27 Temperature Calibration System.

As done for the previous tests, the calibration steps are referred to the procedure supplied by the manufacturer.

Place the plate near the machine and turn it on, it refers to the external plate.

Connect both the thermocouple of the machine and the reference one to the heating plate, the device is equipped with a thermocouple which is used as a sensor for PID control, the other is external.

Maintain 50˚c and compare with the display on PID module, in this phase the values shown on the electrical box and the external thermocouple must coincide, ensuring a good operation.

Control both the set temperature, on thermocouple and pid display and write it down

Repeat the test with other values 100˚C, 200˚C, 300˚C, it is important to repeat at different temperatures to verify the performance of the machine is constant.

The test results are reported in Table 4.12, where it is highlighted the difference measurement between the thermocouple of the machine and the external one. It can be noted that at low temperatures the difference is minimal, while at high temperatures the variation between the two measurements is greater; this effect can be caused by the heating time of the machine, that once received input, takes a longer time to stabilize.

Machine Temperature [°C]	Heating Plate Temperature [°C]	Variation
55	56	-1
98	100	-2
198	200	-2
290	280	10
351	340	11

Tab. 4.12 Heating System Temperature analysis values.

Also in this case it is possible to affirm that the calibration was successful, considering that the higher temperature that will be used during the test will be 100°C.

The instrument used for data treatment is a statistic model defined **Linear Regression** in statistics is an approach for modeling the relationship between a scalar dependent variable *y* (response) and one or more explanatory variables (or independent variables) denoted *X* (control factors). The case of one explanatory variable is called *simple linear regression*. For more than one explanatory variable, the process is called *multiple linear regression*, as in the case of the analysis conducted. Multiple linear regression attempts to model the relationship between two or more explanatory variables and a response variable by fitting a linear equation to observed data. Every value of the independent variable *x* is associated with a value of the dependent variable *y*. In linear regression, the relationships are modeled using linear predictor functions whose unknown model parameters are estimated from the data. Such models are called *linear models*. Most commonly, the conditional mean of *y* given the value of *X* is assumed to be an affine function of *X*; less commonly, the median or some other *quantile* of the conditional distribution of *y* given *X* is expressed as a linear function of *X*. Like all forms of regression analysis, linear regression focuses on the conditional probability distribution of *y* given *X*, rather than on the joint probability distribution of *y* and *X*, which is the domain of multivariate analysis.

4.2.3 DESIGN OF THE EXPERIMENTS

In order to analyze the behavior of steel subject to erosion and the damage due to the different operating conditions, have been planned many types of tests, which will be differentiated by the parameters set initially.

The design of the experiment begins by analyzing the basic parameters of the experiment, already seen in the previous section about the description of the device. The next step is define the parameters so-called fixed that will not vary during the entire analysis and the variables one that could be changed depending on the desired conditions.

The parameters that were fixed during the entire analysis are:

- Discharge velocity = **3 Hz**
- Time = **10 min**

The parameters that have been changed are:

- Material
- Impact angle
- Temperature
- Particles Velocity

The number and type of tests carried out in the entire analysis were planned taking into account of the tests already carried out on the same project, and also trying to recreate the working conditions of the dies.

Therefore it was decided to submit both materials to low temperature (~25°C) and high temperature (100°C) during the tests.

Then have been chosen three different angles of impact, which represents the various conditions of incidence of the erodent on steel, namely, 15°, 45°, 90°.

Finally it was decided to use maximum values of the particles velocity for all types of impact angle, to verify the different behaviors; on the specimens inclined by 15° it has also been used a minimum value of particles velocity for the completeness of the analysis. The tests scheduling is shown in Table 4.13*a*. For the final analysis of the results and the develop of the model, it has been used few data taken from tests performed previously in the company referred to the preliminary draft. Some have the same test conditions planned, and are reported in Table 4.7*b*.

Test N°	Material [steel]	Impact Angle [α]	Temperature [°C]	Particles Velocity [Max/Min*]
1	HH	15	~25	Min
2	HH	15	~25	Max
3	HH	15	100	Min
4	HH	15	100	Max
5	HH	45	~25	Max
6	HH	45	100	Max
7	HH	90	~25	Max
8	HH	90	100	Max
9	BM	15	~25	Min
10	BM	15	~25	Max
11	BM	15	100	Min
12	BM	15	100	Max
13	BM	45	~25	Max
14	BM	45	100	Max
15	BM	90	~25	Max
16	BM	90	100	Max

**The maximum and minimum values, converted into pressure, are respectively Max=1.5Kg/cm^2,and Min=0.2Kg/cm^2.*

Test N°	Material [steel]	Impact Angle [α]	Temperature [°C]	Particles Velocity [Max/Min*]
1	BM	15	25	Min
2	BM	15	100	Min
3	BM	45	25	Min
4	BM	45	100	Min
5	BM	90	25	Min
6	BM	90	100	Min
7	BM	15	25	Max
8	BM	15	100	Max
9	BM	45	25	Max
10	BM	45	100	Max
11	BM	90	25	Max
12	BM	90	100	Max
13	HH	15	25	Min
14	HH	15	100	Min
15	HH	45	25	Min
16	HH	45	100	Min
17	HH	90	25	Min
18	HH	90	100	Min
19	HH	15	25	Max
20	HH	15	100	Max
21	HH	45	25	Max
22	HH	45	100	Max
23	HH	90	25	Max
24	HH	90	100	Max

Tab. 4.7 Test planned for the analysis.

The analysis is experimental, for this it is necessary to perform at least three tests for each type of condition, therefore the total number of the tests is 48.

The procedure of the experiment is very simple and repeatable for all kinds of tests with different parameters. For completeness is indicated the procedure, provided by the manufacturers which is equivalent to all the tests.

Fill the machine through the hopper with alumina, it is important that the alumina is heated and filtered before insertion to prevent the passage inside the machine of crystals of larger size.

Choose wich kind of material to analyze, the specimen of the material required has to be prepared as seen in the previous paragraph, also to accelerate up the process it should be done all different parameters tests planned with that material.

Choose the impact angle to analyze, this information affect both the specimen both the type of holder. As seen before to a different impact angle corresponds a different specimen holder and a different sample.

Set the specimen holder under the nozzle and close the front door, in this step is important to ensure that the specimen is correctly positioned under the nozzle, and that is securely fixed to the system.

Activate the system setting the wanted frequency of discharge, the time, and choosen pressure of air, these are the three parameters that are controlled by the machine, two of which as we have seen before are fixed.

Start the test and wait until the automatic stop, the system is configured that at the end of the set time, it shut down automatically.

Open the door and extract the specimen, after extracting the specimen it is necessary to remove all traces of alumina and preserve it from possible contact with other materials.

Repeat all these operation, changing the parameters request, completed the procedure for the experiment, the specimens are cataloged and ready to be analyzed.

The procedure for the analysis at low temperature and high temperature are equal, the only element that differs is the activation of the heating unit for the tests at 100°C, it is therefore slower the process in order to stabilize the temperature value.

The results for preliminary visual analysis, are shown in Fig 4.28, the pictures show two types of specimens tested. The central marks are left by the flow of the erodent.

It can be seen how different is, depending on the impact angle of the flow of the specimen.

a ***b***

Fig 4.28 Specimen tested at a (45°) and b (15°).

Completed the experimental phase, the tested specimens are ready for the phase of analysis of results, which can be built on two approaches, the erosion rate can be calculated through the lost mass, or using the mark to calculate the eroded volume.

The first approach is very simple, the sample is re-weighed according the same methodology seen in the preparation of the specimen, using a balance with ±0.001mg precision. The measurement is made at least 3 times to ensure the accuracy of the value and avoid measurement errors, from these three values it is calculated an average value that will become the final weight of the specimen eroded.

For each specimen is assigned a code, for every code, using a spreadsheet is easy to obtain the difference in weight, which can also be expressed as mass lost due to the damage given by the flow of erodent.

The code contains all the information about the process and the type of sample, and it is written as:

PRO-XX-YY-ZZ-MM-a/b/c

PRO= Name of the project;

XX= Impact angle[°deg];

YY= [°C];

ZZ= Particle velocity [m/s];

MM= Specimen material;

a= first test, b= second test, c= third test;

Example:

MUS-90-100-64-HH-a

MUS= Project MUSIC

90= 90° angle inclination from to the flow of alumina;

100= 100°C specimen temperature;

64= particle velocity → 64= 1,5 kg/cm^2 ;

HH= specimen steel;

a= first test.

The second approach is more demanding, is based on the volume eroded during the experiment, to calculate how much material has been lost. It is still based on the code of the specimen but is more complicated because requires the use of a confocal microscope. With this device you can get the value of the wear volume through a complete 3D topography, that using the calculation software is able to bring a direct result expressed in µm^3, but it requires a long time for each specimen.

The confocal system is also able to carry out a more simple. analysis of the profile of the print, namely profilometry, obtaining the maximum penetration depth of the mark, a faster process.

To perform this type of analysis it is necessary the use of a precision instrument, the ***Confocal Microscope***, that is a tool based on an optical imaging technique for increasing optical resolution and contrast of a micrograph by means of adding a spatial pinhole placed at the confocal plane of the lens to eliminate out-of-focus light. It enables the reconstruction of three-dimensional structures from the obtained images. This technique has gained popularity in the scientific and industrial communities and typical applications

are in life sciences, semiconductor inspection and materials science. A schematization of the operation of the confocal microscope is shown in figure 4.29.

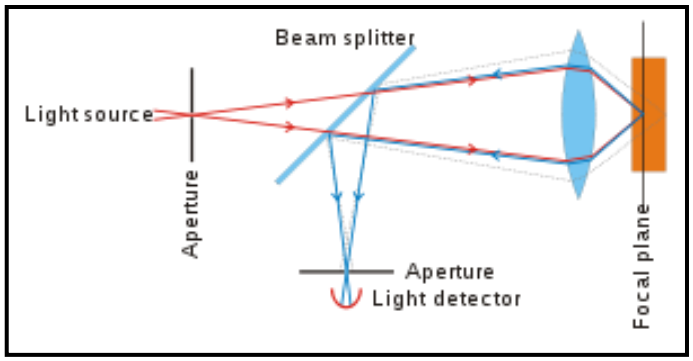

Fig 4.29 Principle of confocal microscopy.

The confocal microscope uses point illumination and a pinhole in an optically conjugate plane in front of the detector to eliminate out-of-focus signal - the name "confocal" stems from this configuration. As only light produced by fluorescence very close to the focal plane can be detected, the image's optical resolution, particularly in the sample depth direction, is much better than that of wide-field microscopes. However, as much of the light from sample fluorescence is blocked at the pinhole, this increased resolution is at the cost of decreased signal intensity – so long exposures are often required. The only one point in the sample is illuminated at a time, 2D or 3D imaging requires scanning over a regular raster (i.e., a rectangular pattern of parallel scanning lines) in the specimen. The achievable thickness of the focal plane is defined mostly by the wavelength of the used light divided by the numerical aperture of the objective lens, but also by the optical properties of the specimen. The thin optical sectioning possible makes these types of microscopes particularly good at 3D imaging and surface profiling of samples.

During the actual analysis carried out with the confocal microscope in the company, it was possible to carry out two different types of techniques for the analysis of the specimen and the degree of penetration inside the material. Both procedures require a thorough cleaning of the sample chosen, which will be positioned correctly on the sliding plane of the instrument. Using the software it is possible to decide on which area of the specimen carrying out the detecting, and in particular whether to make an analysis more or less detailed.

The most detailed is defined as a complete ***3D topography*** of the specimen, in this analysis were analyzed several layers based on the number set by the user then the system creates a graph in three dimensions (three axes) which reproduces the surface of the specimen, as shown in figure 4.30.

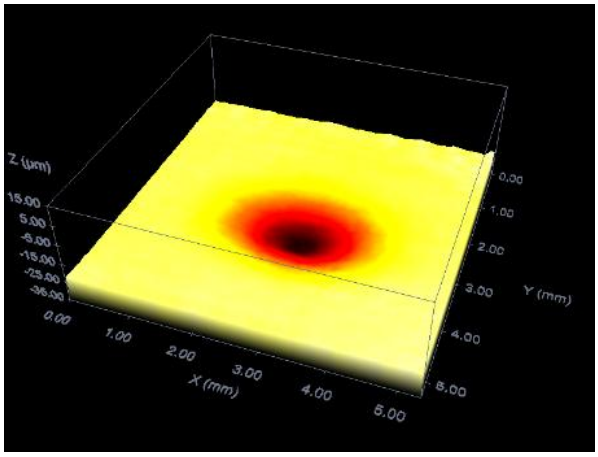

Fig 4.30 3D Topography of specimen.

This technique has several advantages, which are necessary for refined analysis, a **very accurate analysis** of specimen eliminates any measurement error; allows an **experimental calculation of wear volume**, with a high precision, and allows even a **calculation of maximum value of depth**, which is very important to understand how much the flow of alumina penetrates the inside of the specimen. However, the method presents a disadvantage: the analysis time, in fact, to create the complete topography of a single specimen requires about 20±30 minutes. This limit has made sure that it was used another type of technique to investigate the result of the test, given the high number of samples to be analyzed.

The alternative technique for analyzing the *print* of damage is defined ***profilometry***, and as you can be guessed, analyzes the development of the profile of the hole. The results reported are no longer expressed in 3D, but the trend is plotted in a two axes graph, that shows the relative dimensions of the damage expressed in µm. As can be seen in Fig. 5.3 the shape of the hole is similar to a peak, where the zero level is represented by the normal surface of the specimen. As noted above, this technique has the great advantage of taking few minutes to complete, in fact, the confocal microscope lens performs a single linear detection along the profile of the print dimension. The analysis parameter of distance is

defined by the user visually, that detects the area affected by erosion, and set the right number. The graph can get then the **maximum value of depth,** and also the **maximum value of width** of the hole. Through this technique, however, it is not possible to calculate the actual **wear volume**, because the analysis is not into three dimensions. Note that the same method of profilometry is used for measurements of surface roughness, thickening the analysis parameters, you can get the peak surface.

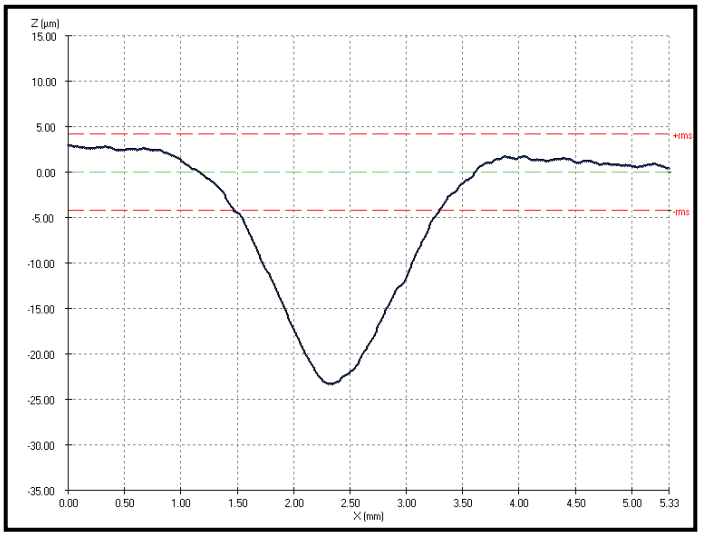

Fig 4.31 Profilometry of the specimen.

As this second process was faster it has been decided to use this method during the actual analysis, and calculate the wear volume in analytical form. To obtain the volume in analytical form, it was analyzed visually the mark left by the effect of the erosion, and then was approximated to half of an ellipsoid, since the surface was not always perfectly circular. The method used is shown schematically in Figure 4.32

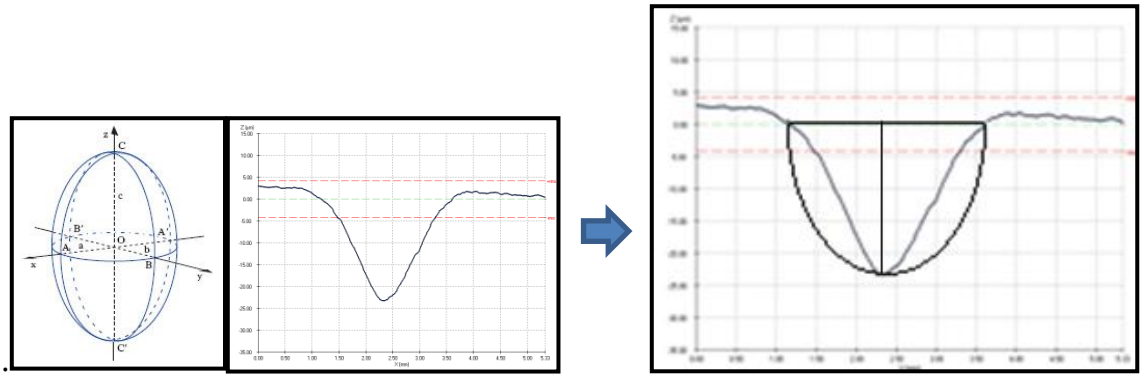

Fig 4.32 Analytical representation of wear volume using a half-ellipsoid.

Chapter 5:

RESULTS AND DISCUSSION

5.1 HIGH TEMPERATURE MECHANICAL FATIGUE TEST

The results of the experiment can be described going over the data of all the tests in order to understand what were the methodologies that led to the determination of the optimum parameters. In particular, it is possible to conduct an analysis both on the progress of the loading history obtained, and on the specimen to highlight the mode of failure that has occurred, using the Microscope system described in the previous chapter.

While the results for the proper fatigue test are given, it is necessary to consider what were the behaviors of tensile tests. As described above (§4.1.2), have been carried out 6 types of tensile test, 3 for each material (H11 and H13), at 300 °, 400 ° and 500 ° C, and the results are shown in the graph 4.4.

The first test lasted approximately 3 days, it was made on a H13 specimen and the temperature remained constant at 500˚C; the machine has carried out the scheduled experiment required. On the analysis of load cycles is it has been noticed that an error has occurred in the loading cycle.

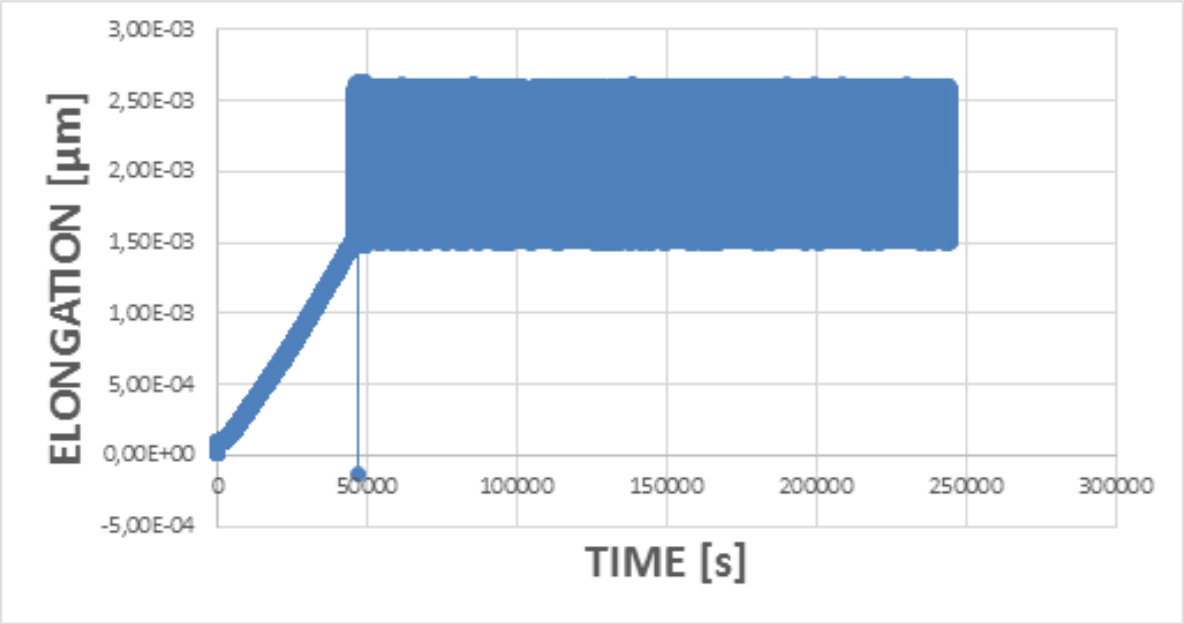

Graph. 5.1 Elongation vs. Time Cycles (I TEST).

As can be seen from the graphic 5.1, the calibration parameters for the amplitude of the cycles of deformation was helpful and has brought good results. The amplitude shown is the one set and the cycle are finally constant.

The problems have occurred in the performance of load. As shown in graphic 5.2, the system has reached a peak and then went into a continuous load decrease.

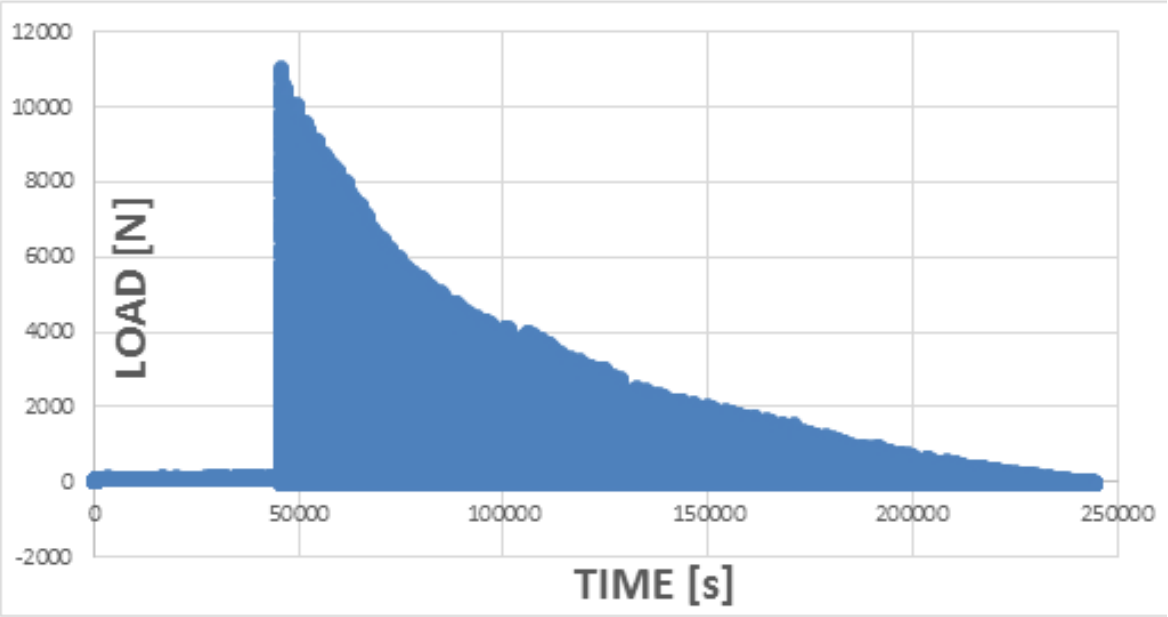

Graph. 5.2 Load vs. Time Cycles (I TEST).

Therefore it has tried to understand the possible causes that could led to such a trend, that may affected the behavior, and can be assumed in:

- Creep phenomenon: this phenomenon of creep may be deleted from the assumptions, because according to the literature the relation that indicates the temperature at which it develops the phenomenon is:

$$T°_{creep} \cong 0.40\, T°_{fusione} \qquad 5.1$$

and in the type of experiment carried out, is not reached the temperature of creep just defined, in fact:

$T°_{fusione}(\text{H13}) \cong 1427$ °C → $T°_{creep}$ (H13) ≅ 570.8 °C

- Deformation in Plastic region: as told before, when the system goes up to a limit too high the specimen deforms plastically. The deformation in plastic zone causes a steady decline of charge to perform the same deformation. So this can be considered a possible cause of the behavior of the load.

- Device problem with unscrewing lower nut: When the system goes down to the lower limit, if it has a load value too low (<600 N), the nut supporting the system is unscrewed, causing a continuous decrease.

In conclusion, the first test, which lasted about 2589 cycles, was not successful but reported incorrect results and thus the specimen breakage has not occurred as an effect of cycles of fatigue, but because of further testing under several loads conflicting, as can be seen from the Fig 5.1.
The images have been obtained through the use of the microscope described previously and describe the breakdown of only one specimen into two halves.

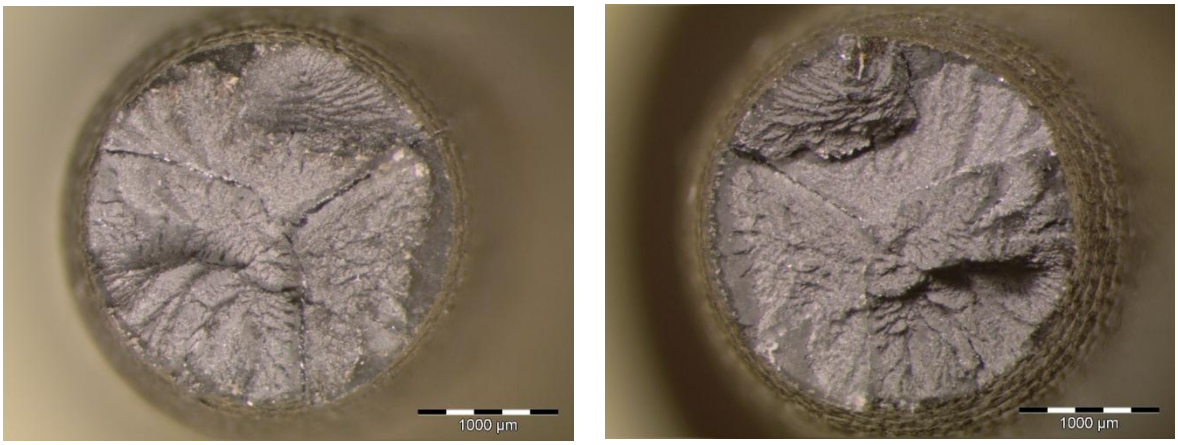

Fig. 5.1 H13 Specimen result from First HTMF Test.

The second test lasted approximately 14 days, the temperature remained constant at 500˚C and the machine has carried out the scheduled solicitation required. The test was stopped a few times, so it is divided into 4 parts.

This time the number of cycles achieved by the specimen was higher, around 18000 and trend of stresses is shown in graphics 5.3 and 5.4.

Given the very high number of data present in the charts, it was decided to report, for simplicity, schemes which are more qualitative, but always referring to the tested specimen. The qualitative graphics are easier to understand and more functional to the analysis of the experiment trend, and in this specific case, they show better the loading history.

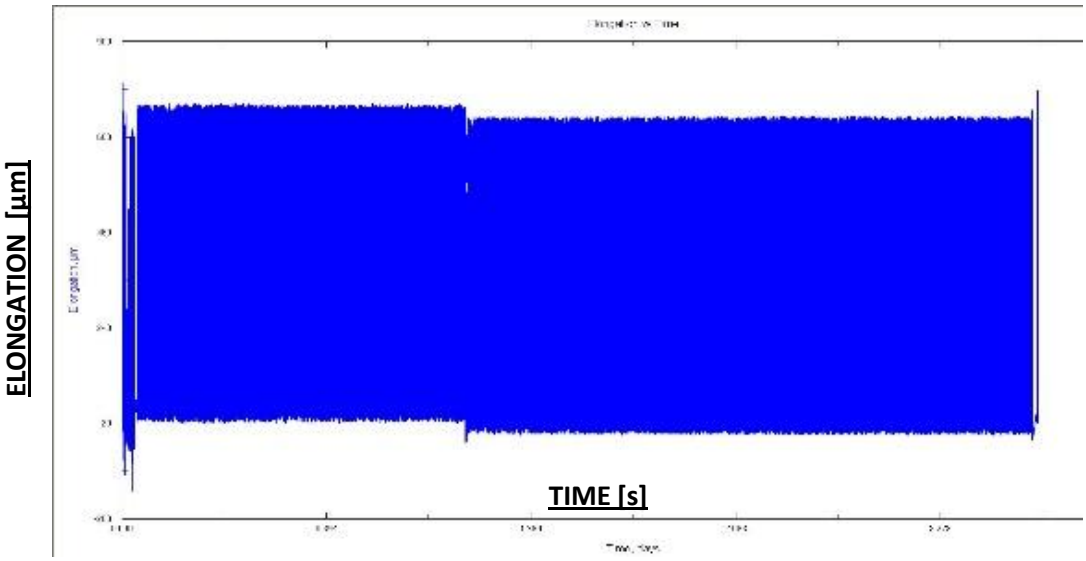

Graph. 5.3 Elongation vs. Time Cycles (II TEST).

As can be seen from the graphs, the trend of the cycles of deformation is constant, just as required.

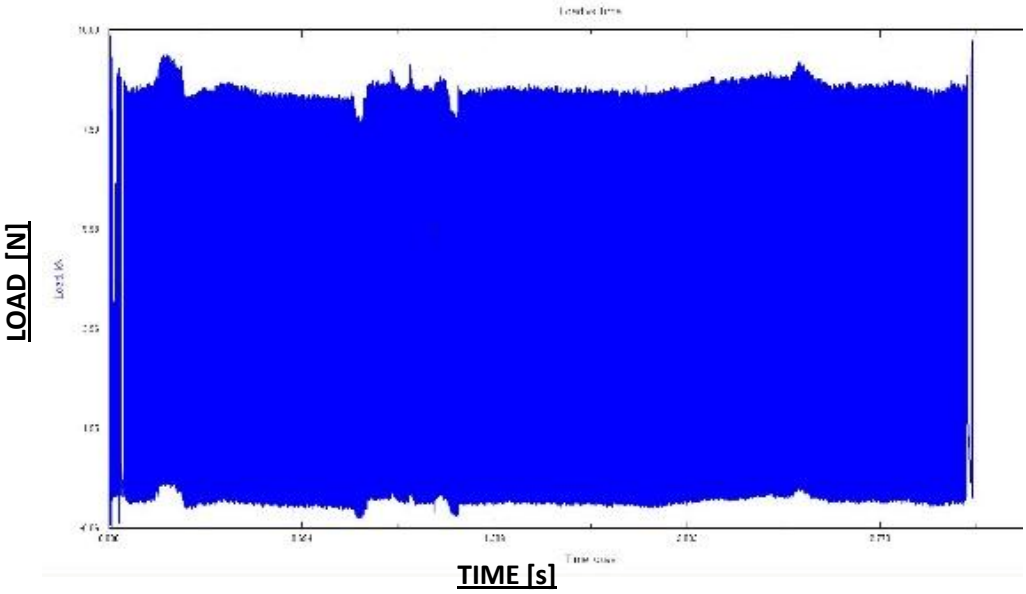

Graph. 5.4 Load vs. Time Cycles (II TEST).

The trend of the Load remains constant, even if decrease or increase, the interval of the cycles amplitude remains the same. The changing have solved the problems of the loading cycles.

The problem occurred in this test is related to its duration and consequently it's number of cycles. Although it is considered a test of *Low Cycle Fatigue*, exceeded 15000 cycles and the plastic field, the specimen did not have an instant break.

After analyzing the two sides of the specimen brought at break, Fig 5.2, it can be stated that the rupture caused by fatigue cycles is begun (see the initial cracks in red), but did not lead to the final break. In this case the breakdown occurred as a brittle failure, as can be seen on left side of the specimen.

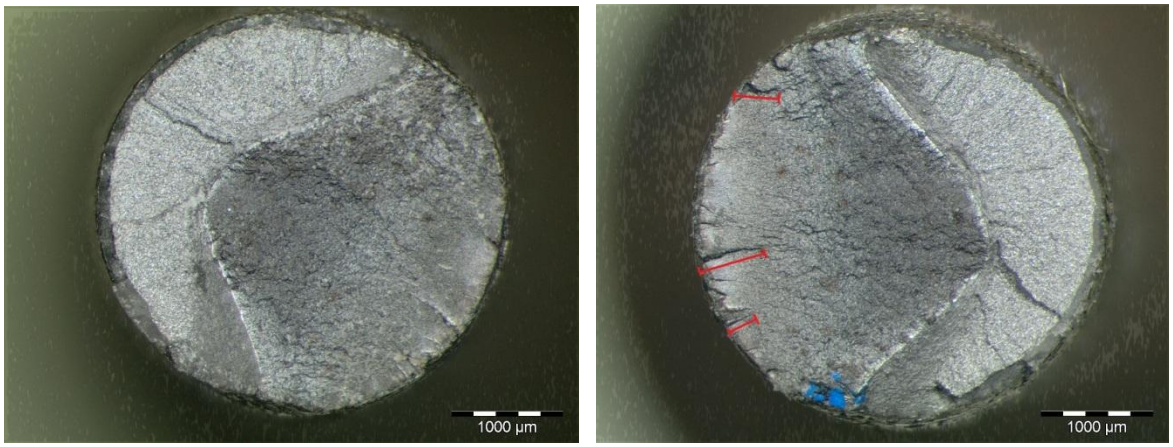

Fig. 5.2 H13 Specimen result from Second HTMF Test.

The third test lasted approximately 10 days, the temperature remained constant at 500°C and the machine has carried out the scheduled solicitation required. The test was stopped a few times, so it is divided into 3 parts.

The test was carried out very similar to the previous one, but as described in the paragraph *Design of the experiment* (4.1.3), some parameters have been changed. In particular during this test it was changed the range of amplitude, in order to obtain higher deformations and consequently a break at a lower number of cycles.

This change made in the parameters has brought the desired effect, reducing to about 11000 the number of cycles to failure.

The trend of the stresses are not shown because they are very similar to those of the previous test, and consequently follow a correct progress.

Analyzing under the microscope the specimen broken (Fig 5.3) it is possible to assume that the problem occurred in this test is related to its break, in fact as before the break that appears seem more plastic than for mechanical fatigue.

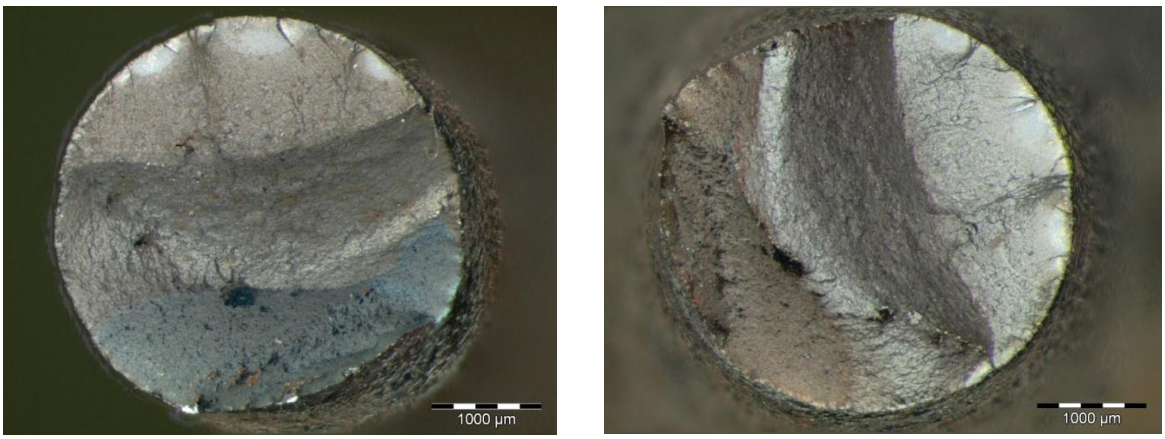

Fig. 5.3 H13 Specimen result from Second HTMF Test.

Even in this case the rupture caused by fatigue cycles is begun, but did not lead to the final break, this one occurred as a brittle failure, as can be seen on one side of the specimen.

It is obvious that the described tests and carried out so far are not sufficient to create a model that can describe the behavior valid for the steels subjected to high temperature fatigue. As the author mentioned previously the tests of this kind require a very long period of exposure, in fact, even though they are low cycles fatigue test, they last at least one week.

For this reason, additional tests than those described, were carried out subsequently using both steels, different deformation range and different temperature.

All the following tests were carried out taking into consideration the corrections in tests described above, and in particular are described in Table 5.1 with the deformation range and the relative cycles. It must however be clear that the results presented have still to be confirmed and in particular work is still in progress.

Some repetitions have been done, where it has left 5 minutes instead of 1 between each loop, to be sure that it arrives to 600N before restart. For 500ºC and 300ºC they are breaking at the same range of cycles, while at 400ºC endure much more.

Material	Stress (MPa)	Strain amp. (µm)	Temperature (°C)	Cycles
H13	908,2492082	390	500	140
H13	853,4016525	365	500	11028
H13	820,4931191	350	500	18000
H13	874,2324423	365	300	3983
H11	856,0505097	365	500	11690
H11	849,08648	365	400	8722
H11	855,6853547	365	300	5073

Tab. 5.1 Results from HTMF Tests.

High temperature tensile tests shown before in paragraph 4.1 are important to understand the mechanical behavior of materials, but dedicated fatigue tests are necessary to support the thermal stress calculation in order to have a reliable thermal cracks appearance prediction. The tests performed on the two steels H11 and H13 didn't show a big different between the two steels, what is reasonable regarding their equal Hardness.

The influence of the temperature have a combined effect that has been explained in the tensile tests part. At lower temperatures, the Young Modulus is higher for the same strain, at 300ºC it is applied higher stress, but it also would have higher maximum stress but on the other side lower maximum elongation. As a good correlation, the relation between the stress and cycles to failure was found and can be described as shown in the next graphic. This equation would be valid for a martensitic steel at 43HRC hardness:

The relation used is taken from both the theory and by regulations. In fact one of the most used methods to understand the residual cycles of a component under fatigue is to compare his behavior with standard Wöhler curves. This tool is usually used for a high number of stress cycles, but in our case, where the cycles are fewer, however, is useful.

Usually in cases with low number of cycles fatigue it is used the Manson-Coffin curve, in particular if the component works in elasto-plastic condition. This statement is also confirmed by the fact that the experiments are carried out in deformation control, as it is fixed the displacement amplitude.

Using the results reported above and the tests performed it is possible to try creating a model, that is typical of the approach of Fatigue Analysis.

For this has been made a curve Stress-Cycles to failure from these results. If it is plot the logarithmic values of the curves (typically made in fatigue), instead of real values, it is still much more lineal.

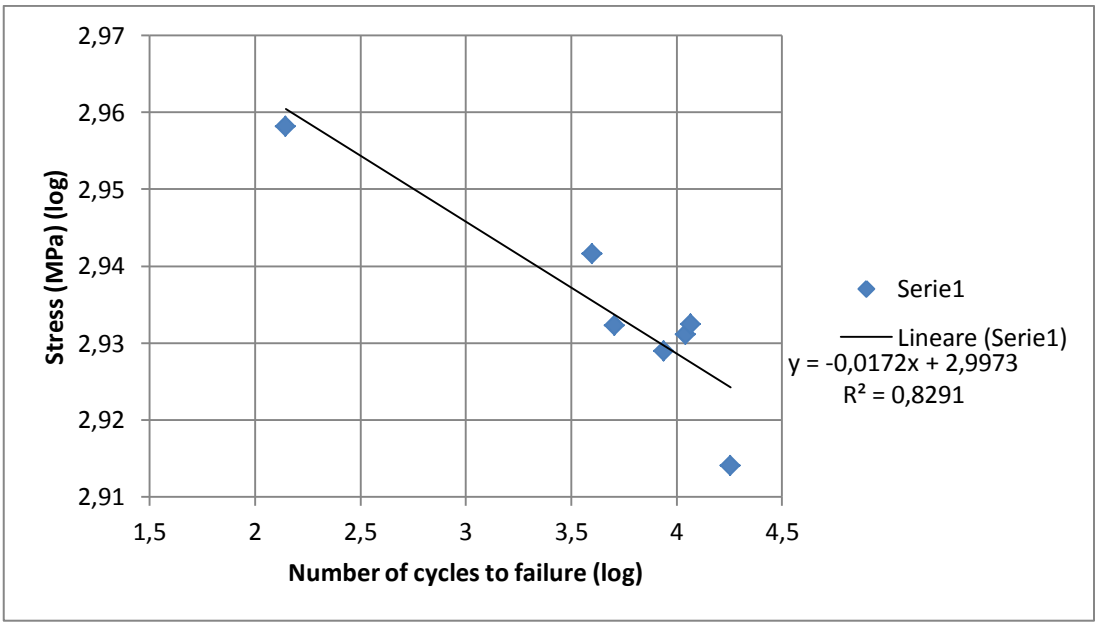

Graph. 5.5 Results of HTMF plotted as Stress vs. Number of Cycles.

As explained previously, the study is a work in progress, there are still many attempts and the tests to be carried out to achieve the certainty of a realistic model. However, already by the first results it can be noted that the values follow a certain trend, which is almost linear. This trend ensures both that the tests carried out up to now can be considered reliable, is that it is possible to predict thanks to a model and to the necessary boundary conditions for the residual life of a component subject to high temperature fatiguing cycles.

The equation that represents the linear trend on the graph, obtained by the use of a spreadsheet is described as:

$$y = -0.0172x + 2.9973 \qquad 5.2$$

y = Stress (MPa) (Log); x = Number of Breaking Cycles (Log).

This equation, of course, will be further validated making more fatigue tests as well with the results of Thermal Fatigue Machine.

5.2 EROSION TEST

As already introduced in the previous sections the results of the experiments can be divided in two categories. The first is the analysis of the amount of mass lost after the erosion process, which is obtained by comparing the same specimen before and after. For the estimation it is used a balance with precision of ±0.001mg, and making at least 3 measurements, from where you will get an average.

Code	Weight av. [g]	Impact angle [°deg]	Temperature [°C]	Air Pressure [kg/cm^2]	Mass Lost [g]	Mass Lost [%]
MUS_15_100_32_HH_b	18,81099	15	100	0,2	0,000236667	0,023667
MUS_15_25_32_HH_b	18,82271	15	25	0,2	0,001416333	0,141633
MUS_15_25_64_HH_a	18,75672	15	25	1,5	0,006763333	0,676333
MUS_15_100_64_HH_a	18,78919	15	100	1,5	0,018136667	1,813667
MUS_90_25_64_HH_b	23,92487	90	25	1,5	0,009723333	0,972333
MUS_90_100_64_HH_c	23,90766	90	100	1,5	0,011000333	1,100033
MUS_45_100_64_HH_b	22,70640	45	100	1,5	0,015424	1,5424
MUS_45_25_64_HH_a	18,77692	45	25	1,5	0,018426667	1,842667

Tab 5.2 Results from lost mass approach.

The percentage of lost mass varies from a minimum 0.02% to a maximum of 2%, then the order of erosion is not extreme, even for the most critical conditions.

As can be seen from the results shown in Table 5.1, the most influential factor on the erosion rate appears to be the air pressure, in fact it is possible to note the clear difference between the percentages of the specimens tested at the minimum particles velocity and maximum.

In fact it can be noted how the two specimens *MUS_15_100_32_HH_b* and *MUS_15_100_64_HH_a*, which differ only in the condition of particles velocity, have respectively a mass loss of 0.02% and 1.8%, proving that just described.

In second place as influencing parameter there is the inclination of the specimen or impact angle, which has as most influential value 45°, then 15° and finally 90° that, under the same conditions, shows the lower erosion rate. Unlike the previous parameter, the impact

angle, is not a parameter which always shows the expected results, but in some cases can affect more or less the specimen. Sometimes this is due to an improper operation of the machine, and in order to avoid such errors is necessary to repeat the test at least 3 times.

Using the parameter of the density of steel the analysis of the lost mass allows to transform the data obtained, in the equivalent volume eroded, thus obtaining an approximate solution of the depth of erosion.

In order to get a more realistic solution about volume, it is possible to use the second approach for evaluate the erosion rate of each specimen: the analysis of the volume, using the Confocal Microscope described in the previous chapter.

The results are approximations, since the figure of the semi-ellipse does not coincide fully with the profile of the peak. To improve the result, it was also supposed to calculate the volume using a cone as a reference figure, but as mentioned before the section of the hole not always appeared perfectly circular. However, it can be accepted the results as reliable, since the dimensions of the holes are of a few µm, and consequently also the volumes. Once established these approximations, calculations were performed using the scheme expressed in Fig. 5.4, and the volume calculated using the formula 5.3

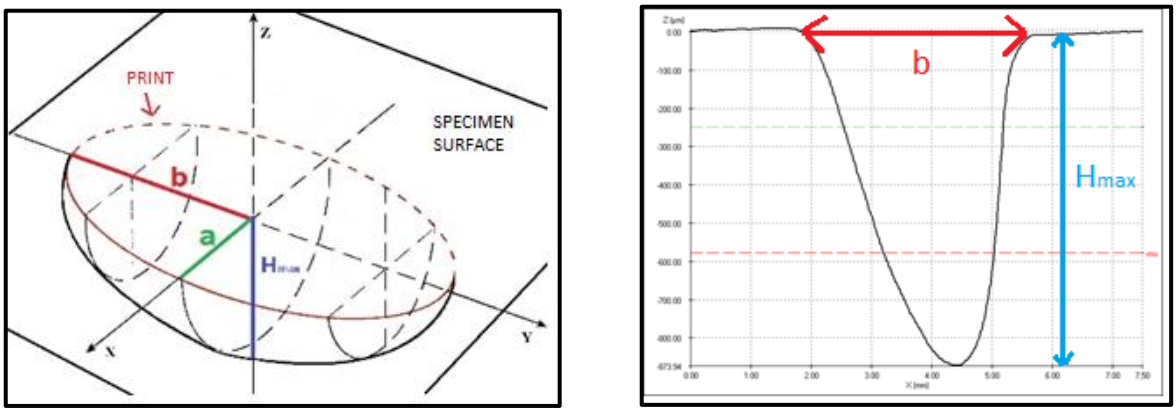

Fig 5.4 Analytical calculation of wear volume using a half-ellipsoid.

$$V = \frac{1}{2} \cdot \frac{4}{3} \pi \, a \, b \, H_{max} \qquad 5.3$$

The values $\mathbf{H_{max}}$ and **b**, are taken directly from the experimental data, as the pic shows.

The value **a**, is set constant: 1000µm for specimens tested with the impact angle of 15˚, 45˚ and 90˚.

Some results obtained by means of a spreadsheet are reported in table 5.3 and 5.4, divided by type of steel.

HH STEEL

SPECIMEN CODE	Hmax [µm]	a [µm]	b [µm]	VOLUME [µm^3]	VOLUME [mm^3]
MUS_90_100_64_HH_c	638,4	1000	1175	1571047654	1,571
MUS_45_100_64_HH_a	659,34	1000	1325	1829716969	1,830
MUS_15_100_64_HH_a	360,05	1000	3500	2639304348	2,639
MUS_15_25_32_HH_b	32,65	1000	3000	205146000,3	0,205
MUS_15_25_64_HH_b	133,03	1000	3500	975160831,6	0,975
MUS_90_100_64_HH_a	162,36	1000	1200	408055186,6	0,408
MUS_90_25_64_HH_a	155	1000	1250	405789051,1	0,406
MUS_45_25_64_HH_b	729,53	1000	1645	2513435077	2,513
MUS_15_100_64_HH_b	414,52	1000	3500	3038590302	3,039
MUS_15_100_32_HH_a	6,69	1000	3195	44766752,84	0,045
MUS_45_100_64_HH_b	743,36	1000	1350	2101800883	2,102
MUS_15_100_64_HH_c	414,89	1000	3500	3041302544	3,041
MUS_90_25_64_HH_c	607,41	1000	1190	1513866270	1,514
MUS_90_100_64_HH_b	672,64	1000	1110	1563739053	1,564
MUS_15_25_32_HH_a	30,6	1000	4000	256353960,5	0,256
MUS_90_25_64_HH_b	596,68	1000	1225	1530862495	1,531
MUS_45_25_64_HH_a	864,63	1000	1695	3069436239	3,069
MUS_15_25_64_HH_a	121,52	1000	4250	1081671295	1,082
MUS_15_100_32_HH_b	7,54	1000	3225	50928358,51	0,051

Tab 5.3 Wear Volume of HH Steel.

BM STEEL

SPECIMEN CODE	Hmax [µm]	a [µm]	b [µm]	VOLUME [µm^3]	VOLUME [mm^3]
MUS_15_25_32_BM_a	18,85	1000	3175	125346928,9	0,125346929
MUS_90_25_64_BM_b	597,42	1000	1045	1307539031	1,307539031
MUS_45_25_64_BM_a	725,88	1000	1345	2044775950	2,04477595
MUS_15_25_64_BM_c	366,09	1000	3875	2971106274	2,971106274
MUS_15_100_32_BM_a	5,92	1000	2810	34840681,41	0,034840681
MUS_90_100_64_BM_a	696,68	1000	1010	1473714412	1,473714412
MUS_45_100_64_BM_a	864,53	1000	1335	2417240976	2,417240976
MUS_15_100_64_BM_c	443,25	1000	3500	3249192202	3,249192202
MUS_15_25_32_BM_b	31,24	1000	2555	167170847,2	0,167170847
MUS_15_25_64_BM_b	388,07	1000	3890	3161682720	3,16168272
MUS_90_100_64_BM_b	600,55	1000	1050	1320678428	1,320678428
MUS_90_25_64_BM_a	179,34	1000	1005	377486861,8	0,377486862
MUS_45_25_64_BM_b	750,69	1000	1500	2358362189	2,358362189
MUS_15_100_64_BM_b	442,58	1000	3500	3244280845	3,244280845
MUS_15_100_32_BM_b	5,8	1000	2760	33527076,8	0,033527077
MUS_45_100_64_BM_b	876,93	1000	1655	3039635720	3,03963572
MUS_45_100_64_BM_c	116,77	1000	1550	379071900	0,3790719
MUS_90_25_64_BM_c	633,46	1000	1175	1558890738	1,558890738
MUS_15_25_64_BM_a	79,41	1000	3730	620358363,3	0,620358363
MUS_15_100_64_BM_a	382,31	1000	3500	2802478671	2,802478671

Tab 5.4 Wear Volume of BM Steel.

Having cataloged all the data collected during the various tests, the next step is to create a model that is able to provide prior information on the type of damage of the steel according to operating conditions. Using the two different approaches developed we are able to distinguish between three different types of **output** data:

- LOST MASS;
- WEAR VOLUME;
- MAX VALUE OF WEAR DEPTH (H_{max}).

Furthermore, referring to the section of the design of experiment, it is possible to express that the **input** data, user-selected, and for this variables are:

- TEMPERATURE;
- IMPACT ANGLE;
- VELOCITY;
- MATERIAL.

The parameters described above may also be called as control factors, for the future analysis.

For simplicity it was decided to continue the analysis by reference to a single output data, in order to build the model out of just one solution that would indicate the degree of erosion on the material. To get a more accurate model has been chosen as the response the **maximum value of wear depth** since it was obtained by means of a tool with high precision, and for that the most accurate.

The model described in the method part was applied to a spreadsheet that implements the tool performing an iterative calculation. However, some changes were needed on the input data, to make the analysis easier and have an input equal. The changes were made on the velocity of the particles, impact angle and temperature of the sample, assigning for each value a numerical code, as summarized in Table 5.5.

IMPACT ANGLE [°deg.]	NUMERICAL CODE
15	-1
45	0
90	1
TEMPERATURE [°C]	**NUMERICAL CODE**
25	-1
100	1
PARTICLES VELOCITY [m/s]	**NUMERICAL CODE**
32	-1
64	1

Tab 5.5 Numerical Codes for Linear Regression .

Finally, after a few attempts, the system provides an equation that relates the maximum value of wear depth and some input parameters. It has been shown that between the four parameters that affect this phenomenon taken in the initial considerations, only two have a significant influence on the final result, the **impact angle** and the **particle velocity**. In fact as could be noticed before, from the results, the temperature did not have a great impact on the erosion rate, or at least up to 100 °C. Even the diversity of the steel does not affect the behavior, which was predictable given the similarity of the two materials. Therefore with a reasonable limit of uncertainty it is possible predict the wear depth, starting from process condition. It was obtained an equation that described the change of the **wear depth** depending on the impact angle and the particles velocity as variables, being negligible material and temperature.

$$\boldsymbol{Hmax}(\mu m) = -607{,}68 + 10{,}27[\boldsymbol{ANG}] + 12{,}09[\boldsymbol{VEL}] + 0{,}1[\boldsymbol{ANG} * \boldsymbol{VEL}] - 0{,}13[\boldsymbol{ANG\text{^}2}] \quad 5.4$$

The equation 5.4 can be defined as a parametric equation, it presents the control factors and their linear combination, also the numeric parameters define “the weight” of every factor.

The equation obtained can be considered a real model, to verify the reliability was compared to the performance of the real data with those predicted by the model, and the comparison is shown in the graph 5.6. The trend can be considered similar, there are some peaks of the actual results (blue line) that can be considered anomalies, for which the model (red line) proceeds much more constant.

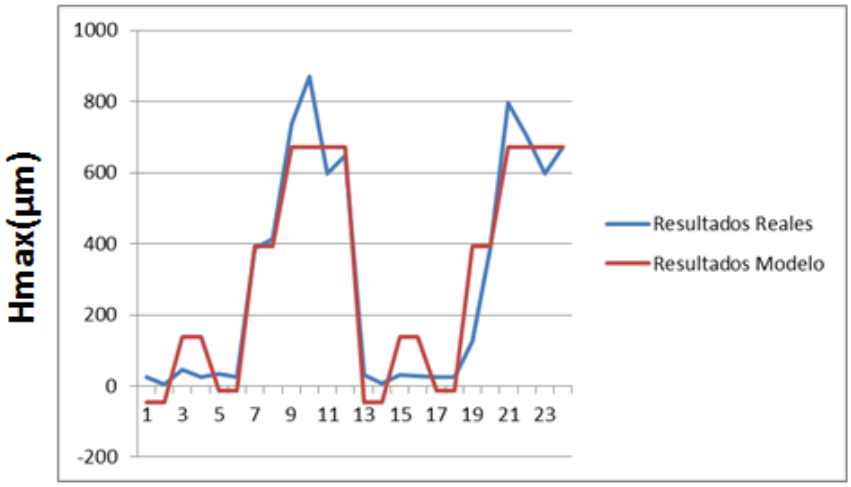

Graph. 5.6 Comparison between Experimental Results and Equation Model.

Example

Determine the erosion rate per cycle of a steel component, on which impacts a flow of aluminum inclined by 30° with a speed of particles of 50 m/s for a given time of 10 minutes.

INPUT DATA:

- *IMPACT ANGLE=30˚*
- *VELOCITY=50m/s*
- *TIME= 10 min= 600 s*

For the calculation it is introduced another parameter, the wear rate because it is important to know the rate of wear for every cycle. According to the literature [51] there is a value that takes into account the fact that in 0.15 seconds will form a layer (skin) of aluminum on the dies. *WEAR RATE = 0,15s/cycle*.

Hence, taking the equation 5.4 and substituting the values is obtained the erosion rate expressed **wear depth per cycle**.

Hmax[(μm)/cycle] =[-607,68+10,27**(30)**+12,09**(50)**+0,1(**30*50)**-0,13(**30^2)**]*__0,15__/600

Hmax[(μm)/cycle]= 0,086863 μm/cycle

Chapter 6:

CONCLUSIONS

The work just presented is part of a much larger project which aims the study of the damage of steels for dies, especially the one used in the HPDC process, that is one of the hardest process. The aim of this part is to study in detail the damage due to the phenomenon of thermal fatigue and erosion inside the dies and trying to develop a model that can express the trend.

The steels used throughout the analysis are H13 and H11, which are the most used materials for the creation of dies thanks to their resistance properties and mechanical characteristics described even previously.

By a mechanical analysis of these two materials result that, despite differences in the chemical composition, when they are subjected to mechanical stress, it can be said that the two materials behave in the same way with minimal differences.

In the first part it has been focus on the study of the effect of thermal fatigue experimenting the behavior of the chosen materials, subject to many cycles in an environment where the temperature was equal to that used during the HPDC process. In fact, the tests have not been precisely take on with a standard *Thermal Fatigue* approach, but specimens were subjected to the one that can be defined as *High Temperature Mechanical Fatigue,* given the similarity of the two phenomenon.

The Thermal Fatigue phenomenon develops as the dies are constantly, for each production cycle, subjected to a very rapid increase in temperature due to contact with high temperature molten material (aluminum, plastic, etc..) followed by an equally rapid cooling that is via spray or cooling channels.

The study has been carried out with the aim to understand how the high temperatures affecting on the remaining life of a component subjected also to mechanical stresses. Some limits were encountered during the testing path, in fact the tests of this type that may be considered in LCF, however, have a very extended duration.

During the trials it were taken into account the fundamental properties of steels, such as monotonic curve of the material, which revealed the yield stress, the maximum stress and the breaking limits. It is also taken into account the variation of the Young's modulus in relation to temperature change; from this analysis it has been obtained a curve that describe the type of behavior and the values to be taken at different temperatures.

With the data obtained in the preliminary analysis, we were able to carry at least seven tests, four with H13 specimens and three with H11 specimens. The experimentation may be considered in the deformation control, since the main parameter that varied in the different tests was the range of amplitude, and then, of course, the temperature.

As it was to be expected to a greater amplitude, and at a constant temperature, correspond a less number of residues cycles of the component, demonstrating, in this way that the most influencing parameter is the amplitude of deformation.

From the results of these tests we have managed to create a chart to show that the actual trend obtained from the data was reliable. From the graph, using a spreadsheet, has been

identified an equation (5.2) that can be considered a good starting point to describe the behavior between applied stress and number of residues cycles to rupture.

It is however necessary to clarify that, the study of the thermal fatigue damage on die-casting dies is still a work in progress, and as already mentioned in the previous chapters, still many tests must be performed to ensure the development of a predictive model.

The erosion damage occurs inside the dies, because it creates a contact between the molten material and the die surface, that, after many cycles produces an erosive reaction, that's going to change the geometry of the die.

For this reason, the other part of experimentation has focused on the damage due to erosion, also this segment has the aim of studying the behavior of the two materials in order to create a model that describes the trend. It was appropriate to introducing and describing the works carried out previously and use them as a starting point to understand which parameters to working with during testing.

From the analysis of the literature previous works it was decided that a reliable study had to involve all the parameters that affect during the process, both for the molten material, i.e., the flow rate, discharge rate, temperature and exposure time, both for the die, then impact angle and temperature of that.

Therefore were carried out about forty tests, twenty using a HH steel, and twenty for the BM steel, to be able to fully describe all the different configurations with different parameters. The experiment was quite simple, since the device allowed to choose the values of discharge rate, the particle velocity and impact angle, also did not require a high time.

Once all the analyzes were done, it was studied the results using three different approaches. The first one, simplest, based on the mass loss obtained with the weight difference between original specimen and eroded one.
The second approach comes from the observation of the type of mark left on the specimen from the erosive flow, which is always similar to a semi-ellipsoid. For this reason it was decided to quantify the eroded volume in order to compare different specimens subjected to different conditions.

The third approach is based on the use of a confocal microscope, able to measure the maximum depth of the mark left by the erosive flow.

From all the approaches it is result that the most affecting factors of all the parameters nearly described, are the impact angle and the velocity of the erodent flow. In particular, as shown in the graph 6.1, obtained by treatment of the data, the mass lost values are inversely proportional to the increasing angle, that is larger values of impact angle corresponds to a less mass lost, while the wear depth has a maximum on 45°, a minimum at 15° and an intermediate value at 90°.

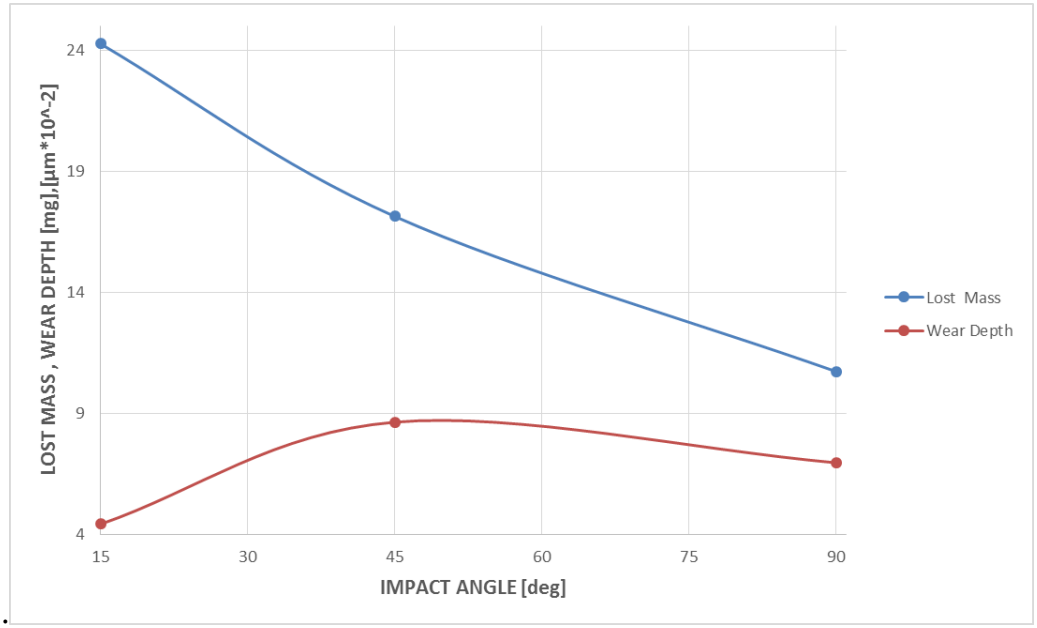

Graph. 6.1 Comparison between Impact Angle and Lost Mass, Wear Depth.

Finally the relationships found between different parameters is demonstrated in the equation 5.3, expressing the maximum value of wear depth in function of the impact angle and the velocity of erodent flow. The report identified is reliable because, even when compared to the basic theory, expresses the same trend. (Graph 5.4).

Chapter 7:

WORK SUMMARY IN ITALIAN

L'argomento sviluppato in questa tesi tratta il danneggiamento causato dal fenomeno di *fatica termica* e di *erosione* degli acciai utilizzati per la produzione di stampi nei processi di *pressocolata*. Il processo di pressocolata è uno dei più utilizzati per la produzione di componenti, varia dalla creazione di oggetti di uso comune, al settore dell'*automotive*, fino all'industria aerospaziale. Durante la pressocolata il materiale fuso (alluminio, plastica, etc..) è pressato all'interno della cavità dello stampo. Caratterizzato da un'elevata velocità di riempimento, questo processo di produzione può produrre componenti con forme e geometrie assai complesse e dettagliate, che non sarebbero possibili con altre tecniche di fonderia. La pressocolata è ideale per produzioni di componenti con grandi volumi e pareti sottili grazie ai rapidi tempi di ciclo; questi variano da pochi secondi ad alcuni minuti a seconda della dimensione della colata e dello spessore di progetto, ciò consente una produzione media di circa 60 stampaggi per ora, da una sola macchina di pressocolata.

Si tratta, infatti del processo più rapido tra tutti i sistemi di fonderia (un componente di 15-20 kg viene prodotto in 40-50 secondi) permettendo così una produttività elevata. Presenta una sola fase, suddivisa in tre passaggi nel quale il metallo liquido (solitamente alluminio) viene iniettato all'interno di uno stampo raffreddato ad acqua o con spray lubrificanti ad elevata pressione e velocità. L'acciaio da stampo ha come funzione principale quella di

assorbire il calore contenuto nella lega iniettata fino a farla solidificare e a far scendere la temperatura della stessa fino al valore più adatto per l'estrazione del getto.

La vita media di uno stampo corrisponde ad una produzione che varia dai 100,000 ai 300,000 componenti, tuttavia talvolta si verifica che alcuni stampi cedano tra i 5000 e i 25,000 cicli. Questo danneggiamento è dovuto al formarsi di difetti all'interno dello stampo causati dalle forti condizioni di lavoro a cui sono sottoposti gli acciai. Durante la pressocolata con alluminio, il materiale fuso viene iniettato a temperature di 670°-710°C, con velocità tra i 30 e 100 m/s e pressioni medie di 70 MPa. Per questi motivi le proprietà più importanti che deve avere un acciaio per stampi sono la resistenza agli *shock termici*, all'*ammorbidimento*, ad *elevate temperature*, stabilità al *rinvenimento*, *tenacità* e *resistenza* all'usura a caldo. I materiali più utilizzati sono acciai della serie H11 e H13. La longevità dello stampo è direttamente legata alla temperatura di colata del metallo fuso, al gradiente sviluppato all'interno della cavità e alla frequenza di esposizione ad alte temperature.

A queste condizioni di lavoro, l'acciaio degli stampi è soggetto a cicli in cui si sviluppa un gradiente di temperatura molto elevato, causato dalla differenza tra fase *calda*, momento in cui il materiale fuso viene a contatto con la superficie, e la fase *fredda*, momento in cui il componente ha lasciato la cavità e lo stampo viene raffreddato o tramite spray lubrificanti o con un sistema di canali di raffreddamento. Contemporaneamente si sviluppa anche un danneggiamento dovuto all'erosione che può essere definito come una graduale rimozione fisica del materiale dal substrato, che avviene ad ogni impatto dell'alluminio liquido Questo avviene a causa del moto della massa fusa di alluminio.

La tesi nasce all'interno del Progetto Europeo "*MUlti-layers control&cognitive System to drive metal and plastic production line for Injected Components*, ***MUSIC***" che ha come partner sia *l'Università degli Studi di Padova* , sia il centro di ricerca IK4-TEKNIKER, presso il quale è stata svolta la parte di sperimentazione. In un processo produttivo come la pressocolata, una delle principali voci di costo riguarda l'investimento iniziale per la progettazione/produzione dello stampo in acciaio e la manutenzione/riparazione dello stesso necessaria a seguito dell'incorrere di stati di usura eccessivi che provoca un elevata riduzione della qualità finale della parte formata. Il processo di manutenzione/riparazione induce quindi un costo di *down-time* e un costo diretto. La riduzione di tale voce di costo, tramite lo studio e la previsione dei meccanismi di usura, è alla base del progetto Europeo di ricerca. *MUSIC* vede coinvolte altre Università, centri di ricerca ed azienda per un totale di 16 partner.

Le fasi del processo di pressocolata sono ben identificate nella figura 7.1, tramite la quale è possibile individuare, in relazione all'avanzamento del pistone, i tre passaggi.

Durante la prima fase, il pistone avanza lentamente ed esercita una pressione limitata. In caso di mancato controllo della velocità si potrebbero creare onde che favoriscono

l'intrappolamento di aria. Quando la lega arriva all'attacco di colata inizia la seconda fase. Questa è caratterizzata da un repentino incremento della velocità del pistone corrispondente ad un incremento di pressione, che porta ad un riempimento dello stampo pressoché istantaneo (qualche centesimo di secondo). Grazie all'elevata velocità permette la realizzazione di geometrie complesse con spessori molto sottili (1-2 mm) riuscendo così a iniettare il metallo anche in zone di difficile raggiungimento.

Una pressione aggiuntiva, ancora una volta fornita dal pistone, caratterizza la terza fase dove questo continua a spingere fino a solidificazione completata. La fase di riempimento vede una velocità massima intorno ai 50m/s e una pressione massima intorno ai 120 MPa durante la fase di solidificazione [47]. Una volta completata la solidificazione, lo stampo sufficientemente raffreddato viene aperto e il getto meccanicamente estratto. Sulla superficie dello stampo viene quindi iniettato un mix di lubrificante e acqua utile non solo per il suo raffreddamento ma anche per la formazione di uno strato separante che impedisce il contatto diretto fra il metallo fuso e l'acciaio dello stampo [48].

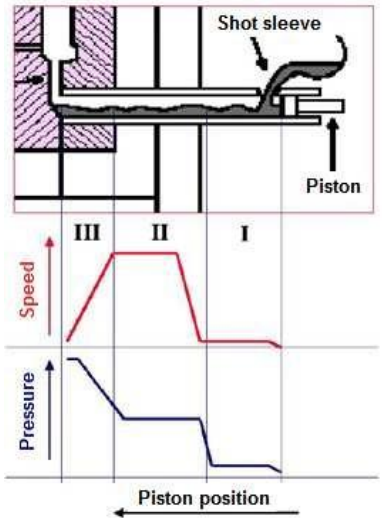

Figura 7.1 Fasi della pressocolata (HPDC) [47]

Dato l'elevato costo della produzione, progettazione e manutenzione degli stampi, numerosi studi sono stati sviluppati per determinare quali potessero essere i principali danneggiamenti riscontrabili sugli acciai, per poter creare modelli che favorissero un migliore sviluppo degli stampi stessi.

Da questi studi è risultato che i fenomeni più influenzanti e affaticanti sono: *die soldering, washout* e *fatica termica,* come si può notare sono quasi tutti termini inglesi, poiché si rifanno ad una letteratura internazionale in cui è comunemente utilizzata la lingua inglese.

Il *die soldering* è un meccanismo di usura è direttamente correlato all'interazione chimica che si manifesta tra stampo e lega. Il meccanismo è stato ampliamento studiato in letteratura ormai da anni; una delle principali pubblicazioni è di HAN e VISWANATHAN [49],il quale descrive in dettaglio quella che è la fenomenologia del meccanismo: come prima cosa si ha la diretta divisione in due grandi sottocategorie:

- **mechanical die soldering:** interazione meccanica tra lega e stampo dovuta a fenomeni di adesione fisico/meccanica (interlooking, adhesion)la quale si manifesta principalmente nelle zone caratterizzate da alta pressione locale e limitate temperature superficiali dello stampo. In tale caso non è presente nessuna interazione chimica tra lega e stampo.
- **chemical die soldering:** interazione chimica tra lega di alluminio e stampo. Alla base di tale processo c'è un processo diffusivo o di adesione chimica. Tale meccanismo si manifesta prevalentemente in zone caratterizzate da bassa velocità ed elevata temperatura superficiale.

In dettaglio, il meccanismo di *soldering* si sviluppa tramite diversi step, come si può vedere in figura 7.2. Dopo che si crea un danneggiamento sulla superficie dello stampo o sul rivestimento, anche se pur piccolo, il materiale fuso arriva a contatto direttamente con lo strato di materiale più debole, andando ad attaccare i bordi dei grani a livello microstrutturale, sciogliendo i grani più duri e le zone di struttura martensitica, dando origine a danneggiamenti denominati *pitting* sulla superficie dello stampo.

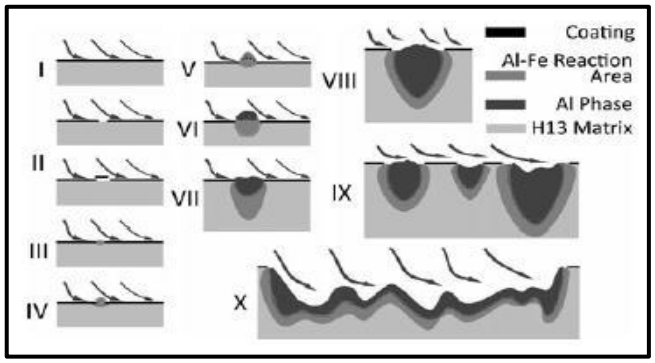

Figura 7.2 Schematizzazione delle fasi di Soldering [12].

Il meccanismo di usura *washout*, che letteralmente significa "*lavar via*", viene utilizzato nel campo della fonderia, ed in particolare nella pressocolata come un tipo di danneggiamento degli stampi, che racchiude al suo interno diversi fenomeni che possono sia coesistere, sia verificarsi singolarmente. I fenomeni che comprende tuttavia hanno comportamenti completamente differenti a livello fisico e chimico all'interno dello stampo.

Si può sviluppare un'usura causata da **corrosione,** poiché gli acciai utilizzati per gli stampi, e più in generale gli acciai da utensili, possono dissolversi in qualche modo nell'alluminio liquido, e le alte temperature di colata possono causare l'ossidazione dello stampo. Talvolta viene identificato come un fenomeno di soldering, ma non rispecchia del tutto la verità, infatti la corrosione può agire a causa dell'alta temperatura, diventando ossidazione e formando uno strato di ossido di ferro sulla superficie, o causa dei legami chimici, il cui comportamento si avvicina di più al soldering. Quest'ultimo, inoltre può influenzare anche altri danneggiamenti, in quanto va a modificare le proprietà meccaniche dello stampo.

All'interno del washout è compreso anche il danneggiamento causato dal fenomeno dell' **erosione**, che può essere definito come una graduale rimozione del materiale, che avviene a causa del veloce movimento dell'alluminio all'interno della cavità. Anche qui sono stati distinti, secondo vari studi, diversi meccanismi che possono essere causa dell'erosione. Esiste l'erosione causata dal *liquid-impingement,* un fenomeno che crea piccoli fori sulla superficie per la velocità con cui impatta il materiale non del tutto fuso e per le alte temperature; la *cavitazione* che è il risultato dello scoppio delle bolle formatesi all'interno del materiale fuso per valori elevati di velocità e pressione d'ingresso; e infine l'erosione detta *solida* che è causata dall'impatto di particelle non sciolte all'interno del flusso durante la fase di riempimento.

L'immagine 7.3 schematizza la maggior parte dei fenomeni che portano al danneggiamento per erosione.

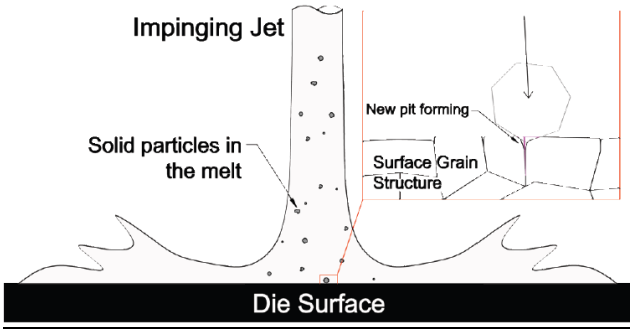

Figura 7.3 Rappresentazione di un Impinging Jet e di alcune particelle solide contro lo stampo [14].

Il terzo danneggiamento, che viene considerato uno dei più deleteri, che verrà approfondito in questo studio è la *fatica termica*. Si manifesta poiché lo stampo, in particolare la sua superficie, è ciclicamente sottoposta a sbalzi di temperature che variano di molti gradi, per questo l'acciaio è sottoposto a tensioni termiche che possono essere considerate affaticanti.

Dall'esperienza e secondo alcuni lavori di analisi, è risultato che queste tensioni che si formano danno origine a delle vere e proprie cricche sulla superficie del materiale, le quali

sommate agli effetti precedentemente descritti portano ad una deformazione notevole dello stampo. La deformazione dello stampo causa un peggioramento netto sul prodotto finito, lasciando segni e difetti non voluti.

Esistono due tipi diversi di cricche nel caso di stampi per pressocolata, la prima è definita *heat checks*¸ sono cricche che si manifestano principalmente sulle zone piatte della superficie, dove elevati gradienti di temperatura danno vita a tensioni di trazione e compressione alternati, in base alla tensione massima che si sviluppa si avrà la direzione di queste cricche. La seconda categoria è definita come *corner crack* (cricche d'angolo), sono più diffuse e si sviluppano in presenza di bordi non raccordati, o cambi di sezione molto duri. Possono svilupparsi o perpendicolarmente al bordo o lungo di esso, a seconda del tipo di deformazione ciclica subita[17]. Nella figura 7.4 si possono vedere due esempi di entrambe le categorie.

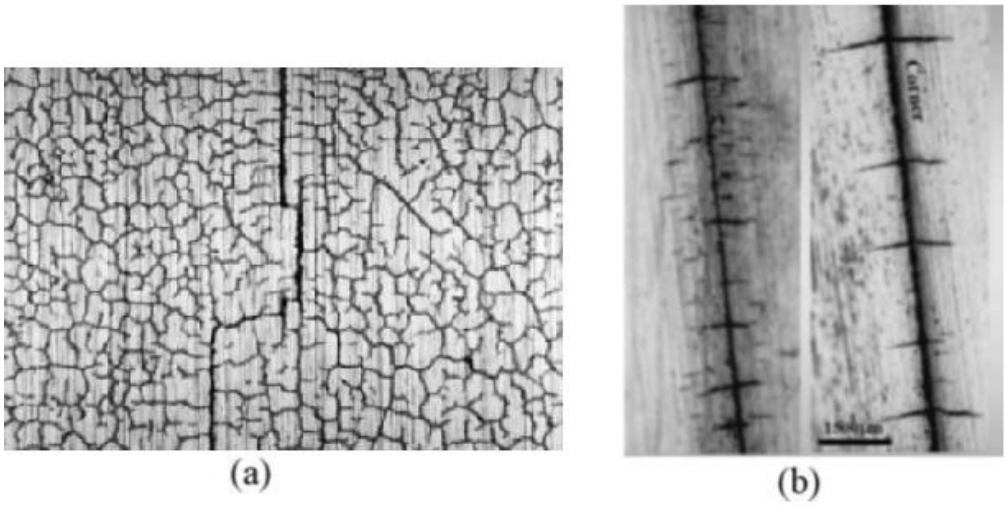

Figura 7.4 Cricche sviluppate sugli stampi (a)Heat checks, (b)Corner cracks [17].

STUDIO DELLA LETTERATURA

Il presente studio, come già evidenziato, si è concentrato sull'analisi dei danneggiamenti causati dal fenomeno di fatica termica e di erosione, entrambi sono stati trattati sia a livello compilativo, andando ad esaminare la letteratura dedicata, sia a livello sperimentale, con prove mirate sugli effetti.

Per quanto riguarda la fatica termica è risultato che molti studi sono stati svolti sia per capire l'effetto, ma anche per sviluppare sistemi di simulazione adeguati, come per l'elaborato *Development of test rig for thermal fatigue testing–preliminary results[40]* nel quale si è sviluppato un anello da porre attorno al provino, che potesse sia riscaldarlo che raffreddarlo mediante getti d'acqua. Infatti è stato anche dimostrato che un modo efficace

di simulare condizioni di fatica termica, in particolare per gli stampi, è quello di usare un bagno di metallo liquido, seguito da una tempra ad acqua [45]

Per spiegare la natura del fenomeno ci si è affidati alla teoria secondo la quale la formazione di cricche *termiche* può essere divisa in 3 fasi: nucleazione, accrescimento iniziale, e continuato accrescimento che porta alla distruzione della superficie[42].
La *nucleazione* della è associata all'accumulazione di effetti di plasticità locale sulla superficie del materiale, che risulta tipico per la fatica a basso numero di cicli (LCF).

Durante la fase calda si avranno tensioni di compressione, mentre durante la fase fredda, le tensioni generate saranno di trazione. L'*accrescimento iniziale* è facilitato dall'ossidazione della parte superficiale dello stampo, che aumenta il volume del strato di ossidazione. Infine L'*accrescimento continuato* è guidato dal riempimento delle cricche precedentemente formatesi, che si riempiono di materiale fuso, anche dovuto al rinvenimento o invecchiamento dello strato superficiale. Questa comportamento è ben riassunto nella figura 7.5.

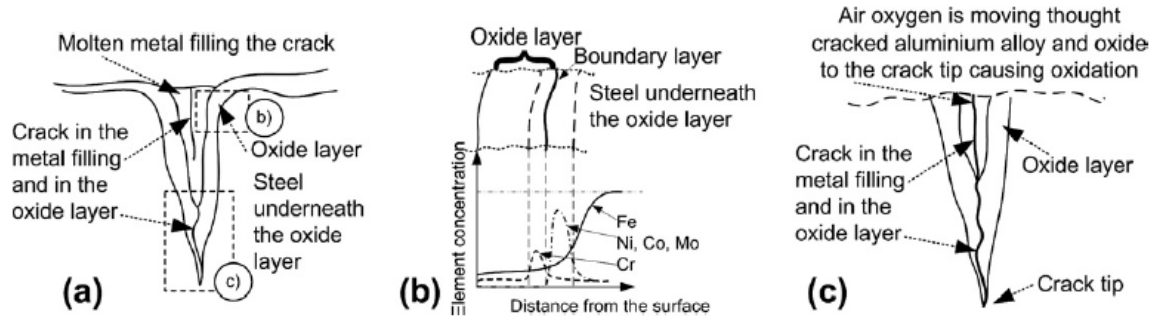

Figura 7.5 Meccanismo di accrescimento della cricca, favorito dall'ossidazione [42].

I test sviluppati per l'analisi della fatica termica sembrano essere molto simili, tutti basati su un sistema che sia in grado di sottoporre il provino ad un alternanza tra alte temperature (bagni di alluminio, riscaldamenti per induzione) e basse temperature (tempra in acqua, spray lubrificanti, etc.) subito dopo. Alcuni si sono concentrati in particolare sulla geometria del provino, che potesse quantificare al meglio la differenza di gradiente tra temperatura superficiale e temperatura interna[42, 43], mentre in altri test il campione è stato messo in rotazione sul proprio asse in modo da eliminare il metallo aderito dalla superficie[45].

I parametri che possono cambiare sono le dimensioni e la geometria del campione, il sistema di raffreddamento e riscaldamento o il tipo di bagno.

Cosa interessante è risultato che la maggior parte degli autori sono d'accordo sui criteri da usare per la valutazione della resistenza a fatica per gli acciai da stampi, cioè *area totale criccata* e *media di lunghezza massima di cricca* [44].

Il criterio di area totale criccata tiene in considerazione i contributi delle cricche, quindi raggiunto un valore critico, allora ci sarà il cedimento dello stampo.
Il secondo criterio è basato sul fatto che se anche una sola cricca è lunga più di un valore limite, l'intero stampo risulta inutilizzabile.
Dai risultati della letteratura si evince che ci si può aspettare che le cricche dovute alla fatica termica si manifestano sulla superficie del provino, dovute alle maggiori temperature e alla diminuzione della resistenza del materiale a questi valori maggiori di temperatura. Quando la superficie più esterna del provino è sottoposta a temperatura più alta di quella dell'interno, le tensioni sono di compressione, viceversa, quando la superfice è a temperature inferiori dell'interno, le tensioni sviluppate risultano di trazione. Infatti quando lo stampo non è in esercizio perde rapidamente calore. Quindi per evitare che si formi un gradiente eccessivo, è buona norma fermare anche il sistema interno di raffreddamento.

Inoltre per migliorare la qualità dello stampo alcuni autori hanno anche fornito delle linee guida che coinvolgono tutto ciò che è legato al processo, dalla progettazione dello stampo, ai parametri di esercizio[41].

Per quanto riguarda lo studio di erosione, per valutare a che punto fosse arrivata l'analisi del fenomeno alcuni elaborati sono stati esaminati. È stato evidenziato dalla teoria di *Barton* [32], che i danneggiamenti da erosione possono essere suddivisi in quattro categorie*: Gate erosion, Washout, Cavitation erosion, Erosion caused by flow separation*. Tutti fenomeni che hanno tratti in comune ma che riportano comportamenti differenti.

Continuando nell'analisi sono stati analizzati i test precedenti sul grado di erosione, per evidenziare le procedure più utilizzate. Si è partito dalla normativa, per vedere quali fossero i principali parametri da considerare per un'analisi efficace di un componente soggetto ad erosione. Che sono risultati essere , velocità del flusso erosivo, angolo di impatto e temperatura.

Uno dei lavori di riferimento è stato sviluppato da *K. Venkatesan and R. Shivpuri* called "*Experimental and Numerical Investigation of the Effect of Process Parameters on the Erosive Wear of Die Casting Dies*" [19]. In questo elaborato, per analizzare i diversi materiali di ricoprimento superficiale, è stato costruito un sistema multi-spina con stampo piatto, in cui sei spine sono state progettate e fabbricate appositamente per il test, come mostra la figura 7.6.

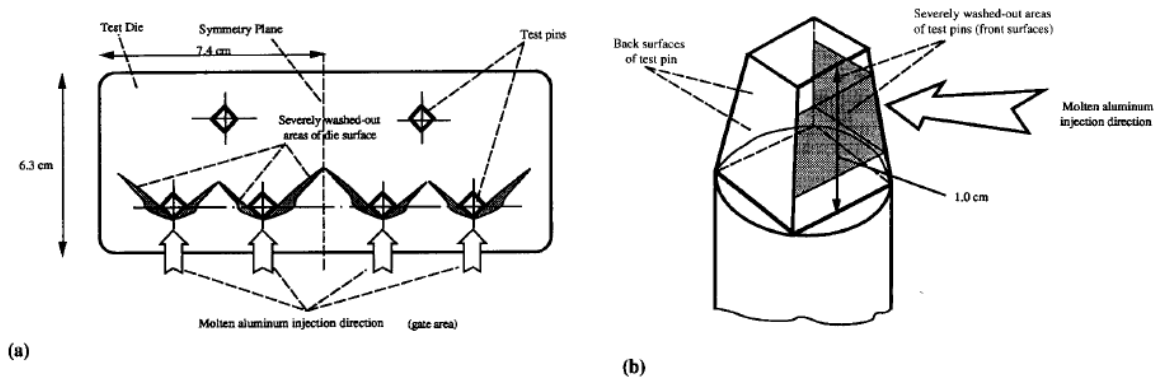

Fig 7.6 Schematizzazione della sezione dello stampo e del layout delle spine più favorevole all'usura[19].

Le spine sono state poste a differenti angolazioni (83°, 75°, 70°, e 65°)rispetto al flusso di erodente. In questo modo l'angolo su cui il metallo fuso impatta è diverso per ciascuna spina, fornendo così un mezzo per valutare l'effetto di angolo di impatto in condizioni sperimentali simili.

Altri tipi di test sono stati studiati da diversi autori, sempre con lo stesso obiettivo di creare un modello che potesse relazionare il grado di erosione con i parametri del sistema di lavoro. I tipi di test possono essere suddivisi essenzialmente in due categorie, quelli in cui l'erodente è in forma di particelle solide, e quelli in cui l'erodente è un flusso di materiale liquido, chiamato anche *liquid impingement* test.

Per la prima categoria ci si può riferire ai test svolti da *J.R. Laguna-Camacho, et al. "Solid particle erosion on coatings employed to protect die casting molds"* [27] e anche all'analisi svolta da *A. Mohammed, et al* "*Development of a Method for Assessing Erosive Wear Damage on Dies used in Aluminium Casting*"[28]. I test sono molto simili, hanno lo stesso sistema di sperimentazione formato da un ugello da cui esce il flusso di erodente, e una piastra su cui fissare il provino da sperimentare che può variare l'angolazione per differenti angoli di impatto. In entrambi si può definire velocità e portata del flusso. Il fattore che le differenzia è che nel primo viene utilizzato un flusso di micro particelle di carburo di silicio con diametro medio massimo di 450µm, mentre per il secondo vengono usate sfere di alluminio con un diametro di 3 mm. Inoltre nel secondo test vengono testati anche provini cilindrici e non solo piatti.

Il comportamento dato invece dal flusso liquido è affrontato da *Shuji Hattori* nel lavoro "*Effects of Impact Velocity and Droplet Size on Liquid Impingement Erosion*" [29].
In questo elaborato il meccanismo di erosione causato dal flusso liquido agisce a causa della fatica. Cioè, i danneggiamenti appaiono a causa di deformazioni plastiche sui bordi grano dei cristalli e le aree producono concentrazioni di stress elevato, con conseguente nucleazione di cricche da fatica e rimozione del materiale.

Analizzando i risultati dei test sull'erosione si capisce immediatamente come i parametri descritti precedentemente, temperatura del metallo fuso, angolo di impatto e velocità del flusso, abbiano un impatto significante sul grado di erosione. Infatti si può affermare che in questo caso gli studi teorici e sperimentali coincidano. Per questo motivo i risultati sono di ogni elaborato vengono presentati sostanzialmente relazionando il grado di erosione a questi fattori. In particolare tutti gli autori concordano nell'affermare che il picco di usura si verifica quando il flusso ha un angolo di impatto di 30°[28], rispetto allo stampo, o a i provini testati, dove è stata identificata la zona di massimo danneggiamento[27]. Che espresso in grafici da il risultato nel grafico 7.1.

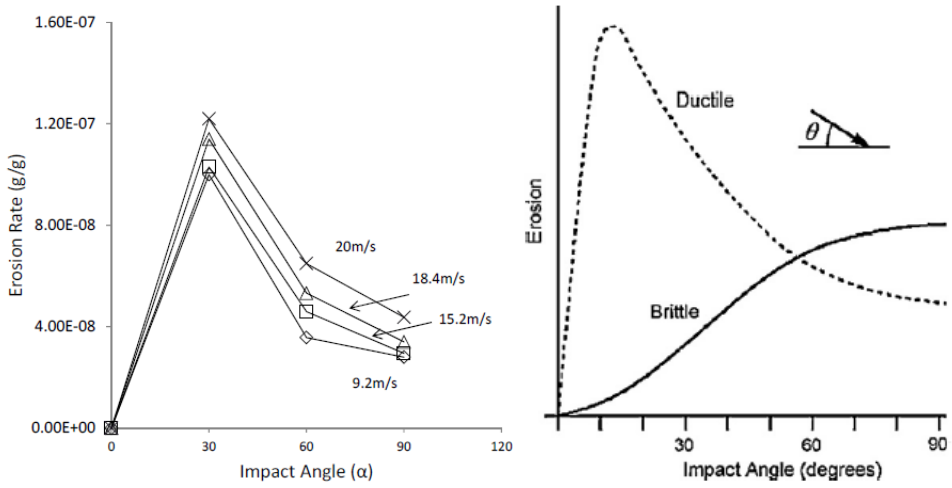

Graf. 7.1 Grado di erosione rapportato alla variazione di angolo di impatto[28, 39]

Dal secondo grafico è anche possibile capire il diverso comportamento tra materiale fragile e duttile. Relazione verificata durante gli studi [27, 28].
In particolare in tutti i casi visti, la dimensione dell'impronta di usura aumenta per bassi angoli di impatto, mentre è ridotta quando l'angolo cresce. Il fattore comune però rimane nella forma dell'impronta, che ad angoli bassi è ellittica, mentre ad aumentare dell'angolo diventa più di forma circolare.

Questo fenomeno può essere spiegato osservando la figura 7.7, tratta dallo studio effettuato utilizzando come erodente delle sfere di alluminio, dove viene spiegato il meccanismo di contatto tra provino e flusso.

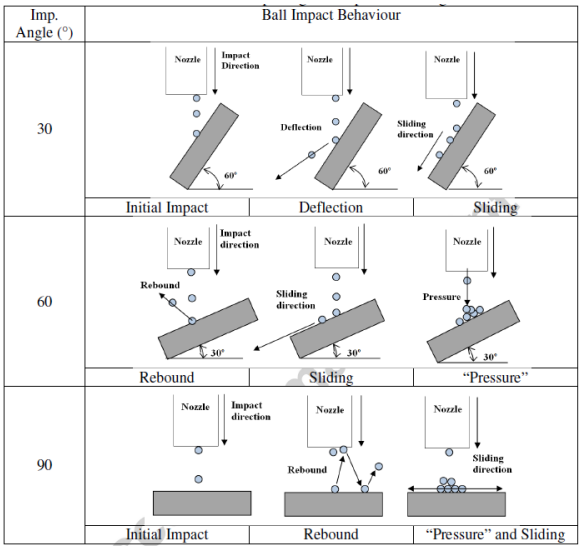

Fig. 7.7 Comportamento di impatto di un flusso di sfere su provini piatti di alluminio a diversi angoli. [28].

Da qui si può vedere infatti che un danno che comporterebbe la perdita di materiale si verifica molto più velocemente quando le sfere strisciano e tagliano il provino, più che quando impattano e formano crateri.
Infine è stato dimostrato che la velocità non ha un impatto così dominante sul grado di erosione come l'angolo di impatto[28], è stato dimostrato che il profilo di velocità calcolata sul bordo della matrice sperimentale utilizzato per lo studio di usura corrisponde strettamente con il profilo di usura misurata, indicando la velocità del metallo come un meccanismo primario di danneggiamento solo per alcuni casi particolari, come ad esempio il *washout*.

PARTE SPERIMENTALE

I risultati degli esperimenti sul fenomeno della fatica termica possono essere descritti analizzando i dati di tutti i test per capire quali possano essere le metodologie che hanno portato alla determinazione dei parametri ottimali. In particolare, è possibile condurre un'analisi sia sul cambiamento della storia di carico ottenuta, sia sul campione per evidenziare la modalità che ha portato il provino a rottura, utilizzando il sistema Microscopio.

È ovvio che le prove descritte e condotte finora non sono sufficienti a creare un modello valido, che possa descrivere il comportamento per gli acciai soggetti a fatica per elevate temperature. Come è stato menzionato in precedenza le prove di questo genere richiedono un lungo periodo di esposizione, infatti, anche se sono test a basso numero di cicli di fatica, durano almeno una settimana.

Tutte le prove sono state effettuate prendendo in considerazione le correzioni sopra descritti, ed in particolare sono descritti nella Tabella 7.1 con il range di deformazione ed i relativi cicli. Deve però essere chiaro che i risultati presentati devono ancora essere confermati e, in particolare, il lavoro è da considerarsi ancora un lavoro in corso.

Material	Stress (MPa)	Strain amp. (µm)	Temperature (°C)	Cycles
H13	908,2492082	390	500	140
H13	853,4016525	365	500	11028
H13	820,4931191	350	500	18000
H13	874,2324423	365	300	3983
H11	856,0505097	365	500	11690
H11	849,08648	365	400	8722
H11	855,6853547	365	300	5073

Tab. 7.1 Risultati dei Test HTMF.

L'influenza della temperatura ha un effetto combinato che è stato spiegato nella parte di prove di trazione. A temperature inferiori, il modulo di Young è maggiore per le stesse deformazioni. Come buona correlazione, è stata trovata la relazione tra la tensione risultante e il numero dei cicli a rottura che viene descritta graficamente (grafico 7.2) Questa equazione sarebbe valida per un acciaio martensitico a 43 HRC di durezza:

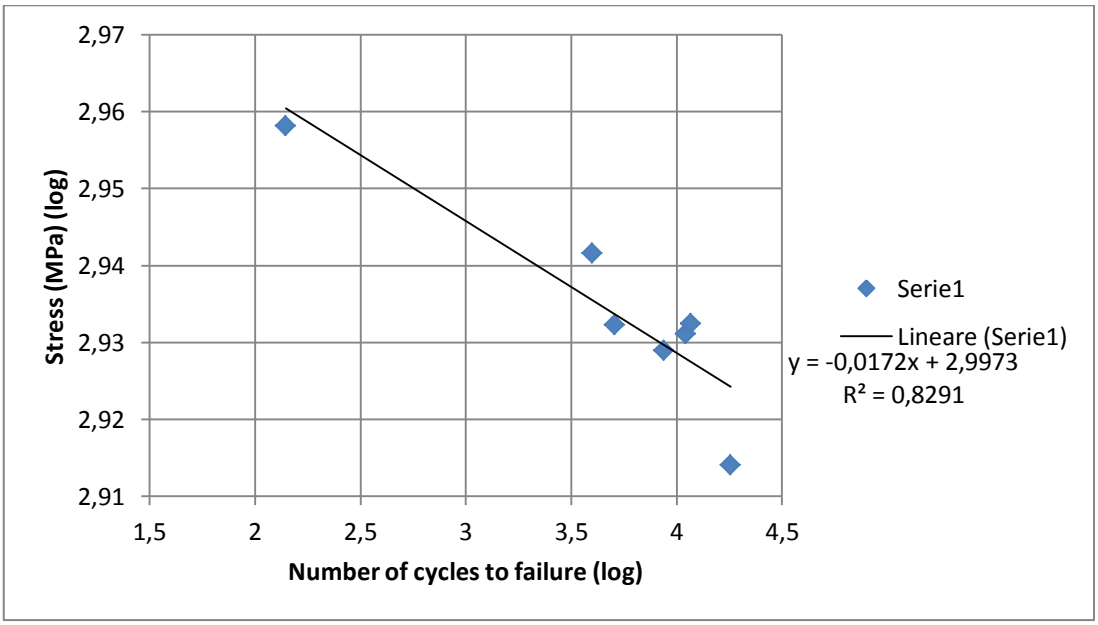

Graf. 7.2 Risultati dei test HTMF dipendenza tra Tensione e Numero di Cicli a rottura.

Da cui mediante un foglio di calcolo è stata ricavata un'equazione che ne descrive il comportamento.

$$y = -0.0172x + 2.9973 \qquad 7.1$$

y = Tensione (MPa) (Log); x = Numero di cicli a rottura (Log).

Come già introdotto nelle sezioni precedenti i risultati degli esperimenti sul fenomeno dell'erosione, possono essere suddivisi in due categorie. La prima è tramite l'analisi della quantità di massa persa dopo il processo di erosione, che viene ottenuta confrontando lo stesso campione prima e dopo. Per la stima viene utilizzata una bilancia con una precisione di 0,001 mg ±, e facendo almeno 3 misurazioni, da cui si ottiene una media.

Come si può vedere dai risultati riportati nella Tabella 7.2, il fattore più influente sulla velocità di erosione sembra essere la pressione dell'aria, infatti è possibile notare la netta differenza tra le percentuali dei campioni testati alla velocità di flusso minima e massima.

Code	Weight av. [g]	Impact angle [°deg]	Temperature [°C]	Air Pressure [kg/cm^2]	Mass Lost [g]	Mass Lost [%]
MUS_15_100_32_HH_b	18,81099	15	100	0,2	0,000236667	0,023667
MUS_15_25_32_HH_b	18,82271	15	25	0,2	0,001416333	0,141633
MUS_15_25_64_HH_a	18,75672	15	25	1,5	0,006763333	0,676333
MUS_15_100_64_HH_a	18,78919	15	100	1,5	0,018136667	1,813667
MUS_90_25_64_HH_b	23,92487	90	25	1,5	0,009723333	0,972333
MUS_90_100_64_HH_c	23,90766	90	100	1,5	0,011000333	1,100033
MUS_45_100_64_HH_b	22,70640	45	100	1,5	0,015424	1,5424
MUS_45_25_64_HH_a	18,77692	45	25	1,5	0,018426667	1,842667

Tab. 7.1 Risultati dei Test di Erosione.

In secondo luogo, come parametro influenzante vi è l'angolo d'impatto del campione, che influisce maggiormente a 45°, poi 15° e infine 90° che, nelle stesse condizioni, mostra il grado di erosione inferiore. A differenza del parametro precedente, l'angolo di impatto, non è un parametro che mostra sempre i risultati attesi, ma in alcuni casi può incidere più o meno sul campione.
Al fine di ottenere una soluzione più realistica sul volume eroso, è possibile utilizzare un secondo approccio per valutare il grado di erosione di ciascun campione: l'analisi mediante il microscopio confocale.

Inoltre, per confrontare e migliorare il tipo di risultati, il volume è stato calcolato anche analiticamente, utilizzando la come formula quella per calcolare il volume di un cono, prendendo come riferimento la figura 7.8.

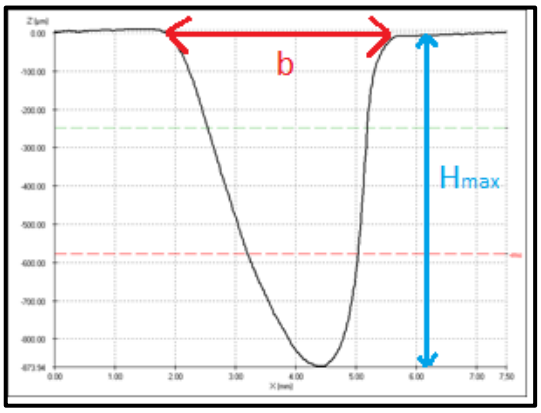

Fig. 7.8 Volume di riferimento per il calcolo analitico del grado di erosione.

$$V = \frac{1}{2} \cdot \frac{4}{3} \pi \, a \, b \, H_{max} \qquad 7.2$$

I valori e **b**, sono stati ripresi direttamente dai dati sperimentali, in riferimento alla figura. Il valore **a** è stato fissato costante: 1000 µm per ogni provino testato con angolo di impatto di 15˚, 45˚ e 90˚.
Per i risultati ottenuti ci si può ricondurre alle tabelle 5.3 e 5.4, del presente lavoro, divise per tipo di acciaio.

Infine è stato utilizzato un modello di regressione lineare per ottenere la dipendenza del grado di erosione solo da alcuni parametri fondamentali. Per rendere il modello più accurato possibile, è stato scelto come fattore di riferimento il valore di massima profondità di usura (H_{max}), dal momento che è stato ottenuto tramite il microscopio confocale che può essere considerato di elevate precisione e accuratezza

Quindi con un limite ragionevole di incertezza è possibile prevedere la profondità di usura, partendo dalla condizione di processo. Per questo è stata ottenuta una equazione che descrive la variazione della profondità di usura a seconda dell'angolo di impatto e della velocità del flusso di erodente come variabili, essendo l'influenza del materiale trascurabile e della temperatura trascurabili.

$$\boldsymbol{Hmax}(\mu m) = -607{,}68 + 10{,}27[\boldsymbol{ANG}] + 12{,}09[\boldsymbol{VEL}] + 0{,}1[\boldsymbol{ANG} * \boldsymbol{VEL}] - 0{,}13[\boldsymbol{ANG\text{^}2}] \qquad 7.3$$

L'equazione 7.3 può essere definita come equazione parametrica, presenta i fattori di controllo e la loro combinazione lineare, inoltre i parametri numerici definiscono il "peso" di ogni fattore.

L'equazione ottenuta può essere considerata un modello reale, per verificare l'affidabilità è stato confrontato l'andamento dei dati reali con quelli previsti dal modello, e il confronto è mostrato nel grafico 7.3.

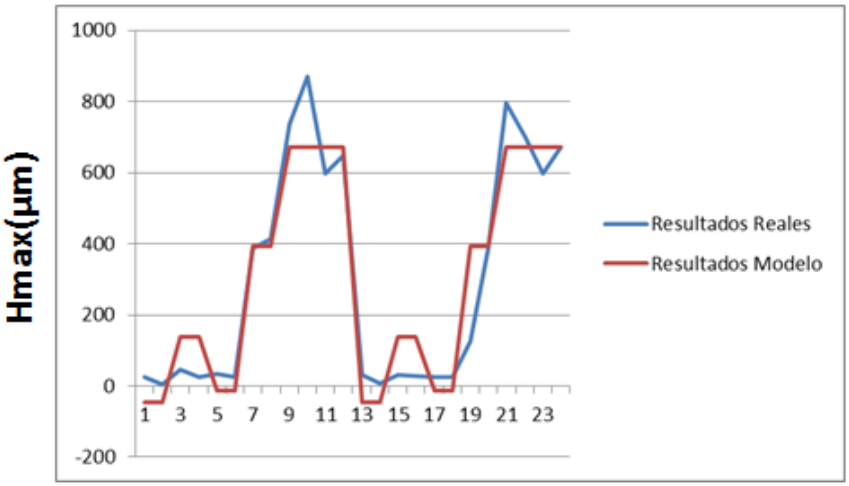

Graf. 7.3 Comparazione tra Risultati Sperimentali e Modello di Previsione.

CONCLUSIONI

Gli acciai utilizzati durante tutta l'analisi sono H13 e H11, che sono i più utilizzati per la creazione di stampi grazie alle loro caratteristiche descritte precedentemente. Dall'analisi meccanica di questi due materiali è risultato che nonostante le differenze a livello di composizione chimica, quando sono soggetti a sforzi di natura meccanica, è lecito affermare che i due materiali si comportino allo stesso modo con minime differenze.

Lo studio è stato affrontato con lo scopo di capire come le alte temperature influissero sulla vita residua di un componente soggetto anche a tensioni meccaniche.

Durante la sperimentazione sono stati presi in considerazione le proprietà fondamentali degli acciai, come la curva monotona del materiale, che ha rivelato la tensione di snervamento, la tensione massima e i limiti di rottura. Si è anche preso in considerazione la variazione del modulo di Young in relazione al cambiamento di temperatura ottenendo una curva che descriveva il tipo di comportamento e i valori da adottare alle diverse temperature.

Con i dati ottenuti nelle analisi preliminari, siamo riusciti ad effettuare almeno sette tests, quattro con provini in H13 e tre con provini di H11, che possono essere considerati in controllo di deformazione, in quanto il parametro principale che variava nei diversi test era l'ampiezza, oltre che la temperatura.

Come era prevedibile ad un ampiezza maggiore, e a temperatura costante, è corrisposto un numero minore di cicli residui del componente, dimostrando in questo modo che il parametro più influenzante è l'ampiezza di deformazione.

Dai risultati si è individuata un'equazione che può essere considerata un buon punto di partenza per descrivere l'andamento del rapporto tra stress e numero di cicli residui a rottura. È comunque necessario chiarire che si tratta di un *work in progress*.

L'altra sezione di sperimentazione si è focalizzata sul danneggiamento dovuto all'erosione, anche qui con lo scopo di studiare il comportamento tra i due materiali in modo da poter creare un modello che ne descrivesse l'andamento. È stato doveroso introdurre e descrivere i test effettuati precedentemente e utilizzati come punto di partenza per poter capire su quali parametri lavorare durante i test.

Quindi sono stati effettuati circa venti test, dieci per un materiale, e dieci per l'altro per riuscire a descrivere a pieno tutte le diverse configurazioni con i diversi parametri. Una volta effettuate tutte le analisi, si sono studiati i risultati utilizzando due diversi approcci: il primo, più semplice, basato sulla massa persa ottenuta con la differenza di peso tra provino originale ed eroso. Il secondo approccio nasce dall'osservazione del tipo di impronta lasciata sul provino dal flusso erosivo, che risulta sempre assimilabile ad un semi ellissoide. Il terzo approccio è basato sull'utilizzo di un microscopio confocale, in grado di leggere la profondità massima del foro lasciato dal flusso erosivo.

Da tutti gli approcci è risultato che i parametri più influenzanti sono l'angolo di impatto e la velocità del flusso di erodente. In particolare, come dimostra anche il grafico 6.1 ottenuto mediante il trattamento dei dati, i valori di massa persa sono inversamente proporzionali all'aumento di angolo, ossia che a valori maggiori di angolo di impatto corrisponde una minor massa persa, mentre

Infine le relazioni trovate appena espresse sono state riassunte in un equazione (5.4) che esprime il valore massimo di profondità di usura in funzione dell'angolo di impatto e della velocità del flusso di particelle. La relazione individuata risulta affidabile anche perché se comparata ai risultati ottenuti, esprime lo stesso andamento. (Grafico 5.4).

Chapter 8:

BIBLIOGRAPHY

[1] E606 – 04´ Standard Practice for Strain-Controlled Fatigue Testing

[2] E2368 – 04´Standard Practice for Strain Controlled thermomechanical Fatigue Testing

[3] Stress Corrosion Cracking Tekniker – technical specifications.

[4] ASTM G129 – 00 Standard Practice for Slow Strain Rate Testing

[5] Rafael Áviles, Análisis de Fatiga en Máquinas, ISBN 8497323440, 2005

[6] G 76 – 95 Standard Test Method for Conducting Erosion Tests by Solid Particle Impingement Using Gas Jets1

[7] INFORME _2738BM_vs_3738HH

[8] Air Jet Erosion Manual, DUCOM TRIBOLOGY

[9] Simulation of High Pressure Die Casting (HPDC) via STAR-Cast

[10] Internal report on methodology for quantitative classification of quality requirements for classes of HPDC/PIM injected product considering their in-service function and performance requirements (AUDI)

[11] A. Srivastava and R. Shivpuri, V. Joshi, Investigating Tribochemical Behavior Of Nitrided Die Casting Die Surfaces,

[12] Jie Song, Tony Denouden, And Qingyou Han, Mechanisms of Soldering Formation on Coated Core Pins.

[13] Z.W. Chen U, M.Z. Jahedi, Die erosion and its effect on soldering formation in high pressure die casting of aluminium alloys.

[14] Zackery Gay, Benefits of Surface Engineering for Aluminum Die Casters.

[15] Flávio José da Silvai, Sinésio D.Franco, Cavitation Erosion Behavior of CrN and AlCrN Coatings Deposited on 34 CrAlNi 7 plasma Nitrided Steel.

[16] Anders Persson, Sture Hogmarkb, Jens Bergström, Failure modes in field-tested brass die casting dies

[17] A. Srivastava, V. Joshi, R. Shivpuri, Computer modeling and prediction of thermal fatigue cracking in die-casting tooling.

[18] Research Stereo Microscope System , SZX16/SZX10

[19] K. Venkatesan and R. Shivpuri, Experimental and Numerical Investigation of the Effect of Process Parameters on the Erosive Wear of Die Casting Dies, Paper No. MS-39, Transactions of NAMRI/SME, Volume XXII, Society of Manufacturing Engineers 1995

[20] J.H. Brunton and M.C. Rochester, Erosion, Treatise on Materials Science and Technology, Vol. 16, Academic, Press, New York, 1979, p 185

[21] I. Finnie, A. Levy, and D.H. McFadden, Fundamental Mechanisms of Erosive Wear of Ductile Metals by Solid Particles, Erosion: Prevention and Useful Applications, STP 664, ASTM, 1979, p 36-58

[22] S. Malm and J. Tidlund, Increased Life for Die Casting Dies, Tenth Int. Die Casting Congress and Exposition, SDCE (Society of Die Casting Engineers), Paper No. 801, 1979

[23] M.L. Yu, and Y.L. Chu, and R. Shivpuri, A Study of Corrosive Wear of Die Casting Die Materials and Coatings for Aluminum Die Casting, Report Number ERC/NSM-C-93-06, Engineering Research Center for Net Shape Manufacturing, The Ohio State University, 1993

[24] Young, J. P., and Ruff, A. W., Journal of Engineering Materials and Technology, transactions of ASME, Vol 99, 1977, pp. 121–125.

[25] Hansen, J. S., in Erosion: Prevention and Useful Applications, Adler, W. F., ed., ASTM STP 664, 1979, pp. 148–162.

[26] Y.L. Chu and R. Shivpuri, Development of a Test Procedure for Erosive Wear in Die Casting Dies, Report Number ERC/NSM-C-93-11, Engineering Research Center for Net Shape Manufacturing, The Ohio State University, 1993

[27] J.R. Laguna-Camacho, L.A. Cruz-Mendoza, J.C. Anzelmetti-Zaragoza, A. Marquina-Chávez, M. Vite-Torres, J. Martínez-Trinidad, Solid particle erosion on coatings employed to protect die casting molds.

[28] A. Mohammed, M.B. Marshall, R. Lewis, Development of a Method for Assessing Erosive Wear Damage on Dies used in Aluminium Casting.

[29] Shuji Hattori, Effects of Impact Velocity and Droplet Size on Liquid Impingement Erosion.

[30] Japan Society of Mechanical Engineers (JSME), "Codes for Power Generation Facilities – Rules on Pipe Wall Thinning Management –", JSME S Ca1-2005, pp.48-70.

[31] ASTM G134-1995, "Standard Test Method for Erosion of Solid Materials by a Cavitating Liquid Jet", 2005, pp.1-13.

[32] H.K. Barton, What Happens When a Die Casting Die Erodes, Foundry, 1965, p 132-136

[33] K. Stellar, T. Krzytofowicz, and Z. Reymann, Effects of Cavitation on Materials in Field and Laboratory Conditions, STP 567, ASTM, 1976, p 153-170.

[34]J.H. Brunton, Proc. of Third lnt. Conf. Rain. Eros., 1970, p 81.

[35] A.J. Davis and M.T. Murray, Seventh Int. Die Casting Congress and Exposition, DCE Paper No. G-T-81-123, Society of Die Casting Engineers, 198 l

[36] Evan Thomas, Mircea Pascovici, Karolina Jablonka and Romeo Glovnea, Experimental investigation into the cavitation phenomena at a slip/non-slip surface, World Tribology Congress 2013, p 2

[37] D.G. Smith, New Approach to an Old Problem--Die Erosion, Transactions of the Third National Die Casting Congress, Paper 25, Society of Die Casting Engineers, 1964

[38] C. Godoy, R.D. Mancosu, M.M. Lima, D. Brandão, J.Housden, J.C. Avelar-Batista, Influence of plasma nitriding and PAPVD Cr1 − xNx coating on the cavitation erosion resistance of an AISI 1045 steel, Surf. Coat. Technol. 200 (2006) 5370-5378.

[39] I.M. Hutchings, Tribology, Friction and Wear of Engineering Materials, Butterworth-Heinemann, Cambridge, 1992.

[40]Matevž Fazarinc, Rado Turk, Goran Kugler, Primož Mrvar, Milan Teršelj, Development of test rig for thermal fatigue testing – preliminary results, Materials and Geoenvironment, Vol. 54, No. l, pp. 33-48, 2007

[41] Damjan, Janez, Thermal stresses in aluminium alloy die casting dies, Computational Materials Science 43 (2008) 1147–1154

[42] D. Klobcˇar, L. Kosec, B. Kosec, J. Tušek, Thermo fatigue cracking of die casting dies, Engineering Failure Analysis 20 (2012) 43–53

[43] D. Klobcˇar, J. Tušek, B. Taljat, Thermal fatigue of materials for die-casting tooling, Materials Science and Engineering A 472 (2008) 198–207

[44] Yulong Zhu, David Schwam, John F. Wallace, Sebastian Birceanu, Evaluation of soldering, washout and thermal fatigue resistance of advanced metal materials for Aluminum die-casting dies, Materials Science and Engineering A 379 (2004)

[45] A. Srivastava, V. Joshi and R. Shivpuri, Numerical Models And Their Validity In The Prediction Of Heat Checking In Die Casting Tooling, Manufacturing Research Group, The Ohio State University, 1971 Neil Avenue, 210 Baker Systems, Columbus, Ohio 43210.

[46] Alastair Long, David Thornhill, Cecil Armstrong, David Watson, Predicting die life from die temperature for high pressure dies casting aluminium alloy, Applied Thermal Engineering 44 (2012) 100-107

[47] G.Timelli, S.Ferraro, F.Grosselle, F.Bonollo, F.Voltazza, L. Capra "Caratterizzazione meccanica e microstrutturale di leghe di alluminio pressocolate", La Metallurgia Italiana 1, 2011, p.5

[48] L.Andreoni, M.Casè, G.Pomesano, "Lubrificazione della cavità dello stampo", Quaderni della colata a pressione delle leghe di alluminio 7, 1996, pp.9-26

[49] Q. Han and S. Viswanathan, Analysis of the Mechanism of Die Soldering in Aluminum Die Casting''+

[50] Andre Pineau, Stephen D. Antolovich, High temperature fatigue of nickel-base super alloys A review with special emphasis on deformation modes and oxidation Centre des Materiaux de l'Ecole des Mines de Paris, UMR CNRS 7633 EVRY Cedex, France, Georgia Institute of Technology, School of Materials Science and Engineering, Atlanta, GA 30332, USA

[51] Z.W. Chen, Skin solidification during high pressure die casting of Al, 11Si, 2Cu, 1Fe alloy, Department of Mechanical and Production Engineering, Auckland University of Technology, Private Bag 92006, Auckland 1020, New Zealand

[52] http://energy.gov/eere/amo/h-series-cast-austenitic-stainless-steels

ANNEX 1

1.2344

Normativa di riferimento DIN 17350
Reference standard DIN 17350

IMS S.p.A.
acciai speciali

COMPOSIZIONE CHIMICA / *CHEMICAL ANALYSIS*							
C	Mn	Si	Ni	Cr	Mo	W	V
0.37	0.30	0.90	-	4.80	1.20	-	0.90
0.43	0.50	1.20	-	5.50	1.50	-	1.10

PUNTI CRITICI / *CRITICAL POINTS*	
Ac_1	860 °C
Ms	340 °C

UNIFICAZIONI COMPARATIVE / *COMPARABLE STANDARDS*						
SIAU	UNI	W.Nr.	DIN	AFNOR	AISI/SAE	BS
MTV	(X40CrMoV51.1KU)	1.2344	X40CrMoV51	-	(H13)	(BH13)

CARATTERISTICHE GENERALI E IMPIEGHI

Acciaio adatto a subire la tempra in aria. Possiede discreta stabilità dimensionale al trattamento termico. Mantiene elevata resistenza all'usura fino a temperature prossime ai 600 °C.

Questo acciaio presenta inoltre ottima tenacità ed elevata insensibilità agli shock ed alla fatica termica.

Per innalzare la durata delle attrezzature realizzate, questo acciaio può essere sottoposto a trattamento di indurimento superficiale, tipo **nitrurazione**.

Tra i principali impieghi ricordiamo:
- stampi per pressofusione di leghe leggere
- attrezzature per estrusione leghe leggere e acciai
- lame di cesoie a caldo
- rulli profilatori (zona saldatrice)

Si consiglia di preriscaldare gli utensili a temperature comprese nell'intervallo 250 ÷ 300 °C prima dell'impiego.

STATO DI FORNITURA

Ricotto HB ≤ 230

TRATTAMENTI TERMICI

Ricottura isotermica:
- riscaldo a 880 °C con permanenza a temperatura da 1/2 ora ad 1 ora;
- discesa libera in forno a 780 °C e permanenza a temperatura per almeno 5 ore;
- discesa 10 °C/h fino a 750 °C;
- raffreddamento in aria.

Durezza massima: 230 HB

GENERAL PROPERTIES AND APPLICATIONS

Steel suitable for air hardening. It is characterized by fairly good dimensional stability during heat treatment
It maintains high wear resistance up to temperatures of around 600 °C.
This steel also possesses excellent toughness and high level insensitivity to thermal shock and thermal fatigue.
*A **nitriding** type surface treatment can be carried out on this steel to increase the service life of the tooling.*
Main applications:
- *dies for the pressure casting of light alloys*
- *tooling for the extrusion of light alloys and steels*
- *hot work shear blades*
- *rolls for profiling tools (welding area)*

The tools should be preheated to temperatures in the range 250 ÷ 300 °C before use.

SUPPLY CONDITION

Annealed HB ≤ 230

HEAT TREATMENTS

Isothermal annealing:
- *heat to 880 °C, hold at temperature for 1/2 h to1h;*
- *furnace cooling to 780 °C and hold at temperature for at least 5 hours;*
- *cool by 10 °C/h to 750 °C;*
- *cooling in air.*

Maximum hardness: 230 HB

1.2344

Distensione:

Da eseguirsi dopo le lavorazioni meccaniche, prima del trattamento termico finale.

- riscaldo a 650 ÷ 700 °C con permanenza di 4 ÷ 6 ore;
- raffreddamento in forno fino a 300 ÷ 350 °C;
- raffreddamento in aria.

Tempra:

- 1 ° preriscaldo a 350 ÷ 450 °C;
- 2° preriscaldo a 750 ÷ 850 °C;
- riscaldo a temperatura compresa nell'intervallo 1000 ÷ 1050 °C con permanenza a regime;
- raffreddamento in aria.

Durezza dopo tempra: 52 ÷ 56 HRC

Rinvenimento:

Nell'intervallo 550 ÷ 630 °C per almeno 3 ore, secondo le esigenze di durezza e le condizioni di esercizio.

Si prescrive di ripetere sempre il rinvenimento una seconda volta, ad una temperatura uguale od inferiore di 20 °C rispetto alla precedente.

Prima del rinvenimento è necessario preriscaldare i pezzi a 200 ÷ 300 °C.

Stress relieving:

To be carried out after machining and before the final heat treatment.

- *heat to 650 ÷ 700 °C, hold for 4 ÷ 6 hours;*
- *furnace cooling to 300 ÷ 350 °C;*
- *cooling in air.*

Hardening:

- *Initial preheating to 350 ÷ 450 °C;*
- *second preheating to 750 ÷ 850 °C;*
- *heat to hardening temperature in the range 1000 ÷ 1050 °C and hold at temperature;*
- *cooling in air.*

Quenched hardness: 52 ÷ 56 HRC

Tempering:

In the range 550 ÷ 630 °C for at least 3 hours according to hardness requirements and conditions of use.

Tempering must be repeated a second time at a temperature equal to or 20 °C lower than the previous.

Before tempering, preheat the parts to 200 ÷ 300 °C.

1.2344

Curva di resistenza a caldo
Hot tensile strength curve

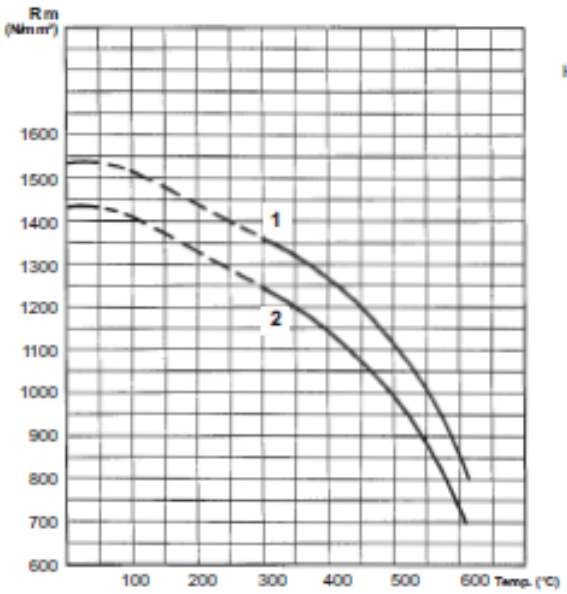

Provetta bonificata a: 1540 N/mm² n°1
Test specimen hardened and tempered at: 1430 N/mm² n°2

Diagramma di rinvenimento
Tempering curve

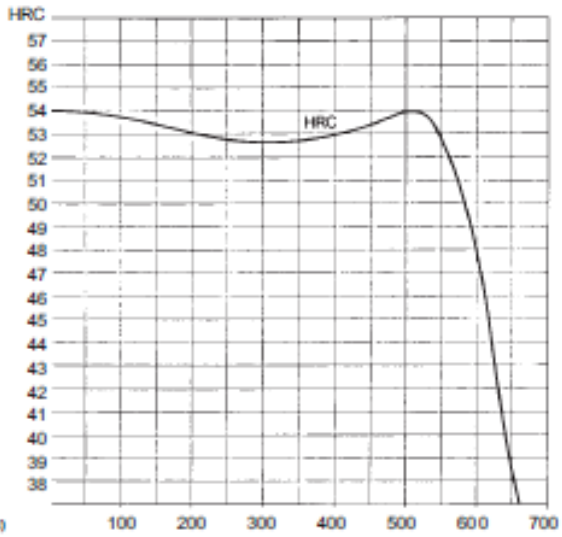

TEMPERATURA DI RINVENIMENTO °C.
TEMPERING TEMPERATURE °C

Quadro: 10 mm
Block: 10 mm

Tempra: 1030 °C in aria
Hardening: 1030 °C in air

Curva C.C.T.
C.C.T. curve

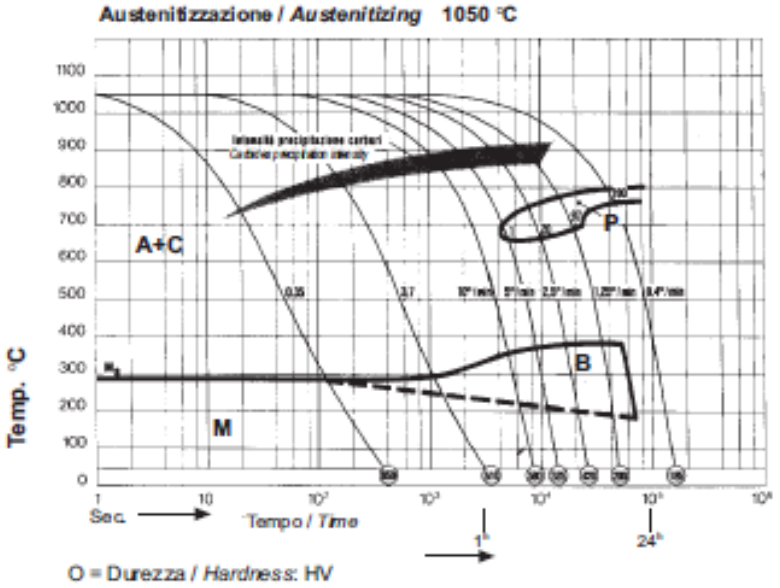

O = Durezza / *Hardness*: HV

IMS S.p.A.
acciai speciali

1.2343

Normativa di riferimento DIN 17350
Reference standard DIN 17350

COMPOSIZIONE CHIMICA / *CHEMICAL ANALYSIS*

C	Mn	Si	Ni	Cr	Mo	W	V
0.36	0.30	0.90	-	4.80	1.10	-	0.25
0.42	0.50	1.20	-	5.50	1.40	-	0.50

PUNTI CRITICI / *CRITICAL POINTS*

Ac_1	840 °C
Ms	310 °C

UNIFICAZIONI COMPARATIVE / *COMPARABLE STANDARDS*

SIAU	UNI	W.Nr.	DIN	AFNOR	AISI/SAE	BS
MTB	(X37CrMoV51KU)	1.2343	X38CrMoV51	Z38CDV5	(H11)	(BH11)

CARATTERISTICHE GENERALI E IMPIEGHI

Acciaio con elevate caratteristiche di resistenza all'usura a caldo, associate a insensibilità alla fatica termica. Questo acciaio può essere sottoposto a tempra in aria il che permette di contenere le deformazioni da trattamento termico. Fra le caratteristiche di questo acciaio è doveroso ricordare che possiede anche ottima tenacità; quindi è adatto per impieghi ove le condizioni di esercizio sono particolarmente gravose.

Questo acciaio trova applicazione per la costruzione di:

- stampi per pressofusione di leghe leggere
- stampi per materie plastiche
- stampi per presse a frizione e meccaniche per lo stampaggio a caldo di acciai, ottone, alluminio e sue leghe.
- matrici per estrusione dell'alluminio
- lame di cesoia a caldo.

In taluni casi può essere conveniente sottoporre gli utensili a trattamenti termochimici di indurimento superficiale.

Si ricorda, allo scopo, che questo acciaio può essere sottoposto a nitrurazione (ionica - salina - gassosa).

Gli utensili, prima di iniziare la lavorazione, devono essere preriscaldati nell'intervallo di temperature comprese fra 250 ÷ 300 °C.

STATO DI FORNITURA

Ricotto HB ≤ 220

GENERAL PROPERTIES AND APPLICATIONS

Steel with high level hot wear strength properties associated with insensitivity to thermal fatigue. This steel can be air hardened which makes it possible to reduce distortions caused by heat treatment. Amongst the properties of this steel, it is worth remembering that it also possesses excellent toughness and is therefore suitable for use in particularly severe operating conditions.

These steels are used to construct:

- *dies for pressure casting of light alloys;*
- *molds for plastic materials;*
- *dies for friction and mechanical presses for hot forming of steels, brass, aluminum and its alloys;*
- *dies for extrusion of aluminum;*
- *hot work shear blades.*

In some cases, it may be advisable to carry out thermo-chemical surface hardening treatments on the tools.

It should be remembered, for this purpose, that this steel can be nitrided (ion- saline – gaseous).

Before machining, the tools must be preheated to a temperature range of between 250 ÷ 300 °C.

SUPPLY CONDITION

Annealed HB ≤ 220

1.2343

TRATTAMENTI TERMICI

Ricottura isotermica:
- riscaldo a 880 °C con permanenza a temperatura da 1/2 ora ad 1 ora;
- discesa libera in forno a 780 °C e permanenza a temperatura per almeno 5 ore;
- discesa 10 °C/h fino a 750 °C;
- raffreddamento in aria.

Durezza massima: 220 HB

Distensione:

Da eseguirsi dopo le lavorazioni meccaniche e prima del trattamento termico finale.
- riscaldo a 650 ÷ 700 °C con permanenza di 4 ÷ 6 ore;
- raffreddamento in forno fino a 300 ÷ 350 °C;
- raffreddamento in aria.

Tempra:
- 1° preriscaldo a 350 ÷ 450 °C;
- 2° preriscaldo a 750 ÷ 850 °C;
- riscaldo alla temperatura di tempra nell'intervallo compreso tra 1000 ÷ 1030 °C con permanenza a regime;
- raffreddamento in aria.

Durezza dopo tempra: 52 ÷ 55 HRC

Rinvenimento:

Nell'intervallo 550 ÷ 650 °C per almeno 3 ore, secondo le esigenze di durezza e le condizioni di esercizio.

Raffreddare in aria calma.

Si prescrive di ripetere sempre il rinvenimento una seconda volta, ad una temperatura uguale od inferiore di 20 °C rispetto alla precedente.

Prima del rinvenimento è necessario preriscaldare i pezzi a 200 ÷ 300 °C.

HEAT TREATMENTS

Isothermal annealing:
- *heat to 880 °C, hold at temperature for 1/2 h to 1 h;*
- *furnace cooling to 780 °C and hold at temperature for at least 5 hours;*
- *cool by 10 °C/h to 750 °C;*
- *cooling in air.*

Maximum hardness: 220 HB

Stress relieving:

To be carried out after machining and before the final heat treatment.
- *heat to 650 ÷ 700 °C, hold for 4-6 hours;*
- *furnace cooling to 300 ÷ 350 °C;*
- *cooling in air.*

Hardening:
- *Initial preheating to 350 ÷ 450 °C;*
- *second preheating to 750 ÷ 850 °C;*
- *heat to hardening temperature in the range 1000 ÷ 1030 °C and hold at temperature;*
- *cooling in air.*

Quenched hardness: 52 ÷ 55 HRC

Tempering:

In the range 560 ÷ 650 °C for at least 3 hours according to hardness requirements and conditions of use.

Cooling in still air

Tempering must be repeated a second time at a temperature equal to or 20 °C lower than the previous.

Before tempering, preheat the parts to 200 ÷ 300 °C.

1.2343

Curva di resistenza a caldo
Hot tensile strength curve

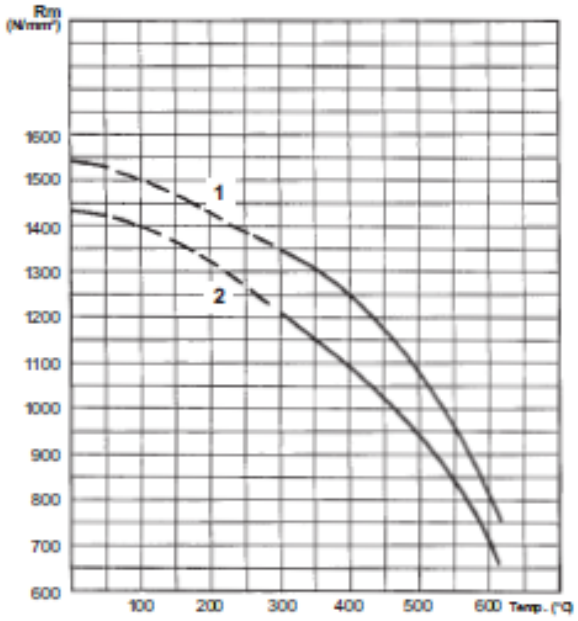

Diagramma di rinvenimento
Tempering curve

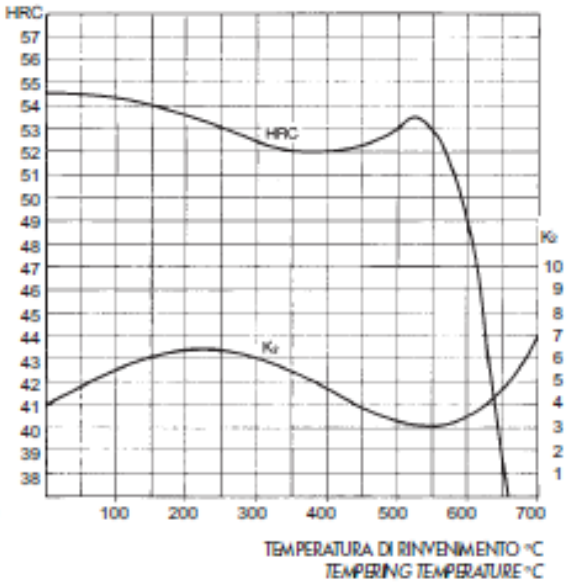

Provetta bonificata a: 1540 N/mm² n°1
Test specimen hardened and tempered at: 1430 N/mm² n°2

Tempra: 1030 °C in aria
Hardening: 1030 °C in air

Saggio: quadro 10 mm
Test specimen: 10 mm square

Diagramma C.C.T.
C.C.T. diagram

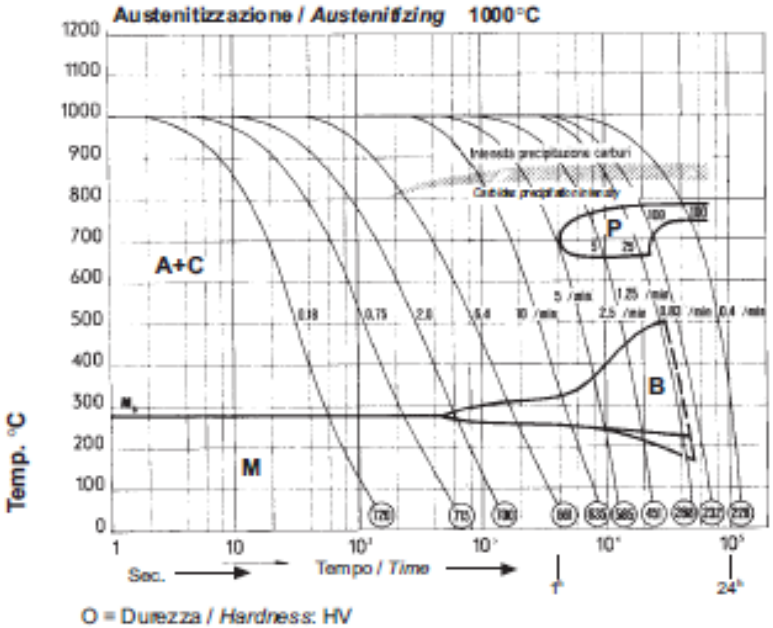

O = Durezza / *Hardness*: HV